NTNU
Norwegian University of
Science and Technology

# Global buckling of pipelines

A study on different soil models

Seoyeon Park

Marine Technology
Submission date: June 2016
Supervisor: Svein Sævik, IMT

Norwegian University of Science and Technology
Department of Marine Technology

NTNU – Trondheim
Norwegian University of
Science and Technology

# Global buckling analysis of subsea pipelines

# A study on different soil models

SeoYeon Park

June 2016

SUPERVISOR : PROFESSOR SVEIN SÆVIK

DEPARTMENT OF MARINE TECHNOLOGY

NORWEGIAN UNIVERSITY OF SCIENCE AND TECHNOLOGY

# Preface

This paper is the result of the two-year international master program at Department of Marine Technology at Norwegian University of Science and Technology. The thesis has written wishing to deliver practical judgments in initial pipeline design step and operation events of pipelines laying on the irregular foundation.

All of case studies has mainly computed by finite element method software SIMLA which is developed by professor Svein Sævik and MARINTEK. Empirical examples included into SIMLA are referred in this thesis.

I am appreciative to all people who involved in this thesis. I would like to thank professor Svein Sævik for his guidances in many ways. Thanks to his work, the software could be continuously updated for accurate and precise outcomes. I also thank professor Bernt Johan Leira for contributing to stochastic parameter theories of underwater soil. I am grateful to Ph.D candidate Tianjiao Dai for extensive guidances in several stages. Last, I want to thank my family and friends for their sincere support

Trondheim, 2016-06-10

_____

SeoYeon Park

# Summary

Pipelines are essential units as a energy transportation method nowadays. Buckling behaviors have been recognized as majority because it can cause sudden disconnection of pipelines and this may lead the pipeline to difficulties such as rupture (Andrew C. Palmer (2007)). Moreover, for exposed pipelines on the sea floor, global buckling is the major phenomenon observed (Hong (2014)). Global buckling has sensitivity of several features which are pressure, temperature, embedment, pipe-soil interaction, initial pipeline configuration, and etc. An issue is that vulnerable hydrocarbon is exposed to high temperature and pressure under the deep sea (Andrew C. Palmer (2007)). In order to operate the oil and gas transportation safely, therefore, pipelines eventually face challenges. Many researchers have previously discussed about pipe-soil interaction, and proposed soil force-displacement models such as Mohr-Coulomb model, DNV model, PONDUS model, and SAFEBUCK model. The scope of this paper is to analyse the global buckling response from different interaction models along with parametric studies. The founding shows that geology data of the foundation has a strong correlation with global buckling more than typical stochastic data. On the other hand the stochastic data has an influences on stabilization of moments, which affect initial design layout for simulations determining length of the operation simulation time. As representative soil models, Coulomb model and DNV model which soil berm formation algorithm under cyclic loading is implemented into, are compared. The DNV model displays conservative resultants in certain extend.

# Contents

# List of Figures

# List of Tables

# Symbols and Acronyms

**Roman letters**

| | |
|---|---|
| C | Damping |
| C | Adhesion coefficient |
| D | Nominal outside diameter of steel pipe |
| D | Embedment of the maximum diameter section |
| DNV | DET NORSKE VERITAS |
| E | Young's Modulus |
| FE | Finite Element |
| f | Local element force |
| G | Initial shear modulus of soil for infinitesimal strains |
| HT/HP | High temperature and high pressure |
| i | iteration step number |
| $I_p$ | Plasticity index |
| k | time step number |
| $K_T$ | Global stiffness for the entire structure |
| $K_L$ | Lateral dynamic stiffness in clay |
| $K_v$ | Lateral dynamic stiffness in clay |
| $\hat{K}$ | Effective stiffness matrix |
| KP | Kilometer point |
| M | Mass |
| $M_{cr}$ | Critical moment |
| $M_P$ | Plastic moment |

| | |
|---|---|
| $M_y$ | Y-axis bending moment |
| $M_z$ | Z-axis bending moment |
| $\Delta r$ | Displacement increment |
| R | Radius of foundation in contact with soil |
| $R^E$ | External force vector |
| $R^I$ | Internal force vector |
| $\Delta R$ | Load increment |
| S | Surface |
| u | local element displacement |
| $\ddot{u}$ | local element acceleration |
| v | Node displacement |
| V | Volume |
| Y | lateral displacement |

**Greek letters**

| | |
|---|---|
| $\alpha$ | Damping correction coefficient from HHT-$\alpha$ method |
| $\delta\varepsilon$ | Infinitesimal strain |
| $\theta$ | Local element rotation |
| $\mu$ | Friction coefficient |
| $\nu$ | Poisson coefficient |
| $\xi$ | Non-dimensional coordinate parameter |
| $\rho$ | Density |
| $\sigma$ | Stress |
| $\tau_f$ | Shear strength of soil |
| $\phi$ | Angle between soil and foundation material curve |

# Chapter 1

# Introduction

## 1.1 Motivation

In 1947, the first offshore rig 'Superior' was installed in Louisiana, United States. The first page of offshore structure history has written with the offshore structure installed in 6 m depth of water. Today, offshore structures are normally placed in more than 2,000 meter of water depth (Randolph and Gourvenec (2011)). As time passes, transportation methods including pipeline transportation system for multi-phase hydrocarbon products have become diverse.

Conveyance of resources through pipelines introduces some challenges with regards to exceeding bending moment during operation events that may result in failure of pipelines under high temperature and pressure. To ensure safe operation pipeline control is crucial. In consequence, there were some attempts to interpret highly nonlinear pipe-soil interaction. Soil response models have developed as the models reflect nature of soil response better, and numerous researchers have previously discussed the idea of dominant parameters on global buckling. However, needs for more sophisticated nonlinear analyses including uneven foundation profile and stochastic variable, have increased.

## 1.2 Objectives

The main objectives of this thesis are

1. pipeline simulation for installation and operation
2. examination of response from different implemented soil models
3. parametric study for geological stochastic variables

To simulate the models, strong finite element(FE) analysis program for pipelines, SIMLA is introduced. Handful case studies are performed based on several simplifications as the least to keep involving significant nonlinear requirements to meet the objects.

## 1.3 Organization of the thesis

This paper is constructed as follows:

**Chapter 2** provides general prospective of theories behind the analyses and methodologies for post processes.
**Chapter 3** gives a big overview of the pipeline-soil interaction technology.
**Chapter 4** deals with assumptions implemented in the models
**Chapter 5** presents the main findings. First, parametric studies of geological stochastic variables are performed. Next, components consisting resultant of outcomes from typical two soil models are compared and examined
**Chapter 6** includes the impact that the results bring on soil-pipeline interaction technology. This chapter also contains comments what the research sought early of this paper.
**Chapter 7** suggests how next step can be continued.

# Chapter 2

# Theory and Method

In this chapter theories behind this thesis are elucidated. Analyses implemented in this thesis are computed by finite element analysis software SIMLA. Basic principles of interpretation of non linear behaviour are described hereby.

## 2.1 SIMLA : Finite element analysis program

### 2.1.1 An overview of SIMLA

SIMLA is a finite element method based program system specialized for pipelines in non-linear static and dynamic analyses. The software has several distinctions. This specialized program can simulate most of non-linear conditions that pipelines face often during installation and operation.

This program mainly cover four parts of non-linearity that pipelines may experience which are aspects of contact condition, soil model, and material. First, applying specific contact conditions implies that highly uneven seabed profile can be adopted, which can cause extremly non-linear response of the pipeline. In addition, the route of the pipes can be divided into parts, and it can make the analysis run with different soil properties as per subdivision.

Pipe-soil interaction models heavily affect responses of behaviour. From simply linear spring model to non-linear soil berm model, users can select an appropriate model depending on scope of projects.

Traditional material models are employed in SIMLA. Both steal material for pipelines and soil material which consists of probabilistic data are included. For steal material linear elastic or elasto-plastic behaviour with isotropic and kinematic hardening are available.

To visualize the result from SIMLA a program called X-post inside of SIMLA is equipped.

However to increase legibility of computed result from the analysis SIMPOST file is required to extract data sets from the model and read the result manually.

### 2.1.2 Solution algorithms

The model is analysed by the finite element method program SIMLA which is a specialized program for underwater pipelines and risers. The theories behind the program are based on virtual work weak form equations for each elements. Since required data from the pipeline is only bending moment and axial forces at each nodes, the pipeline is modelled as a long beam structure.

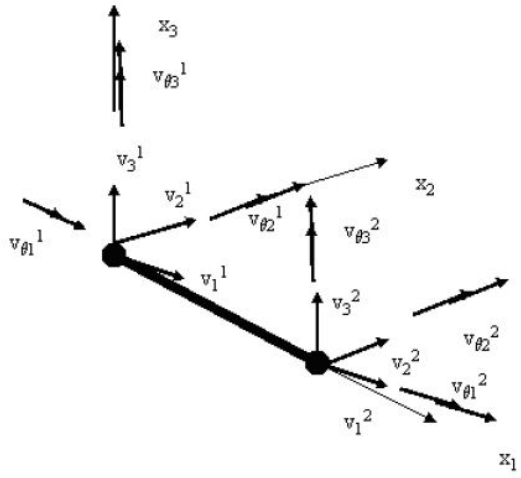


Figure 2.1: Dofs for PIPE elements (Sævik (2008))

In Figure 2,1, one beam element consisting of two nodes with six degree of freedom, is drawn. By movement of the two nodes the beam bends as linear interpolation curve and cubic interpolation curve for axial and torsion displacement and transverse displacement respectively. In a beam structure analysis, instead of finite infinitesimal size of mesh size of one beam length is adopted.

In virtual work weak form equations, in short, sum of multiplication of virtual displacement and sum of force is zero for one node. General form of virtual work weak form equation in a vector form is following.

$$\int_V (\rho \ddot{u} - f)\delta u dV + \int_V \sigma : \delta \epsilon dV - \int_S t\delta u dS = 0$$

The interpolation curve by nodes on a beam can be reinterpret as a shape function with non-dimensional coordinate parameter $\xi$.

$$\begin{pmatrix} u_1 \\ u_2 \\ u_3 \\ \theta_1 \end{pmatrix} = N \begin{pmatrix} v_1^1 \\ v_2^1 \\ v_3^1 \\ v_{\theta 1}^1 \\ v_{\theta 2}^1 \\ v_{\theta 3}^1 \\ v_1^2 \\ v_2^2 \\ v_3^2 \\ v_{\theta 1}^2 \\ v_{\theta 2}^2 \\ v_{\theta 3}^2 \end{pmatrix} \tag{2.1}$$

Where N is the matrix with non-dimensional parameter $\xi$

$$N = \begin{pmatrix} 1-\xi & 0 & 0 & 0 & 0 & 0 & \xi & 0 & 0 & 0 & 0 & 0 \\ 0 & 1-3\xi^2+2\xi^3 & 0 & 0 & 0 & l\xi(\xi-1)^2 & 0 & 3\xi^2-2\xi^3 & 0 & 0 & 0 & -l\xi^2(\xi-1) \\ 0 & 0 & 1-3\xi^2+2\xi^3 & 0 & l\xi(\xi-1)^2 & 0 & 0 & 0 & 3\xi^2-2\xi^3 & 0 & -l\xi^2(\xi-1) & 0 \\ 0 & 0 & 0 & 1-\xi & 0 & 0 & 0 & 0 & 0 & \xi & 0 & 0 \end{pmatrix} \tag{2.2}$$

Here, $\delta u$ is virtual displacement, $\ddot{u}$ is acceleration in a degree of freedom of the element.

Then local element displacements and rotation $u_1, u_2, u_3, and \theta_1$ are found from node data. Integrated local element displacements and rotations matrix along the element are also discovered. Weak form equations of virtual work can be applied again along the element. The total equilibrium in a local element level is found including action-reaction force and virtual displacements caused by reaction forces. Then the local element stiffness can be identified by the

relationship between force and displacement.

By adapting transformation matrix, global stiffness matrices in element level can be found from the local element stiffness matrices. Then all global stiffness matrices in a element level is assembled to find a global stiffness for the entire structure, $K_T$. A equilibrium of global force and displacement is formulated as following.

$$\Delta R = K_T \Delta r$$

Here, non-linearity takes into account on the total global stiffness matrix term. The total matrix includes material and geology non-linearity. With the total global stiffness matrix, expected displacement $\Delta r$ from the force-displacement equilibrium equation is found as following.

$$\Delta r = K_T^{-1} \Delta R$$

To satisfy the equilibrium equation $\Delta R = R_{ext} - R_{int} \approx 0$, implicit time integration with Newton-Raphson iteration at each load steps are solved. Here, external force, $R_{ext}$, is temperature and pressure loads, and internal force,$R_{int}$, is obtained from resultants of entire structure's reactions.

However, nonlinear dynamic problems cannot use the same modal superposition procedures. Consequently, direct time integration of the equilibrium of motion should be computed. For time efficiency and numerical stability, implicit method which use information from both previous load step and the current step is employed, and new iteration equilibrium with Newton-Raphson iteration scheme is introduced as below (Sævik (2008)).

$$\hat{K}_k^i \delta r_{k+1}^{i+1} = (1+\alpha)[R_{k+1}^E - R_{k+1}^{I,i} - C\dot{r}_{k+1}^i] - M\ddot{r}_{k+1}^i - \alpha(R_k^E - R_k^I - C\dot{r}_k^i)$$

Where $R^I$ is internal force vector, $R^E$ is the external force vector, $k, k+1$ is number of time step, $i$ is iteration step number, and C is damping. $\hat{K}$ is the effective stiffness matrix which is expressed as sum of mass, damping, and global tangent stiffness matrix with coefficients. $\alpha$ is a factor from HHT-$\alpha$ method to have a damping correction.

# Chapter 3

# Literature review

Pipeline is devised to carry a fluid from one to another point. As a transportation method, underwater pipelines are widely used in oil and gas industry nowadays rather than tank option. Using a vessel to carry oil or gas is preferred due to flexibility and low capital costs despite high operation costs. However, pipeline option has fairly small operation and maintenance expenses besides less energy consumption compared to liquefaction and re-gasification (Andrew C. Palmer (2007)). An issue is that vulnerable hydrocarbon is exposed to high temperature and pressure under the deep sea. In order to operate the oil and gas transportation safely, thus, pipelines eventually face challenges.

During hydraulic pressure test and installation procedure, pipelines on seabed may obtain residual lay tension. Operation process entails high temperature and pressure (HT/HP) condition in order to ensure the flow of crude oil and gas. Thermal stress by high temperature and internal pressure of pipeline cause longitudinal expansion (DNV (2007)). Meanwhile pipelines restricted by soil contacts and boundary conditions on the seafloor introduce compression. Consequently sudden deformation appears as a reaction from soil resistance, which denotes global buckling. Global buckling is not a failure mode. However, global buckling reduces the axial carrying capacity, which may trigger failures such as local buckling collapse or cyclic fatigue failure (DNV (2007)). Moreover, pipelines with initial imperfections also can work for by global buckling failure under thermal stress and internal pressure actions. Global buckling can be divided into lateral buckling and upheaval buckling. Lateral buckling intends horizontal curvature accompanied the bending on exposed pipelines while vertical buckling deforms the exposed pipelines by vertical bending. Upheaval buckling also intends vertical bending but it is defined only trenched pipelines undergo vertical bending. Therefore, without trenching or

planned berms, pipelines laid on the sea floor may develop lateral or vertical buckles. Hobbs (1981) revealed that when pipelines are under HT/HP state, lateral modes will be dominant because lateral buckling mode occurs at lower axial load than vertical mode. Hassan Karampour (2013) also found that the vertical mode needs higher compressive axial force P and higher temperature to be bucked in comparison with lateral buckling mode. During entire designed operation life, frequently occurring lateral buckling contributes to berm formation process. Repeated horizontal movement by heating and cooling by shut-down and start-up accumulates neighboring soil at side ways of pipelines. Over long period of operation, the repeated lateral movements may strengthen berms, which causes increased stiffness of the soil berms and influences back to the lateral buckling. With increasing demand of underwater developments, lateral buckling becomes highlighted for safe operations. This demanding has brought radical advance for robust pipeline design principles for lateral global buckling (D. Bruton (2006)).

There are various factors which may effect on global buckling of pipelines. For instance, classic aspects are following:

- Pipe-soil interaction model
- Pressure and temperature
- Imperfection of pipeline (out of straightness)

Disregarding the wave-current load, the governing forces on pipelines can be listed as the submerged weight of the pipeline with its contents, hydrostatic pressure, internal pressure, temperature load and soil resistance (Zhaohui Hong (2015)). By selection of pipe-soil interaction model, the resultant response shows significant different responses for each model. Pipe-soil interaction models are known as the most important factor in global buckling phenomenon especially for the uneven sea floor model to predict correct behavior of pipelines. In order to discover meaningful result, therefore, uneven seabed geology should be included. As well as the seabed profiles, both internal and external pressure, and temperature of pipelines are influential factors in responses of pipelines. Internal pressure and thermal energy contribute to variation in total moment while external pressure reduces moment-tension growth (Yong Bai (1997)). Net

pressure also plays an important role. In a shuts-down of piping system, supplement of pressure and temperature stops, and then internal pressure becomes zero immediately while temperature of petroleum and gas slowly goes down. Due to residual temperature and hydrostatic pressure on the surface of the pipelines, the pipelines may face great instability which induces large bending moment. However, failures during operation may be more dangerous than shut-down instability because it is tough to foretell when and why the operation failures occur. At last, imperfections of pipelines are also a main aspect contributing on global responses. Pipeline imperfection has been spotlighted as a governing parameter since 19th century because it is shown that initial imperfections behavior critically toward integrity of pipelines. When initially imperfect are small, buckling is expected to occur as a dynamic 'snap', i.e. a sudden uncontrolled buckle as the axial equilibrium becomes unstable. On the other side, as the initial imperfections become larger, the buckles shows less sudden behaviors and eventually the snap is eliminated (Per R. Nystrom (1997)). Buckling management system may be also induced initial imperfection of pipelines along with out of straightness (F. Van den Abeele (2015)). Therefore, different type of installation such as snake lay has introduced.

Hobbs (1981) analyzed upheaval and lateral behaviors of submarine pipelines based on pipeline behaviors in railroad track. The work proposes four classic pipeline global buckling modes with analytical solutions. However, it was assumed that the pipeline is ideally straight and perfectly elastic pipe with a relatively small slope. Taylor and Gan (1986) revealed the impact that initial imperfections affects global buckling by an analytical approach. However, the pipelines are also idealized and perfectly straight. Afterward, numerous researchers, such as Kyriakides and Shaw (1982), and Croll (1997), studied about effect of initial imperfections with responses and stability of pipelines. By Kyriakides and Shaw (1982), interaction tendencies among initial curvatures, maximum moment, and elasto-plastic material property under combined bending and external pressure are invested. Croll (1997) suggested closed form solutions for upheaval thermal buckling system with initial imperfections in order to prevent damage by upheaval buckling. However, their studies are conducted with assumptions that pipelines are laying on flat soil and nonlinear pipe-soil resistance is not considered.

Since the 20th century, era of finite element analysis has begun. Finite element method finds approximate solutions of complex solid mechanics problems. It has widely used instead of solving strong form formulas and conducting costly experiments. Some pioneer softwares for pipeline analysis, which are PIPLIN-III (Structural Software Development, 1981), PlusOne (Andrew Palmer and Associates, 1995), PIPSOL (Nixon, 1994) and ABP (Zhou and Murray, 1994), have been tested in the last twenty years, and become the first generation in a history of pipeline analysis programs (R. A. Einsfeld (2003)). Those softwares aim for only simple calculations in idealized situations. It denotes that cross-sectional deformation, including ovalization and local buckling cannot be simulated. To overcome the shortcomings, another types of software has introduced for pipelines such as ABAQUS and ANSYS. The tools guarantee detailed modelings and accurate results for both global and local levels. However, a main drawback of those programs are extremely time-consuming for actual size of underwater structures. It has allowed to develop specialized pipeline analysis softwares. The second generation aims for faster calculations and realistic models including structure-soil interaction and berm formation. PLAXIS by PLAXIS bv, BIFURC by Norwegian Geotechnical Institute(NGI), and SIMLA by MARINTEK are examples. Especially software SIMLA includes berm formation while others use a simple beam-spring theory for soil models.

FEM program works for both 2D and 3D models. Between 2D and 3D modeling, despite an advantage of 2D modeling, which is fast calculation, 3D design is preferred because 2D model does not have enough degree of freedom for lateral direction (Hassan Karampour (2013)). In addition, Per R. Nystrom (1997) found that the 3D buckling outcomes presents significantly lower stresses and strains in the buckles compared to 2D buckling results for the same seabed route and loads. It refers that 2D model gives greater conservative outcomes. Afterwards, 3D buckling analysis has actively developed with the growth of finite element method programs. A study of Per R. Nystrom (1997) is conducted for 3D buckling and cyclic effect behavior with initial imperfect and a uneven seabed profile in HT/HP condition. Even though this study includes most of aspects for buckling investigation close to reality, the study is carried with only simple sea bed friction resistance and no dent presumption on cross section of pipelines.

Thanks to rapid development of FEM tools, it became possible to reflect realistic details on models such as initial imperfection, various free spans, a uneven soil model, and pipe-soil interaction. Carlos OliveiraCardoso (2004) studied horizontal and horizontal buckles subjected to free-spans and thermal loads, and its interaction. In this study Mohr-Coulomb model is used for pipe-soil interaction interpretation, and results from FEM simulation is compared with real data from Campos Basin-Brazil. However, even though berm formation is observed from the sea, the 3D model in this report does not include advanced soil model than Mohr-Coulomb model. Another lateral and upheaval buckling study of subsea pipelines is investigated by Hassan Karampour (2013). The work formulates effect of half-wave length local imperfection for lateral and upheaval by different effective weight, initially stressed, contact condition with seabed, and Coulomb friction. However, the model uses simple Coulomb friction model and generally even foundation which does not reflect real seabed conditions. Zhaohui Hong (2015) found a relationship between global lateral buckling and governing parameters in global buckling. The parameters are pipeline properties,which are pipe thinkness t and diameter D, single soil resistance coefficient in Mohr–Coulomb model, and imperfection properties. However, simple assumption such as Mohr–Coulomb soil model and flat seabed without free spans are weak to predict actual pipeline displacement.

As shown above most of researches about global buckling analysis with pipe-soil interactions are conducted on deterministic and simple linear soil properties despite complexity of soil model. The linear soil response model can be used successfully for some flow-line design calculations and can be employed in conceptual evaluation of lateral buckling. However, the linear ground model is not accurate to simulate actual seabed conditions. Because soil strength has the most largest uncertainty and constant soil stiffness cannot be a realistic assumption (J. Michael Duncan (2014)). In addition, the lateral-buckling solution is extremely sensitive to pipe-soil interaction. It denote that a simple coefficient of friction is not appropriate in detailed numerical modeling for lateral-buckling design. There have been difficulties in characterizing behaviors of seabed soils by a lack of detailed description of the soil mechanics.

The early concept of soil modeling was based on assuming that the pipelines does not allow

big displacements from the original position except extreme storms. Bjerrum (1973) aroused the importance of soil properties by presenting studies for local soil contact in North Sea. It is found out that the soil properties including imperfection of underwater structure are governing features on structure's behaviors. It implies that selecting a precise soil model is strongly critical to predict structure failures. Kenneth J. Nyman (1982) suggested a modeling scheme as springs for the soil restraints in four dominant directions, which are vertical-uplift, horizontal lateral, vertical-bearing, and longitudinal-axial. The model describes the development of soil force surrounding pipelines by a function of displacement.

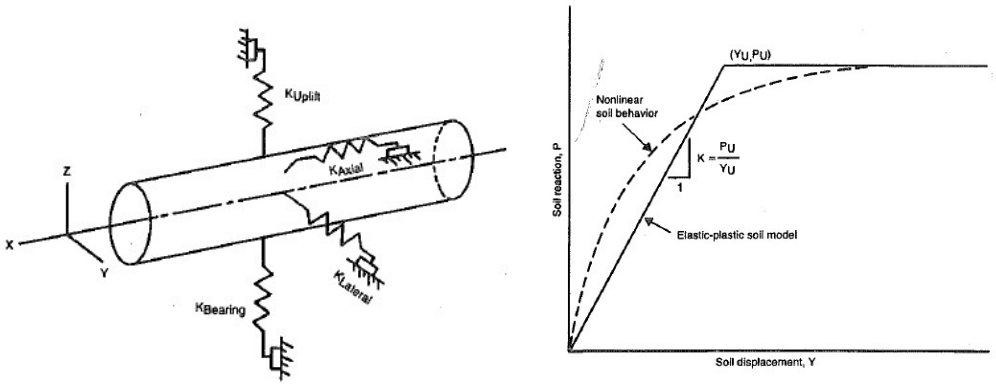


Figure 3.1: Bilinear Representation of Soil Response (Nyman (1982))

However, David A. Wagner (1989) suggested a global lateral buckling response equation containing cyclic movements. It is found that a simple friction model is not enough to describe lateral displacement caused by cyclic loading, which leaves the possibility for next advanced models.

Along with development of soil response models, other aspects of soil-pipe interaction including parametric study also have researched. David A. Wagner (1989) discovered that for general offshore soil clay content is not highly sensitive. It implies that the tests on clay show that a pipe on soft clay has greater resistance to lateral motion than the same pipe on stiff clay. Thus, stiff clay can be considered as soft clay, which is a conservative design approach for pipelines. In recent pipeline design, lateral pipeline displacement is allowed. It is because if sufficient lateral buckles are not formed, the pipelines will be overloaded. However, this must not lead pipe overstraining. This indicates that sufficient displacement potential is required for number of

buckles (D. Bruton (2006)). Paulo Teixeira (2011) studied global buckling responses from the soil-pipe interaction by finite element analysis program. Various case studies are conducted in order to figure out influence of inherent parameters in operations. Internal Pressure, friction coefficient, temperature increment, curvatures of pipelines, internal pressure, and model length are included. Most of parameters shows dependence toward critical stresses and global buckling response. However, the work is conducted with a simple soil model which does not cover berm formation effect. M. Masood Haq (2013) presented comparisons of effective axial forces found by different lateral buckling models such as Hobbs (1984),Lindholm (2007), and Abauqs FE solution. The paper also shows parameter studies of several governing factors in lateral buckles like wall thickness (D/t) ratio, pipe out of straightness (OOS). However, horizontal rigid surface and a simple friction model are adopted for the axial and lateral pipe. Run Liu (2014) attributed to induce the global lateral buckling equation with a term of buckling amplitude by the energy method. In the paper, case studies are also conducted to verify the equation by numerical simulations. In addition, the factors determining the lateral buckles are researched. However, Mohr-Coulomb model and flat sea surface condition are adopted, which gives less accurate resultants compared by ones with uneven seabed profile and non linear soil-pipe interaction models.

Non-linear soil models for cohesive soil (clay) are essential variables in order to analyze global buckling of pipelines laid on the uneven seabed. On the other hand, as can be seen above a simple linear model is selected often for buckling study due to its complexity. There are numerous researches to establish soil-pipe interaction models that are close to the reality. It is found that the soil resistance force consists of two parts, a pure friction part and a passive resistance part which depends on penetration model of pipe (DNV (2010)). Under most conditions on clay, passive resistance is more important (Olav Aamlid (2010)). As a passive resistance model several researchers suggested soil models including soil berm formation by cycles and its loads. Carlos Oliveira Cardoso (2006) presented a pipe-soil interaction model with soil berms formed by cyclic displacements and loads. The new interaction model is designed mainly focusing on equivalent lateral friction. In 10 cycles, cyclic soil behaviors with berms and operating loads are observed. Hong (2014) proposed a updated kinematic hardening model for sub-marine stiff clay under cyclic loading conditions.

Beside of several researches mainly only four models are utilized frequently for industry and academic purposes; Mohr-Coulomb, PONDUS, DNV, SAFEBUCK model.

## 3.1 Mohr-Coulomb model

Mohr-Coulomb model is a simple approximation of complexed grounds model with known uniform friction coefficient which is called Coulomb's law of sliding friction. Experiments of sliding friction in the 15th to 18th century show that frictional force is independent of contact area and velocity magnitude, and friction coefficient depends on pairs of materials (Mason (2012)). Inherent limitations of Mohr-Coulomb model is that nonlinearity is not included such as large displacement effect. Moreover, effects of cyclic loads are also ignored, which indicates Mohr-Coulomb model is a unrealistic model. Despite these disadvantages Mohr-Coulomb model has widely been used in both industries and studies of under marine pipeline buckling until now. In addition a typical soil resistance model can be illustrated as two parts which are a pure Coulomb friction part and a passive resistance due to the build-up of soil penetration as the pipe moves laterally (DNV (2010)). Consequently Coulomb friction is also referred often.

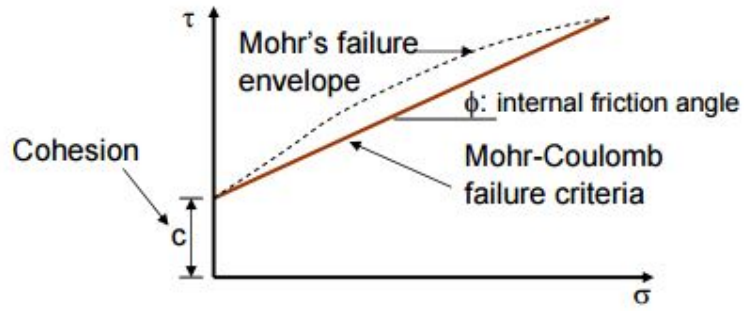


Figure 3.2: Mohr-Coulomb's friction force against loading (Pervizpour)

## 3.2 PONDUS

Verley. R (1995) presented a non-linear pressure-penetration formula for soil-pipelines interaction placed on clay soils. It is modeled based on flat seabed condition and deterministic shear strength of soil without cyclic load effects. Passive resistance on clay is affected by actual pipe penetration. Total penetration is sum of two types of penetrations. Initial penetration is caused by self-weight, piping, penetration during installation while the other penetration is due to pipe movement under waves and current loads DNV (2010). Relationship between total seabed penetration and ground pressure is found by Verley. R (1995) which is shown in Figure 6.

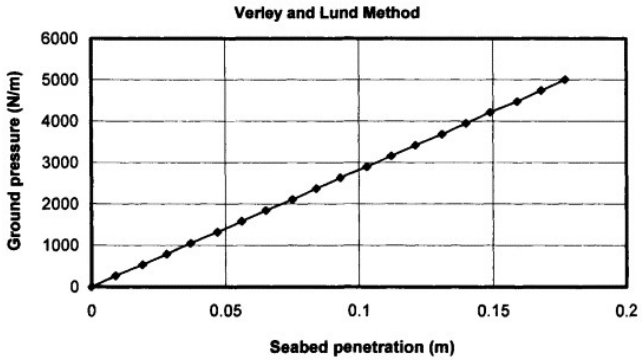


Figure 3.3: Penetration curve of soil model against pressure (Yong Bai (2005))

Subsequently the Verley model also was implemented inside the PONDUS program that was developed by MARINTEK. Figure 7 illustrates the implemented Verley model in the PONDUS program. Figure 7 shows that soil force Fs is related with elastic and plastic lateral displacement ve and vp respectively. Furthermore, the soil resistance Fs in the plastic range is defined as summation of elastic and plastic soil force (SINTEF).

The dynamic lateral response of pipelines under wave and current loads is computed by PONDUS. FEM program PONDUS solves equations of motion of the pipeline using small deflection theory in the time domain. PONDUS deals with time dependent interaction of pipeline and soil with non-linear material behavior model and partial burial model (SINTEF). It denotes that PONDUS is proper to analyses tension effects, pressure effects, temperature effects, and elasto-plastic soil model. However, PONDUS can build only straight pipeline model on hori-

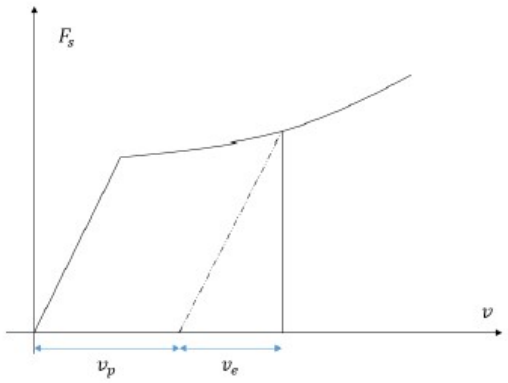


Figure 3.4: Soil resistance-displacement curve by PONDUS (Irman (2015))

zontal sea-bottom using two degrees of freedom, which denotes lateral deflection and axial soil force along the pipe are not considered. The model also uses small deflection theory which allows only small rotations for the beam elements.

## 3.3 DNV model

The HotPipe Joint Industry Project (HOTPIPE JIP) has started to prepare a DNV Recommended Practice for structural design of HT/HP pipelines as one project of DNV New Offshore Class in 1998 (Collberg (1999)). The HOPPIPE JIP in 2005 proposed various type of soil analysis models and conducted uncertainty sensibility study by different soil models for for both uplift and downward resistance (Stig Goplen (2005)).

DNV recommended practice F-109 published in 2010 reveals an updated typical model for passive soil resistance consists of four distinct regions in Figure 9. In the elastic region, the model introduces constant penetration which is equal to the initial penetration. A region where lateral displacement is between 0.02 and 0.5 percent of the pipe diameter causes an increment of the penetration, and then the pipeline response consequently enhances passive resistance and penetration. In the region $Y_2 \leq Y \leq Y_3$, accumulated work becomes zero, and penetration and passive resistance also become reduced. When the pipeline displacement surpasses the pipe diameter, the following passive resistance and penetration remain constant (DNV (2010)).

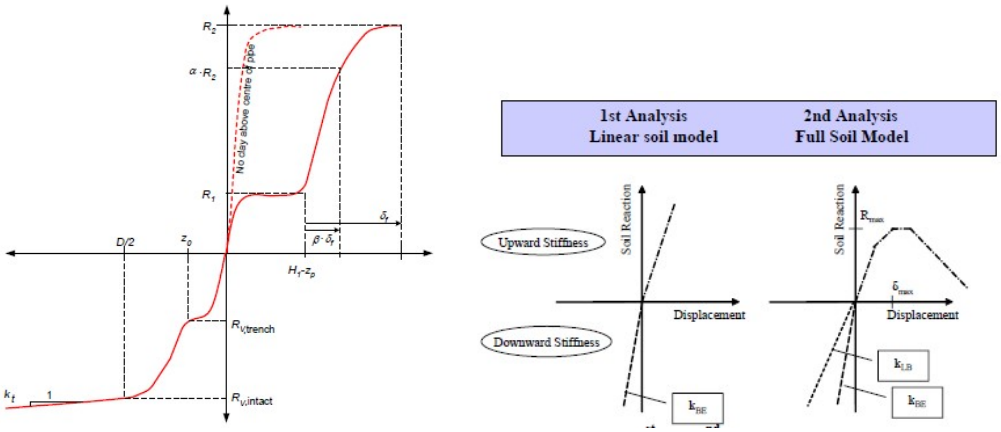


Figure 3.5: A full non-linear mobilication of both upward and downward soil resistance and its simplification (Stig Goplen (2005))

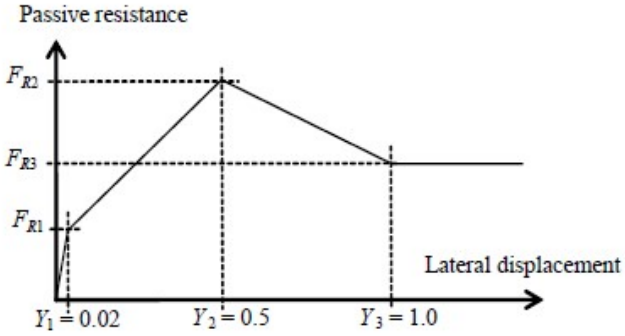


Figure 3.6: Passive resistance by DNV model (DNV (2010))

## 3.4 SAFEBUCK

The SAFEBUCK JIP (joint industry project) has begun in the early of 2000s. The objective of the SAFEBUCK JIP is to improve confidence and safety at the design approach for lateral-buckling (D. Bruton (2006)). D. Bruton (2006) proved this by various experimental results.

The key parameter for successful soil model behavior by cyclic loads is to seizure the reaction force from the static berm. After the first cycle have formed the static berms, the berms provides a significant reaction toward further horizontal displacement. Figure 10 illustrates a typical force-displacement of lateral friction response. It also proves that the cyclic response

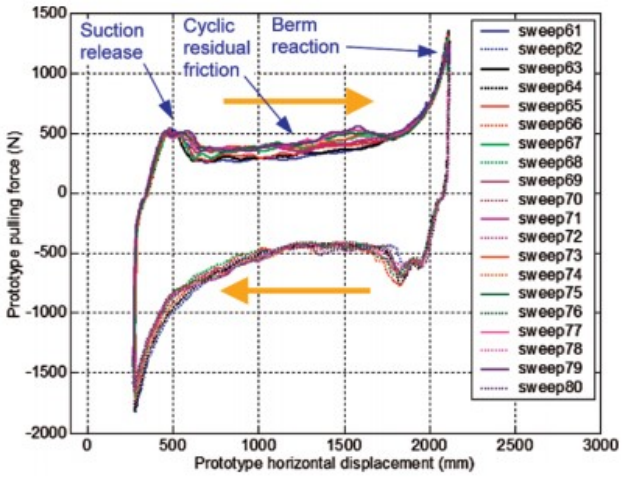


Figure 3.7: A typical cyclic lateral-force-displacement response (D. Bruton (2006))

remains almost constant despite a large number of cycle with static soil berms cyclic (D. Bruton (2006)). The results conducted by D. Bruton (2006) develop suitable equations of lateral buckling subjected to cyclic loads including embedment of pipeline, breakout phenomenon during buckling, and large displacement in the construction of soil berms.

## 3.5 Soil models with uncertainty

Meanwhile probabilistic analysis for soil-pipe interaction becomes spotlighted year by year. There are reasonable grounds. The lateral soil resistance is primarily a function of the pipe characteristics including the soil strength profile and pipe embedment. Especially soil strength is a major source of uncertainty such as the in-situ shear strength (D. Bruton (2006)). It denotes that design of pipeline involves both deterministic and probabilistic aspects (D.J. White (2014)).

First, J. D. Murff (1989) divided range of penetration of pipelines in cohesive soil into upper and lower bound assuming upper and lower bound cause minimax and minimum result and values in between the bounds do not show sudden reaction response. The paper shows that the outcome from the bounds are reasonably close to data by experiments. D. Bruton (2006) also adopted an idea that lower bound approach guarantees conservative result for lateral soil resis-

tance and lateral buckling.

Afterwards, some attempts have been made to adopt stochastic method such as the Monte Carlo simulation for predicting buckling capacity including uncertainty in soil resistance. The required information that non-linear finite element analysis needs for calculation is not obtainable at the design stage. Pipe-soil interaction is significantly uncertain. To use FEM, therefore, it becomes necessary to predict unspecified information. The uncertainty in design is normally accounted for by introducing safety factors. However, high level of uncertainty for soil strength and inter-dependent relationships between global response and parameters ask additional needs of specialized randomness treatments. Particularly shear strength of soil is sensitively varied by cyclic loads or seismically actives (Qinglai Fan (2007), Smith and Kaynia (2015))

In 2007, SAFEBUCK started to include inherent uncertainty of pipe-soil interaction. The research studied by D. Bruton (2006) describes uncertainty diminution methods; improve penetration testing technique, new laboratory testing technique, measurement technique of pipe-soil resistance, and lateral resistance. SAFEBUCK JIP has been constantly improving engineering models and testing methods of pipe-soil interaction with challenges dealing with out of straightness and uncertainty of soil by releasing another program BUCKFAST (D.A.S. Bruton (2011)).

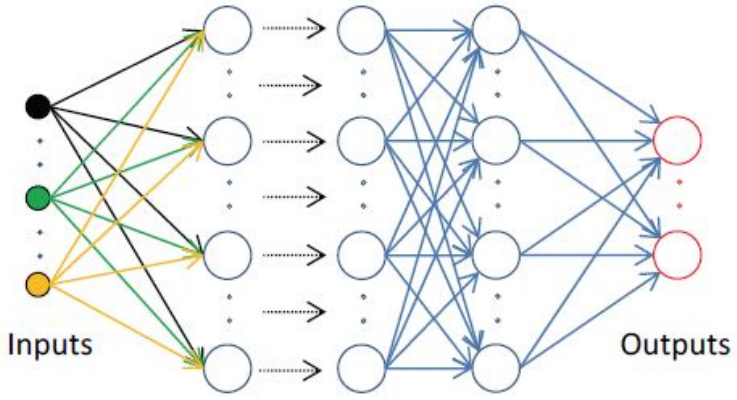


Figure 3.8: Diagram for artificial neural network method (Carlos Sicilia (2014) )

Carlos Sicilia (2014) assessed lateral buckling response of pipelines by artificial neural networks(ANN) and Monte Carlo method. Input variables are generated by Monte Carlo simulation and ANN method predicts lateral buckling response which is can be seen in Figure. These probabilistic assessments combined with FE models show acceptable resultant which can reduce costs with the required levels of safety. McCarron (2015) investigated random nature of parameters which affects buckle capacity. Mainly flowline embedment and out-of-straightness are considered as random parameters, which denotes that magnitude of the parameters is generated by Monte Carlo simulation. The outcomes present an agreement that buckle capacity distributions are influenced by distributions of the parameters in a certain degree. However, in this paper other geology properties are over-simplified.

To sum up, global buckling under high pressure and temperature have studied for decades. Various soil friction models have introduced and typical four models are widely used nowadays. In order to compute soil-pipe interaction study with probabilistic assessments combined with finite element method have recently researched based on an idea that full nonlinear behavior of global buckling response has a limitation that it cannot predict exact movements by deterministic data. Over adapting safety factor, therefore, more fundamental treatments have asked. Due to big uncertainty at soil properties such as shear strength Monte Carlo simulation have applied. In this paper DNV model containing berm formation effects and Mohr-Coulomb are compared as soil models. Because of simplicity Mohr-Coulomb model becomes an industry standard while DNV model and PONDUS model stand for hydrostatic stability checking purpose. DNV model added with berm formation effect is appropriate to illustrate soil stress and strain curve. Moreover, probabilistic assessments are implemented by Monte Carlo simulation.

# Chapter 4

# Model description

The parameters of soil and pipeline properties for global buckling are simplified herein. Both general simplified assumptions and assumptions made for finite element model are considered. General assumptions come from realistic data based on previous projects. The assumptions also include simplifications on a way to target at global buckles. Finite element model assumptions are made by design convenience.

## 4.1 General Simplified Model

### 4.1.1 Pipeline

With consideration of expense and safety standard X65 standard steal is chosen having yield stress 450 Mpa. During the operation diameter of the pipeline remains constant under high pressure and temperature. It is because that since design purpose analysis is examined in this report loading conditions do not exceed capacity of pipelines.

| Parameter | Value | Parameter | Value |
|---|---|---|---|
| Radius | 0.1365 m | Wall thickness | 0.0190 m |
| Radial drag coefficient | 1.0 | Tangential drag coefficient | 0.1 |
| Radial added mass coefficient | 2.0 | Tangential added mass coefficient | 0.2 |
| Dry mass | 191.5 kg/m | Submerged mass | 39.47 kg/m |
| External wrapping outer diameter | 0.4346 m | External wrapping fraction | 0.5 |
| X65 standard yield stress | 450 Mpa | | |

Table 4.1: Parameters adopted in the analyses

### 4.1.2 Rock berms

It is assumed that the pipelines are laying on the irregular foundation with several rock berms. Rock berms is artificially built by filing small stones on the pipeline as can be seen in Figure 4.1. As a practical view of projects building rock berms is a necessary process to support the free-spans for pipeline stabilization, prevent serious fatigue issue and have cost effectiveness. To control global buckling in each sections rock berms are spread evenly like Figure 4.2. In this thesis, rock berms are idealized containing great resistance but not fully fixed. The stiffnesses are shown in Figure 4.3. This assumption neglects interactions between rock berms and pipelines.

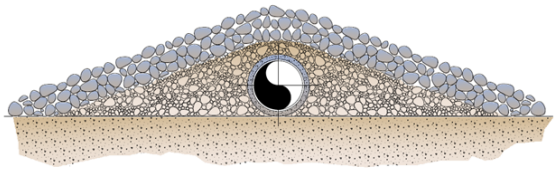

Figure 4.1: Rock berm to control global buckling (Pty (2014))

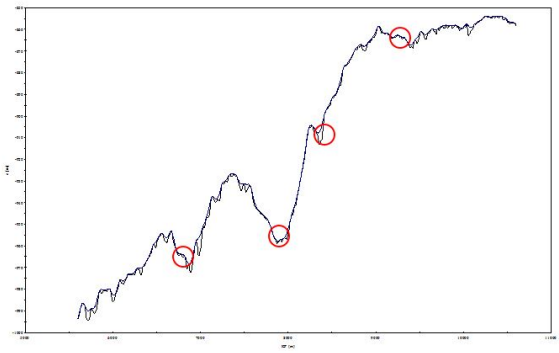

Figure 4.2: Rock berm to control global buckling

### 4.1.3 Uncertainty of soil-model

Underwater soft clay characteristics such as shear strength are major sources of uncertainty in a design, and the geology inputs influence on response of pipelines (D.J. White (2014)). Typical data in North Sea condition is that shear strength follows normal distribution with average shear

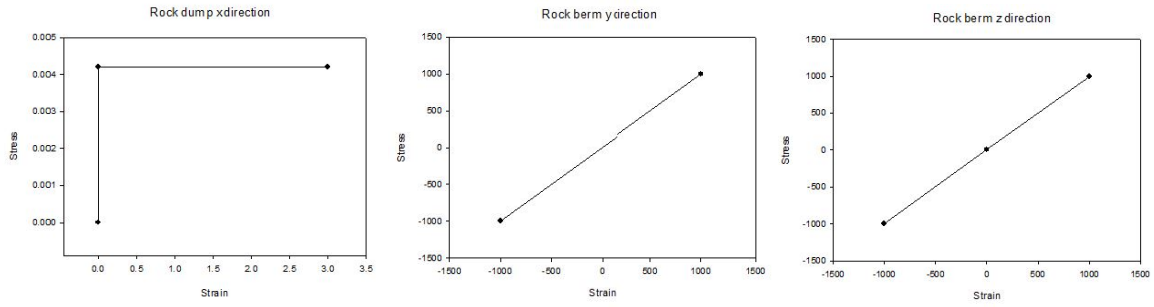


Figure 4.3: Rock berm resistance details in x,y,and z direction

strength 2KPa and standard deviation 0.2. The distribution is shown in Figure 4.4. Thus, shear strength can be generated by Monte-Carlo method based on the normal distribution.

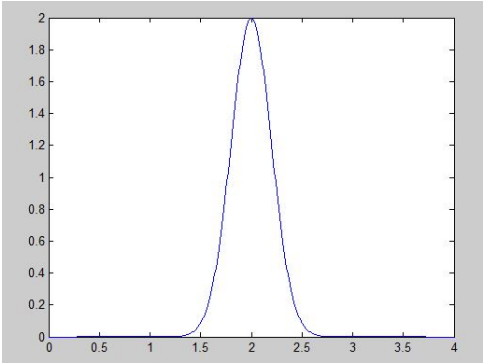

Figure 4.4: Normal distribution with mean 2Kpa and 0.2 standard deviation

Lateral dynamic stiffness and vertical dynamic stiffness of soil are found in DNV (2006).

$$K_L = 0.76G(1+\nu)$$

$$K_v = \frac{0.88G}{1-\nu}$$

Where

R = Radius of foundation in contact with soil.

G = Initial shear modulus of soil for infinitesimal strains. $G_{max} = \frac{300S_u}{Ip}$ (DNV (2006))

Ip = Plasticity index. Plasticity index in Ormen Lange, Ip = 30 (Kåre Senneset (2005))

$\nu$ = Poisson's ratio. 0.45 (Mckenzie and Pender (1996))

D = Embedment of the maximum diameter section. Embedment should be smaller than the height of berms (DNV (1992)).

| Parameter | Value |
|---|---|
| Radius | 0.1365 m |
| Ip | 30 |
| $G_{max}$ | 10 $S_u$ |
| $\nu$ | 0.45 |
| D | R = 0.1365 m |

Table 4.2: Inputs for soil in Ormen Lange with randomness

By following the equations it is found that $G_{max}$ is dependent on uncertain shear strength generated by Monte Carlo, and it affects back lateral and vertical dynamic stiffness. Found lateral stiffnesses are applied to elastic soil stiffness part in the costumed soil model. Averaged vertical stiffness is adopted in z-direction stiffness of the costumed soil.

| Stiffness | Value |
|---|---|
| $K_L$ Range | 7.11 - 39.68 KN/m |
| $K_v$ | 32.62 KN/m |

Table 4.3: Lateral and vertical dynamic stiffness

### 4.1.4 Soil friction model

Soil friction is a basis for the reaction force of pipeline laying on the soil. It is crucial to build a robust model that can describe highly non-linear behavior of soil under cyclic loading. Typical soil friction models are Mohr-Coulomb, PONDUS, DNV, SAFEBUCK models. Among those Mohr-Coulomb model is widely used as a industry standard due to its simplicity. DNV model and PONDUS model are adopted for hydrostatic tests purpose. DNV model and PONDUS model shows similar response tendency. For the sake of limiting amount of work DNV model is examined. In this report, global buckling responses of Coulomb model and DNV model combined with soil berm formation from SAFEBUCK when cyclic loads are applied, are reported.

Mathematic model of Mohr-Coulomb is written as following.

$$\tau_f = C + \sigma tan\phi$$

Here, $\tau_f$ shear strength of soil.

C = adhesion coefficient.

$\sigma$ = total stress.

$\phi$ = angle between soil and foundation material curve.

The mathematic model is valid for sand and consolidated/unconsolidated clay. However, in Orman Lange clay is over-consolidated and undrained (Petter Bryn (2005)). In industry Coulomb friction coefficient depends on empirical data. This paper employs a friction coefficient from contact element force examined by DNV soil model. The average value is selected ranged over time.

$$\frac{SoilcontactYforce}{SoilcontactZforce} = \mu$$

Where $\mu$ = friction coefficient.

The chosen friction is multiplied by force on the pipeline to get reaction force back. In SIMLA the force-displacement curve of the friction coefficient is illustrated as a bilinear curve with three points as can be seen in Figure 4.5.

DNV soil model with soil berms is subdivided into a curve before berm formation and a curve after berm formation. Before development, DNV soil model follows typical resistance-lateral displacement curve. After berm development by cyclic loads, the model tracks cyclic force-displacement curve suggested by the SAFEBUCK project. DNV model implemented into SIMLA requires various parameters.

| Parameter | Value | Parameter | Value |
|---|---|---|---|
| Elastic soil stiffness | 7.11 - 39.68 KN/m | Dry soil specified weight | 1.80E+04 $kg/m^3$ |
| Undrained shear strength | Generated by Monte Carlo | Soil strength gradient | Shear strength * 0.2 |

Table 4.4: Parameters in DNV soil model

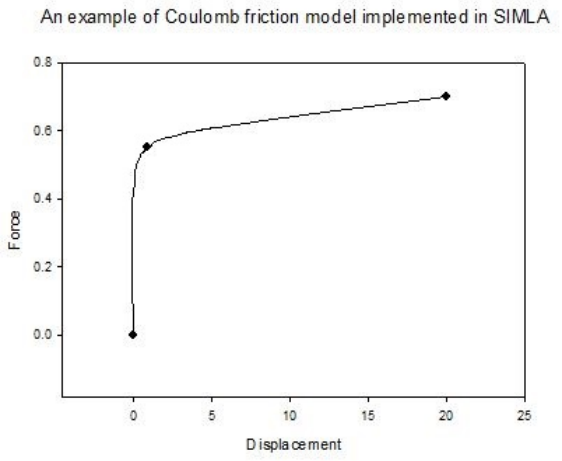


Figure 4.5: An example of force-displacement curve with a Coulomb friction factor

Where elastic soil stiffness is found in lateral dynamic stiffness by DNV class written in chapter 4.1.3. Dry soil specified weight is typical data in North Sea. Undrained shear strength is generated by Monte Carlo simulation with mean value 2Kpa and standard deviation 0.2. Soil strength gradient is gained from the products of shear strength and ordinary value 0.2 for very soft clay.

### 4.1.5 Operation

In the simulations of global buckling analysis conducted in this thesis, operation procedures are also clarified. Operation simulation should start from pipeline laying out process in order to include initial placement and pretension of the pipeline into the analysis. 5km long pipeline is installed on uneven foundation. The pipeline experiences a hydrostatic test and cyclic production events. Operation time schedule is displayed below.

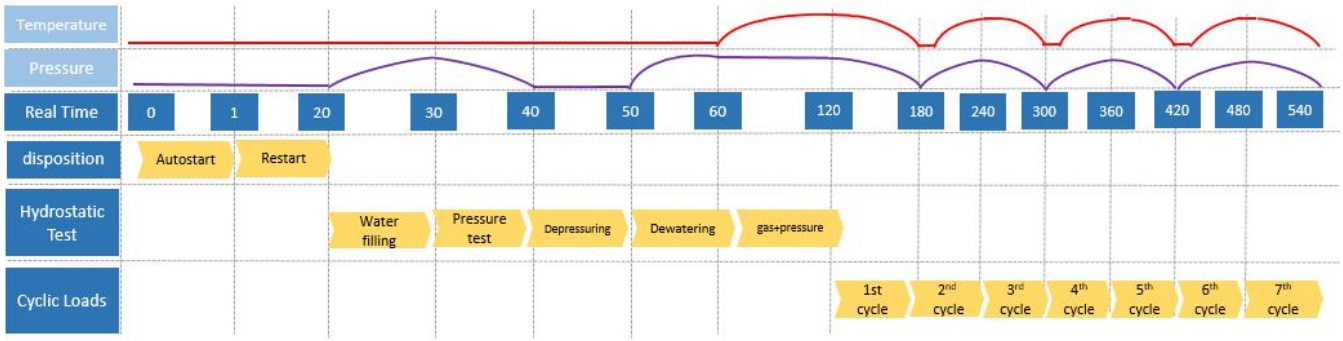


Figure 4.6: Simulated operation time schedule in SIMLA

| Time | Number of maximum and minimum points |
|---|---|
| 120 | First maximum |
| 180 | First minimum |
| 240 | Second maximum |
| 300 | Second minimum |
| 360 | Third maximum |
| 420 | Third minimum |
| 480 | Fourth maximum |
| 540 | Fourth minimum |

Table 4.5: Time and cycles

### 4.1.6 Load history

The load model includes a hydro-pressure test behind the pipelines installation procedure. During cyclic loading, pressure loads decrease and increase faster than temperature because of the natural characteristic that thermal conduction works slowly.

Aspects that can affect the loading condition like dry mass, buoyancy, external pressure, and tension, are also considered in SIMLA. However, since the loads act constantly afterwards hydrostatic test it does not affect significantly the global buckling.

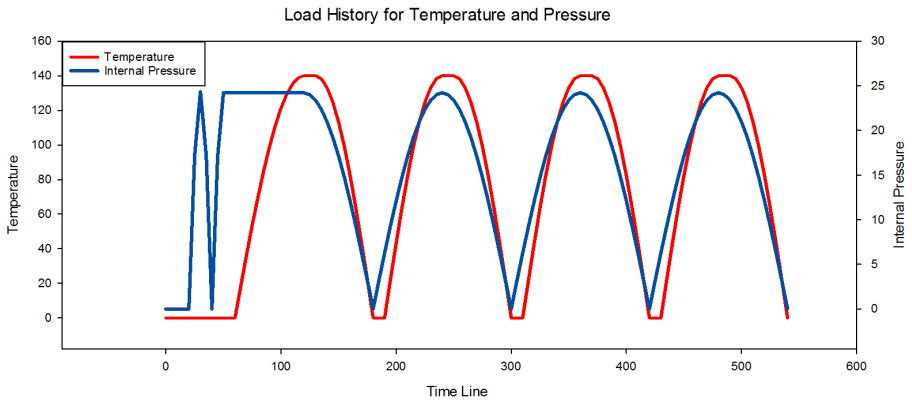


Figure 4.7: A load history plot for temperature and internal pressure

## 4.2 Finite element model

### 4.2.1 Contact elements

In the finite element program, pipeline element is defined as PIPE33 which describes 3D beam constant axial strain and torsion. This 3D 2-noded beam element consists of thin walled tubular cross-sections with constant radius and thickness along each element. Seabed and rock berms elements employ 1-noded element. For sea floor elements, material curves in the x, y and z directions are introduced with torsion while rock berms allows the user to specify linear springs properties.

### 4.2.2 Geographic model

Figure 4.8 shows implemented pipeline in SIMLA with small and big spans.

The coordination of the route is described by kilometer point (KP). The pipeline is stretched out from KP 5600 to KP 10600. Since the pipeline is 5km long 1m corresponds with 1KP.

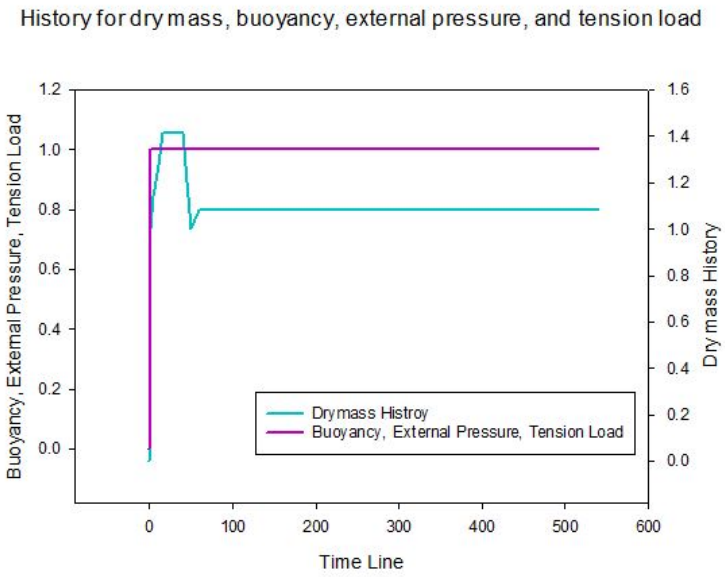


Figure 4.8: A load history plot for dry mass, buoyancy,external pressure, and tension

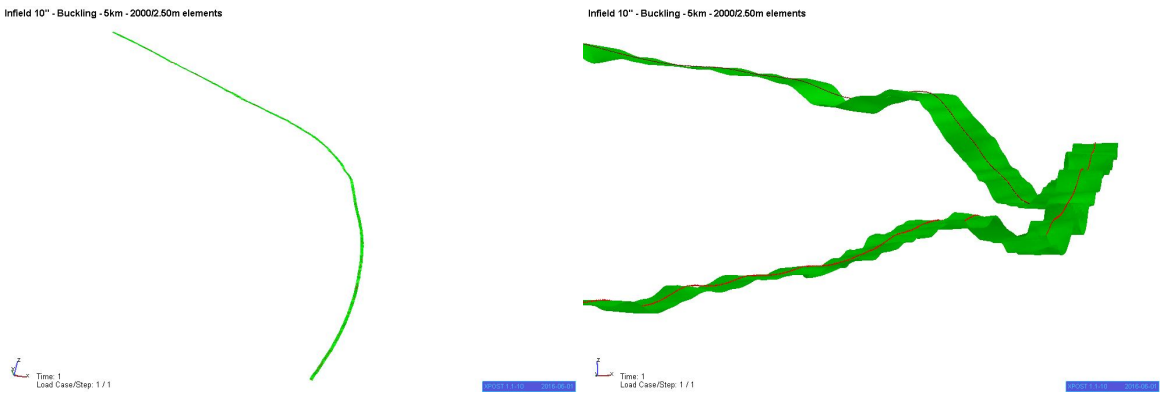


Figure 4.9: The implemented pipeline model in SIMLA

# Chapter 5

# Case study

## 5.1 Impact of shear strength intervals

In this section parametric studies of shear strength '$S_u$' have conducted. In order to find the influence of shear strength on global buckling, the route is subdivided into several numbers from 1 to 300 as can be seen in Figure 5.1.

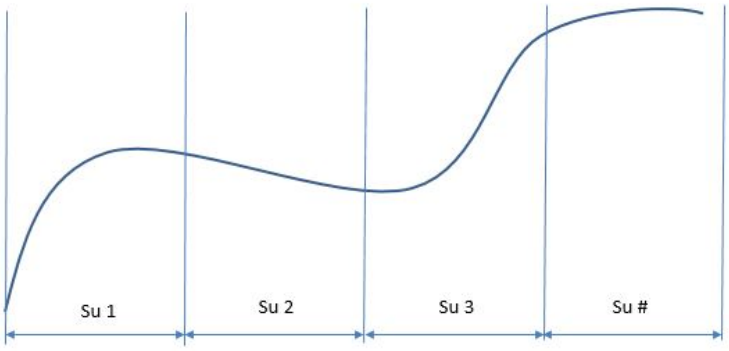


Figure 5.1: A pipeline divided by number of shear strength intervals

This studies are carried out based on an idea that soil strength may be changed over the time due to installation, water-filling and hydrostatic test, and operation events because the events can remodel and reconsolidate the foundation (D.J. White (2014)). Therefore, applying same $S_u$ along the whole structure for the entire operation events, does not reflect the reality enough, and is also unreasonable.

Finite element method program SIMLA has computed numerous analyses with different number of intervals on the irregular seabed. The total bending moment, which is given by $\sqrt{M_Z^2 + M_Y^2}$, is the resultant from the analyses by SIMLA. Particularly Z-moment governs lateral displacement of the pipeline, which influences on strength of stiffness of the berms.

First, impact of shear strength value on total bending moment distribution is researched. In Appendix A.2, it is observed that overall bending moment distribution plots exhibit superficial resemblance between the plots regardless of magnitude of shear strength. Table 5.1 displays kilometer points (KP) where maximum and minimum total bending moments appear. The table reveals that as cycles goes by, maximum total bending moments appear only at KP 6944 while minimum total bending moments develop invariably at KP 8234. KP 6944 and KP 8234 are located on shoulder of the deepest free-spans disregarding of existence of rock berms in Figure 5.2. When accumulated force becomes strong enough to generate an extra maximum bending moment point at high cycle, near shoulder of next deepest free-spans such as KP 10060 the maximum occurs. Moreover as can be seen in Appendix A.1, distribution graphs of shear strength and total bending moment are not correlated. For instance, high numerical value of shear strength does not guarantee big total bending moment according to Appendix A.1. To sum up, it is interpreted as maximum and minimum bending moments are dependent on geology parameters such as depth of free spans and slope of seabed, rather than magnitude of shear strength.

| Number of intervals | KP with max total moment | KP with min total moment |
|---|---|---|
| 1 | 6944,6947 | 8234 |
| 5 | 6944,10063 | 8234 |
| 10 | 6944,6946,10060 | 8234 |
| 20 | 6944,10063 | 8234 |
| 40 | 6944 | 8234 |
| 60 | 6944,10063 | 8234 |
| 80 | 6947 | 8234 |
| 100 | 6944 | 8234 |
| 200 | 6944 | 8234 |
| 300 | 6944 | 8234 |

Table 5.1: KPs where show maximum and minimum total bending moment

Z-moment distribution graphs from Appendix A.4 also present relatively similar moment

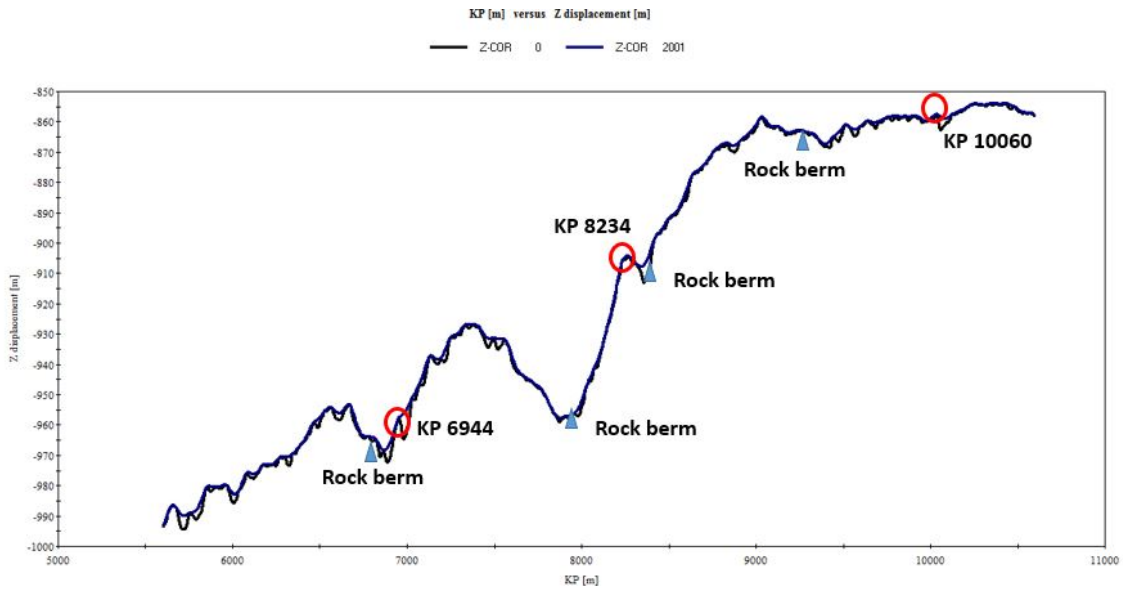


Figure 5.2: A pipeline divided by number of shear strength intervals

distribution tendency regardless of number of intervals and cycles. It means that Z-moment does not affected by shear strength intervals too. However, small changes in Z-moment between KP 7000 and 8000, are captured irregularly in the distribution plots.

In this sensibility test of shear strength intervals, it is possible to check convergence of total bending moment by different number of intervals. Numerical values by each cycles at KP 6944 and KP 8234, which are points for maximum and minimum of total bending moment distribution, are plotted in Figure 5.3. It demonstrates that at high cycle total moment converges at near 200 intervals. Choosing number of shear strength interval is strongly related with analyzing time and costs. In order to select the most effective intervals, buckling length needs to be checked first. Buckling length is defined as a distance between points having zero bending moment including single envelope inward. Depending on a type of models or assumptions, moment distribution and buckling length vary. Employing buckling length as the length of shear strength intervals is a reasonable choice for cost efficiency. An analysis with big interval length makes small number of intervals. Therefore when small number of interval is applied one should be aware of the possibility that the result could be overestimated or underestimated because of the convergence trends.

It is also found that big shear strength with large number of intervals than average, con-

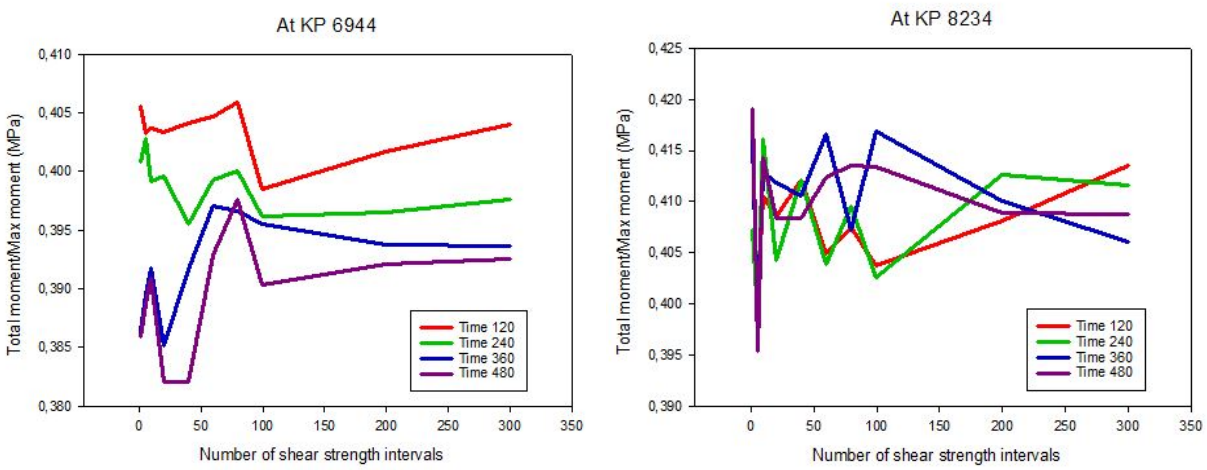


Figure 5.3: A pipeline divided by different number of shear strength intervals

tributes to develop extra moment maximum point. It proves that in reality pipelines do not have extra maximum points by shear strength. It is because actual pipeline is considered as sum of infinitesimal elements, which implies that interval length of the pipeline is very small. KP 10063 is a point where shows extra maximum bending moment value when some special condition is met. Figure 5.4 displays the convergence tendency at KP 10063. Contrary to KP 6944 and KP 8234, KP 10063 does not show convergence and requires more cycles to be stabilized, which implies that only KPs offering constant maximum or minimum can be utilized for pipeline design. Since maximum and minimum values bring the most severe results, it is reasonable in the pipeline design for global buckling.

In Table 5.2 non-absolute mean shear strength and standard deviation by different number of intervals, are tabulated. As can be shown in Figure 5.5, mean value and standard deviation vary slightly depending on number of intervals. Accordingly a relation between properties of intervals and Z-axis bending moment has handled. Table 5.3 presents averaged and non-absolute mean and standard deviation values from Z-moment by different number of intervals in order to find relevance with shear strength data. Table 5.4 exhibits comparisons between standard deviation of shear strength and Y, Z, and total-moment which are distinctive data than mean value. Standard deviation of shear strength by number of intervals presents a constant decline while standard deviation of moments shows irregularities. Table 5.4 supports that shear strength in this model has an uncertain connection with Z-moment. Table 5.4 also proves that Z-moment

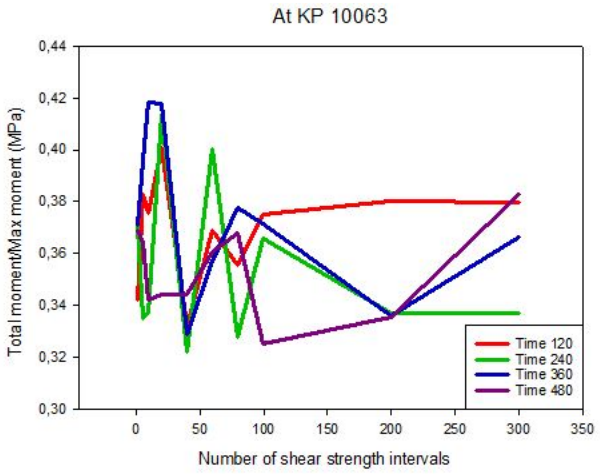


Figure 5.4: A pipeline divided by different number of shear strength intervals

and total moment have small standard deviation values.

| Figure | Mean value (MPa) | Standard deviation |
|---|---|---|
| 1 interval | 0.002240452 | - |
| 5 intervals | 0.002115707 | 0.00068062 |
| 10 intervals | 0.002279187 | 0.000740258 |
| 20 intervals | 0.002297213 | 0.000661741 |
| 40 intervals | 0.002135762 | 0.000618469 |
| 60 intervals | 0.002097695 | 0.000543436 |
| 80 interval | 0.002065644 | 0.000526346 |
| 100 intervals | 0.002055045 | 0.000519841 |
| 200 intervals | 0.002055045 | 0.000518533 |
| 300 intervals | 0.002039012 | 0.000479589 |

Table 5.2: Mean shear strength and standard deviation by number of intervals

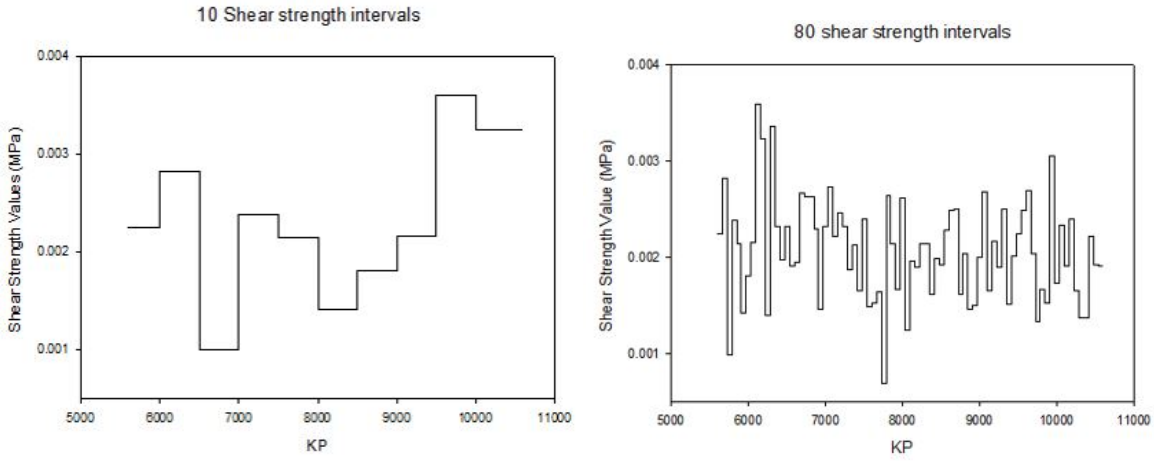


Figure 5.5: Examples of twp shear strength distribution plots

| Figure | First max | Second max | Third max | Fourth max |
|---|---|---|---|---|
| Mean value with 1 interval | 0.0011 | 0.0010 | -0.0052 | 0.0037 |
| Standard deviation 1 interval | 0.0892 | 0.0905 | 0.0763 | 0.0733 |
| Mean value with 5 interval | 0.0011 | 0.0025 | 0.0008 | 0.0014 |
| Standard deviation with 5 intervals | 0.0897 | 0.0868 | 0.0853 | 0.0867 |
| Mean value with 10 interval | -0.0071 | 0.0021 | 0.0019 | 0.0021 |
| Standard deviation with 10 intervals | 0.0710 | 0.0753 | 0.0615 | 0.0790 |
| Mean value with 20 interval | 0.0008 | 0.0022 | 0.0031 | 0.0014 |
| Standard deviation with 20 intervals | 0.0932 | 0.0907 | 0.0780 | 0.0827 |
| Mean value with 40 interval | 0.0014 | 0.0014 | 0.0013 | -0.0076 |
| Standard deviation with 40 intervals | 0.0903 | 0.0667 | 0.0886 | 0.0724 |
| Mean value with 60 interval | -0.0007 | 0.0008 | 0.0004 | 0.0020 |
| Standard deviation with 60 intervals | 0.0732 | 0.0943 | 0.0633 | 0.0912 |
| Mean value with 80 interval | 0.0011 | 0.0027 | 0.0011 | -0.0029 |
| Standard deviation with 80 intervals | 0.0904 | 0.0865 | 0.0893 | 0.0719 |
| Mean value with 100 interval | 0.0019 | 0.0010 | 0.0020 | 0.0030 |
| Standard deviation with 100 intervals | 0.0876 | 0.0865 | 0.0746 | 0.0810 |
| Mean value with 200 interval | -0.00056 | 0.0022 | 0.00184 | 0.0018 |
| Standard deviationl with 200 intervals | 0.0680 | 0.0865 | 0.0893 | 0.0890 |
| Mean value with 300 interval | 0.0016 | 0.0023 | 0.0010 | 0.0006 |
| Standard deviation with 300 intervals | 0.0877 | 0.0863 | 0.0878 | 0.0838 |

Table 5.3: Mean and standard deviation from Z axis bending moment by number of intervals and cycles

| Figure | Standard deviation of shear strength | Standard deviation of Z- moment | Standard deviation of Y- moment | Standard deviation of total moment |
|---|---|---|---|---|
| 1 interval | - | 0.0733 | 0.1129 | 0.0830 |
| 5 intervals | 0.00068062 | 0.0867 | 0.1024 | 0.0833 |
| 10 intervals | 0.000740258 | 0.0790 | 0.1110 | 0.0849 |
| 20 intervals | 0.000661741 | 0.0827 | 0.1057 | 0.0824 |
| 40 intervals | 0.000618469 | 0.0724 | 0.1055 | 0.0855 |
| 60 intervals | 0.000543436 | 0.0912 | 0.1009 | 0.0844 |
| 80 interval | 0.000526346 | 0.0719 | 0.1157 | 0.0840 |
| 100 intervals | 0.000519841 | 0.0810 | 0.1081 | 0.0839 |
| 200 intervals | 0.000518533 | 0.0890 | 0.1037 | 0.0851 |
| 300 intervals | 0.000479589 | 0.0838 | 0.1065 | 0.0834 |

Table 5.4: Mean and standard deviation from shear strength and Z, Y, total-moment at the last cycle by number of intervals

## 5.2 Uncertainty sensibility test

The most sensitive soil property is shear strength $S_u$. In this section analyses to find sensitiveness of magnitude or distribution of shear strength on global buckling behavior, are conducted. Two sets of shear strength distribution are generated by Monte Carlo simulation with 2KPa mean value and 0.2 standard deviation as can be seen in Figure 5.6. Numerous DNV models are examined with different number of intervals from 1 interval to 300. Total bending moment from different shear strength distribution, which is square root of Y-moment squared and Z-moment squared of the pipeline, is compared.

As found in Appendix B.1, distribution trends of shear strength do not significantly change tendencies of the total bending moment distribution plots. Despite some captured changes in absolute averaged magnitude of bending moment in Table 5.5, in overall small changes do not affect greatly global buckling.

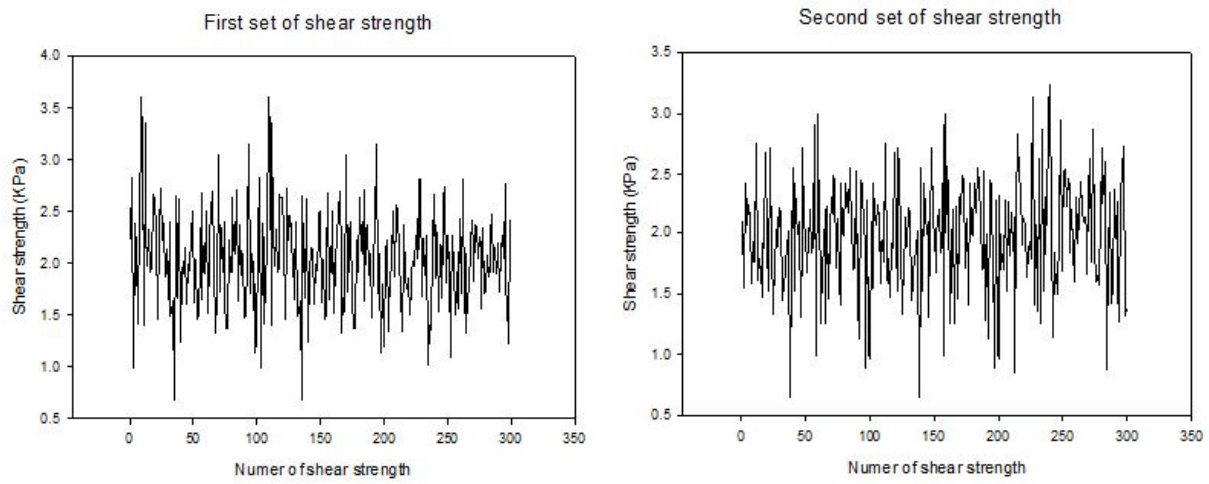


Figure 5.6: Two sets of shear strength by Monte Carlo

| Figure (MNm) | 1st max by set 1 | 1st max by set 2 | 2nd max by set 1 | 2nd max by set 2 | 3rd max by set 1 | 3rd max by set 2 | 4th max by set 1 | 4th max by set 2 |
|---|---|---|---|---|---|---|---|---|
| $M_{tot}$ with 1 interval | 0.1084 | 0.1095 | 0.1098 | 0.1084 | 0.1051 | 0.1084 | 0.1061 | - |
| $M_{tot}$ with 60 intervals | 0.1094 | 0.1088 | 0.1084 | 0.1088 | 0.1066 | 0.1085 | 0.1067 | 0.1065 |
| $M_{tot}$ with 80 intervals | 0.1089 | 0.1089 | 0.1084 | 0.1075 | 0.1085 | 0.1086 | 0.1074 | 0.1059 |
| $M_{tot}$ with 100 intervals | 0.1087 | 0.1087 | 0.1072 | 0.1074 | 0.1073 | 0.1074 | 0.1059 | 0.1066 |
| $M_{tot}$ with 200 intervals | 0.1092 | 0.1088 | 0.1074 | 0.1083 | 0.1078 | 0.1084 | 0.1070 | - |
| $M_{tot}$ with 300 intervals | 0.1082 | 0.1090 | 0.1070 | 0.1079 | 0.1081 | 0.1071 | 0.1068 | 0.1060 |

Table 5.5: Maximum bending moment values by sets and cycles

In Appendix B.2, two total bending moment graphs from two different set of shear strength distribution have matched by time. Since the analysis converges near number of intervals 200, only limited interval number near convergence points such as 60, 80, 100, 200, and 300 are studied. The graphs of two bending moments by two different shear strength distribution plots in Appendix B.2, shows reasonably proportional straight lines. The proportional straight lines stand for fairly alike outcomes, while scattered plots refer that shear strength distribution has strong influence in global buckling phenomenon. Most of plots present linear proportionality with some exceptional points, which indicates that total bending moment is influenced by shear strength in certain extend, but not strong connection with typical stochastic shear strength data in North Sea. Different mean shear strength value, however, may display dissimilar outcomes.

## 5.3 Comparison of soil response models

In this section, Coulomb models and DNV models added berms are compared. Typical Coulomb friction is between 0.2-0.5 in North Sea. From the analysis of DNV model with 100 intervals in the case study 5.1, Coulomb friction is found as 0.4 which is an average by time. To study about influence of Coulomb friction on the resultant bending moment, two additional Coulomb frictions are selected and analyzed in this paper. In Table 5.6, absolute average value of Z-bending moment, Y-bending moment, and total bending moment are tabulated by cycles. The table describes that generally the average bending moments is decreased by time for all Coulomb friction models. On the other hand some trends are seen that average absolute Z-bending moment values are slightly developed at the last cycle in friction 0.4 and 0.6. This indicates that for friction 0.4 and 0.6 bigger lateral displacement of pipeline is expected, and higher Coulomb friction causes large Z-bending moment as cycles develop. In addition, as a nature of pipe-soil interaction, Z-axis moment becomes stiffer by cycles grow. Thus, it can be seen that the Coulomb models with friction 0.4 and 0.6 stabilize faster than the model with friction factor 0.3.

| Figure (MNm) | First max | Second max | Third max | Fourth max |
|---|---|---|---|---|
| Z-moment with Coulomb friction 0.3 | 0.0511 | 0.0446 | 0.0425 | 0.0499 |
| Y-moment with Coulomb friction 0.3 | 0.0724 | 0.0717 | 0.0724 | 0.0679 |
| Total moment with Coulomb friction 0.3 | 0.1001 | 0.0972 | 0.0961 | 0.0957 |
| Z-moment Coulomb friction 0.4 | 0.0451 | 0.0488 | 0.0502 | 0.0521 |
| Y-moment Coulomb friction 0.4 | 0.0784 | 0.0772 | 0.0748 | 0.0725 |
| Total moment Coulomb friction 0.4 | 0.1024 | 0.1027 | 0.1010 | 0.1012 |
| Z-moment Coulomb friction 0.6 | 0.0474 | 0.0516 | 0.0512 | 0.0577 |
| Y-moment Coulomb friction 0.6 | 0.0827 | 0.0752 | 0.0764 | 0.0687 |
| Total moment Coulomb friction 0.6 | 0.1061 | 0.1029 | 0.1034 | 0.1031 |

Table 5.6: Absolute average numerical values for each maximum points

The numerical values from various Coulomb friction models in Table 5.6, are compared with

data from DNV models in Table 5.8. It is observed that in DNV models total bending moments have a reduction trend through the intervals. The trend is not necessarily proportional to the number of intervals. However, the results from the DNV models shows bigger total bending moment than Coulomb friction models, which implies that DNV model brings more conservative results in pipeline design.

| Figure (MNm) | First max | Second max | Third max | Fourth max | Fifth max | Sixth max |
|---|---|---|---|---|---|---|
| $M_Z$ of DNV model with 100 interval | 0.0538 | 0.0537 | 0.0542 | 0.0542 | 0.0534 | 0.0584 |
| $M_Y$ of DNV model with 100 interval | 0.0773 | 0.0768 | 0.0758 | 0.0760 | 0.0759 | 0.0726 |
| $M_{tot}$ of DNV model with 100 interval | 0.1086 | 0.1075 | 0.1070 | 0.1065 | 0.1063 | 0.1072 |

Table 5.7: Absolute average numerical values with longer number of cycles for each maximum points

Table 5.7 tells that absolute Z-bending moment decreases with some fluctuating at the start while absolute Y-bending has a decreasing trend. It implies that as cycles progress lateral movement of the pipeline develops instead of rolling motion of the pipe. However, total bending moment becomes diminished, which seems to have a reduction due to built berms aside the pipeline. Unlike the tendency in Table 5.7, data from Table 5.8 exhibits non-constant trends, which implies that number of intervals of shear strength has the importance. With certain number of intervals the tendency of the moment becomes stabilized better. For instance, Z- bending moment with 200 intervals growth by cycles while Z- bending moment with 300 intervals declines.

| Figure (MNm) | First max | Second max | Third max | Fourth max |
|---|---|---|---|---|
| $M_Z$ of DNV model with 1 interval | 0.0550 | 0.0564 | 0.0447 | 0.0467 |
| $M_Y$ of DNV model with 1 interval | 0.0762 | 0.0758 | 0.0807 | 0.0821 |
| $M_{tot}$ of DNV model with 1 interval | 0.1084 | 0.1098 | 0.1051 | 0.1061 |
| $M_Z$ of DNV model with 5 interval | 0.0557 | 0.0536 | 0.0540 | 0.0542 |
| $M_Y$ of DNV model with 5 interval | 0.0765 | 0.0757 | 0.0747 | 0.0727 |
| $M_{tot}$ of DNV model with 5 intervals | 0.1099 | 0.1069 | 0.1052 | 0.1053 |
| $M_Z$ of DNV model with 10 interval | 0.0421 | 0.0474 | 0.039 | 0.0502 |
| $M_Y$ of DNV model with 10 interval | 0.0900 | 0.0803 | 0.0876 | 0.0789 |
| $M_{tot}$ of DNV model with 10 intervals | 0.1087 | 0.1056 | 0.1057 | 0.1065 |
| $M_Z$ of DNV model with 20 interval | 0.0571 | 0.0552 | 0.0458 | 0.0535 |
| $M_Y$ of DNV model with 20 interval | 0.0744 | 0.0750 | 0.0825 | 0.0754 |
| $M_{tot}$ of DNV model with 20 intervals | 0.1095 | 0.1081 | 0.1072 | 0.1059 |
| $M_Z$ of DNV model with 40 interval | 0.0557 | 0.0430 | 0.0555 | 0.0463 |
| $M_Y$ of DNV model with 40 interval | 0.0760 | 0.0863 | 0.0757 | 0.0843 |
| $M_{tot}$ of DNV model with 40 intervals | 0.1093 | 0.1079 | 0.1080 | 0.1061 |
| $M_Z$ of DNV model with 60 interval | 0.0452 | 0.0590 | 0.0404 | 0.0564 |
| $M_Y$ of DNV model with 60 interval | 0.0858 | 0.0726 | 0.0869 | 0.0720 |
| $M_{tot}$ of DNV model with 60 intervals | 0.1094 | 0.1084 | 0.1066 | 0.1067 |
| $M_Z$ of DNV model with 80 interval | 0.0559 | 0.0540 | 0.0563 | 0.0423 |
| $M_Y$ of DNV model with 80 interval | 0.0754 | 0.0772 | 0.0750 | 0.0830 |
| $M_{tot}$ of DNV model with 80 intervals | 0.1089 | 0.1084 | 0.1085 | 0.1074 |
| $M_Z$ of DNV model with 100 interval | 0.0538 | 0.0537 | 0.0542 | 0.0542 |
| $M_Y$ of DNV model with 100 interval | 0.0773 | 0.0768 | 0.0758 | 0.0760 |
| $M_{tot}$ of DNV model with 100 interval | 0.1086 | 0.1075 | 0.1070 | 0.1065 |
| $M_Z$ of DNV model with 200 interval | 0.0426 | 0.0539 | 0.0557 | 0.0555 |
| $M_Y$ of DNV model with 200 interval | 0.0885 | 0.0758 | 0.0742 | 0.0734 |
| $M_{tot}$ of DNV model with 200 intervals | 0.1092 | 0.1074 | 0.1078 | 0.1070 |
| $M_Z$ of DNV model with 300 interval | 0.0540 | 0.0533 | 0.0550 | 0.0533 |
| $M_Y$ of DNV model with 300 interval | 0.0761 | 0.0761 | 0.0766 | 0.0772 |
| $M_{tot}$ of DNV model with 300 intervals | 0.1082 | 0.1070 | 0.1081 | 0.1068 |

Table 5.8: Absolute average numerical values of DNV models at maximum points

Plastic and critical moment in the pipeline model are computed in Table 5.9. Plastic bending moment capacity is computed by multiplication of yield stress and plastic section modulus for thin wall structure. Critical bending moment is found in limit state design principle of DNV-OS-F101 submarine pipeline systems, i.e.: $M_{cr} = \frac{M_p}{\gamma_m \gamma_{SC}}$ where $\gamma_m$ and $\gamma_{SC}$ are material safety factor 1.15 and safety class resistance factor 1.138 respectively. According to Table 5.9, total bending moment from Coulomb friction model is below critical bending moment. In a force-displacement graph, below bifurcation point, which implies critical point and it is elastic region, rapid value change is expected by small difference due to steep slope of elastic modulus. It denotes that small differences between figures from Table 5.6 matter considerable. Table 5.10 displays gap percentages of numerical total bending moment values between different Coulomb frictions. In consequence choosing Coulomb friction coefficient strongly affects averaged total moment, but DNV model gives better outcomes in a conservative side.

| Moments | Equation | Value |
|---|---|---|
| Plastic bending moment $M_p$ | $\sigma_y D^2 t$ | 0.826 MNm |
| Critical bending moment $M_c$ | $\frac{M_p}{\gamma_m \gamma_{SC}}$ | 0.6312 MNm |

Table 5.9: Plastic and critical moment for the pipeline

| Total moment difference between models | First max | Second max | Third max | Fourth max |
|---|---|---|---|---|
| Coulomb friction 0.4 vs 0.3 | 2.246 % | 5.355 % | 4.851% | 5.435% |
| Coulomb friction 0.4 vs 0.6 | 3.6133 % | 0.1947 % | 2.3762 % | 1.8775 % |
| Coulomb friction 0.3 vs 0.6 | 5.994 % | 5.8642 % | 7.5963 % | 7.7325 % |

Table 5.10: Difference percentages of total moment values by friction coefficients

# Chapter 6

# Conclusion and discussion

The main objective of this thesis is to investigate global buckling behavior under high temperature and pressure on irregular foundation for very soft soil. 3D finite element analysis program SIMLA is applied. During operation events the pipeline may experience exceeding bending moment by unknown threat, which can lead the pipeline to failure. Numerous researches including DNV-RP-F105 'free spanning pipelines' suggest detailed guidance for multi-span response. However, since global buckling is highly non-linear phenomenon controlling the buckles is dependent on empirical information. In consequence this thesis focuses on parametric study and response observation from different soil models.

From the sensibility tests for shear strength intervals and different distribution trends, the resultants distinguish priority among parameters that governs global buckling with the soft soil condition an fixed mean shear strengths. Properties of shear strength such as distribution trend and magnitude show less influence on global buckling than geology characteristics of the seabed generally. Especially free-spans tend to govern the growth patterns of total bending moment and Z-moment because depth of free-span can provide elasticity to the pipeline by allowing extra bending further downward into the space of free-spans. On the other hand, some changes in the distributions of Z-axis bending moment have discovered at random.

Regarding different soil response models, outcomes from Coulomb model and DNV with berm formation model demonstrate that there is no significant differences in magnitude of total bending moment and Z-moment. However, DNV model causes slightly larger numerical value, which denotes DNV model is more conservative. In order to have same amount of reaction as DNV model, big Coulomb friction than empirical data that it widely used in the industry is required. It is also found that Z-moment grows as cycles develop with some value oscillations at the start. According to observations of DNV models with different shear strength intervals,

number of the intervals causes to appear differences on fluctuating trends of Z-moment. This implies that number of shear strength interval has some influences on moment stabilization, which gives awareness of selection of interval number when time and resources are limited in FEA.

# Chapter 7

# Further work

In this thesis it is proved that geology parameters mainly governs distribution of bending moment in global buckling on irregular foundation. In order to verify sensibility of other parameter on the global buckles and control the buckles, additional studies are required.

The most potential geology factor is depth of free-spans. In Figure 5.2 it has found that maximum and minimum total bending moment always appear near the deepest free spans. As a consequence, parametric studies for depth and width of free spans correlated with diameter of the pipeline, are recommended to find a key for global buckling control on uneven seabed. Investigations for other geology parameters could be interesting as well such as slopes of uneven foundation.

In North Sea, irregular sea-surface can be simplified as wave shapes with different height of peaks and troughs. On peaks, due to nature of erosion soil stiffness is softer than those on troughs. Therefore, simulations with different stiffness by height of the sea profile can reflect the reality better, which brings accurate results.

Last, the rock berms installed in this thesis have short length and medium degree of stiffness, which does not produce strong enough rigidity to isolate buckles into each subdivisions. Firm stiffness or long berms, can be analyzed to verify impact of rock berm properties.

# Bibliography


Andrew C. Palmer, R. A. K. (2007). *Subsea Pepieline Engineering*. PennWell.

Bjerrum, L. (1973). Geotechnical problems involved in foundations of structures in the north sea. *Géotechnique*.

Carlos Oliveira Cardoso, Marcio Martins Mourelle, A. M. C. A. A. C. S. A. (2006). Hp-ht pipeline cyclic behavior considering soil berms effect. *International Conference on Offshore Mechanics and Arctic Engineering*.

Carlos OliveiraCardoso, Marcio Martins Mourelle, A. M. C. A. A. C. S. A. (2004). Global buckling of a heated pipeline in the campos basin brazil in a region with free-spans. *International Pipeline Conference*.

Carlos Sicilia, Emilien Bonnet, P. A. C. (2014). Probabilistic lateral buckling assessment. *International Ocean and Polar Engineering Conference*.

Collberg, L. (1999). Introduction to the update of dnv'96, dnv os f101; submarine pipeline systems. *International Offshore and Polar Engineering Conference*.

Croll, J. G. (1997). A simplified model of upheaval thermal buckling of subsea pipelines. *Thin-Walled Structures*.

D. Bruton, D. White, C. C. M. B. M. C. (2006). Pipe/soil interaction behavior during lateral buckling. *Offshore Thchnology Conference*.

D.A.S. Bruton, M. C. (2011). Overview of the safebuck jip. *Offshore Technology Conference*.

David A. Wagner, James D. Murff, H. B. O. S. (1989). Pipe-soil interaction model. *Ocean Engineering*.

D.J. White, Z. J. Westgate, Y. T. (2014). Pipeline lateral buckling: Realistic modelling of geotechnical variability and uncertainty. *Offshore Technology Conference*.

DNV (2007). Recommended practice dnv-rp-f110 global buckling of submarine pipelines structural design due to high temperature/high pressure. Technical report, DET NORSKE VERITAS.

DNV (2010). On-bottom stability design of submarine pipelines dnv-rp-f109. Technical report, DNV.

DNV (February 1992). Foundation classification notes no 30.4. Technical report, DET NORSKE VERITAS AS.

DNV (FEBRUARY 2006). Recommended practice dnv-rp-f105 free spanning pipelines. Technical report, DNV.

F. Van den Abeele, F. Boël, D. H. D. S. (2015). An integrated numerical approach to design offshore pipelines susceptible to lateral buckling. *International Conference on Ocean, Offshore and Arctic Engineering*.

Hassan Karampour, Faris Albermani, J. G. (2013). On lateral and upheaval buckling of subsea pipelines. *Engineering Structures*.

Hobbs, R. E. (1981). Pipeline buckling caused by axial loads. *Journal of Constructional Steel Research*.

Hong, P. (2014). An elastoplastic model with combined isotropic–kinematic hardening to predict the cyclic behavior of stiff clays. *Computers and Geotechnics*.

Irman, A. A. (2015). Non-linear soil models for pipeline and riser analysis. Master's thesis, Norwegian University of Science and Technology.

J. D. Murff, D. A. Wagner, M. F. R. (1989). Pipe penetration in cohesive soil. *Géotechnique*.

J. Michael Duncan, Stephen G. Wright, T. L. B. (2014). *Soil Strength and Slope Stability*. John Wiley & Sons.

Kenneth J. Nyman, A. M. A. (1982). Soil response against oblique motion of pipes. *ASCE*.

Kåre Senneset, Kaare Flaate, J. O. L. (2005). *Landslides and Avalanches. Norway 2005: Proceedings of the 11th International Conference and Field Trip on Landslides, Norway, September 2005*. CRC Press.

Kvalstad, T. J. (2005). *Ormen Lange - an integrated study for safe field development in the Storegga Submarrine Slide Area*. Elsevier.

Kyriakides, S. and Shaw (1982). Response and stability of elastoplastic circular pipes under combined bending and external pressure. *International Journal of Solids and Structures*.

M. Masood Haq, S. K. (2013). Lateral buckling response of subsea hthp pipelines using finite element methods. *OMAE*.

Mason, M. T. (2012). Lecture note, friction, mechanics of manipulation. Technical report, Carnegie Mellon University.

McCarron, W. (2015). Subsea flowline buckle capacity considering uncertainty in pipe–soil interaction. *Computers and Geotechnics*.

Mckenzie, N. P. and Pender, M. J. (1996). Representative shear modulus for shallow foundation seismic soil-structure interaction. *Eleventh World Conference on Earthquake Engineering*.

Moan, T. (2003). *Finite Element Modeling and Analysis of Marine Structures*. NTNU.

Nyman, K. J. (1982). Soil response against oblique motion of pipes. *ASCE*.

Olav Aamlid, Knut Vedeld, H. S. (2010). Effects of free spans on on-bottom stability of pipelines – a global approach. *OMAE*.

Paulo Teixeira, Marco Gonzalez, N. L. (2011). Effects of soil-pipe interaction on the global buckling response of submarine pipelines. *Pressure Vessels & Piping Division Conference*.

Per R. Nystrom, Knut Tomes, Y. B. P. D. (1997). 3-d dynamic buckling and cyclic behaviour of hp/ht flowlines. *International Offshore and Polar Engineering Conference*.

Pervizpour, M. Performance evaluation of constructed facilities. Widener University, 2004.

Petter Bryn, Kjell Berg, C. F. F. A. S. T. J. K. (2005). Explaining the storegga slide. *Marine and Petroleum Geology*.

Pty, A. (2014). No cover rock berm. *http://atteris.com.au/no-cover-rock-berm-1/*.

Qinglai Fan, Maotian Luan, Q. Y. (2007). Three dimensional nonlinear finite element analyses for horizontal bearing capacity of deeply-embedded large-diameter cylindrical structure on soft ground. *Soft Soil Engineering*.

R. A. Einsfeld, D. W. Murray, N. Y. (2003). Buckling analysis of high temperature pressurized pipelines with soilstructure interaction. *Journal of the Brazilian Society of Mechanical Sciences and Engineering*.

Randolph, M. and Gourvenec, S. (2011). *Offshore Geotechnical Engineering*. Spon Press.

Run Liu, Wenbin Liu, X. W. S. Y. (2014). Global lateral buckling analysis of idealized subsea pipelines. *Central South University Press*.

SINTEF. Pondus program. https://www.sintef.no/projectweb/pipelines/products-services/pondus-pipe/pondus/.

Smith, V. and Kaynia, A. (2015). Pipe-soil interaction under rapid axial loading. *Frontiers in Offshore Geotechnics III*.

Stig Goplen, Pål Strøm, E. L. K. J. M. (2005). Hotpipe jip: Hp/ht buried pipelines. *OMAE*.

Sævik, S. (2008). Simla-theory manual. Technical report, MARINTEK.

Taylor, N. and Gan, A. B. (1986). Submarine pipeline buckling imperfection studies. *Thin-Walled Structures*.

Verley. R, Lund, K. (1995). A soil resistance model for pipelines placed on clay soils. *OMAE*.

White, D. J. and Randolph, M. F. (2007). Seabed characterisation and models for pipeline-soil interaction. *The International Societyof Offshore and Polar Engineers*.

Yong Bai, Q. B. (2005). *Subsea Pipelines and Risers*. Elsevier.

Yong Bai, Ragnar T. Igland, T. M. (1997). Tube collapse under combined external pressure, tension and bending. *Marine Structures*.

Zhaohui Hong, Run Liu, W. L. S. Y. (2015). A lateral global buckling failure envelope for a high temperature and high pressure (ht/hp) submarine pipeline. *Applied Ocean Research*.

# Appendix A

# Case study 1

## A.1 Effects of cyclic loads in total bending moment

Following graphs exhibit total bending moment distributions along the route by each time (cycles) to study influences of the shear strength distributions on global buckling. In order to provide approachable material interpretation for readers, the total bending moment value is divided by maximum bending moment which is plastic bending moment. Consequently the readers easily comprehend scale of magnitude of resultant total bending moment.

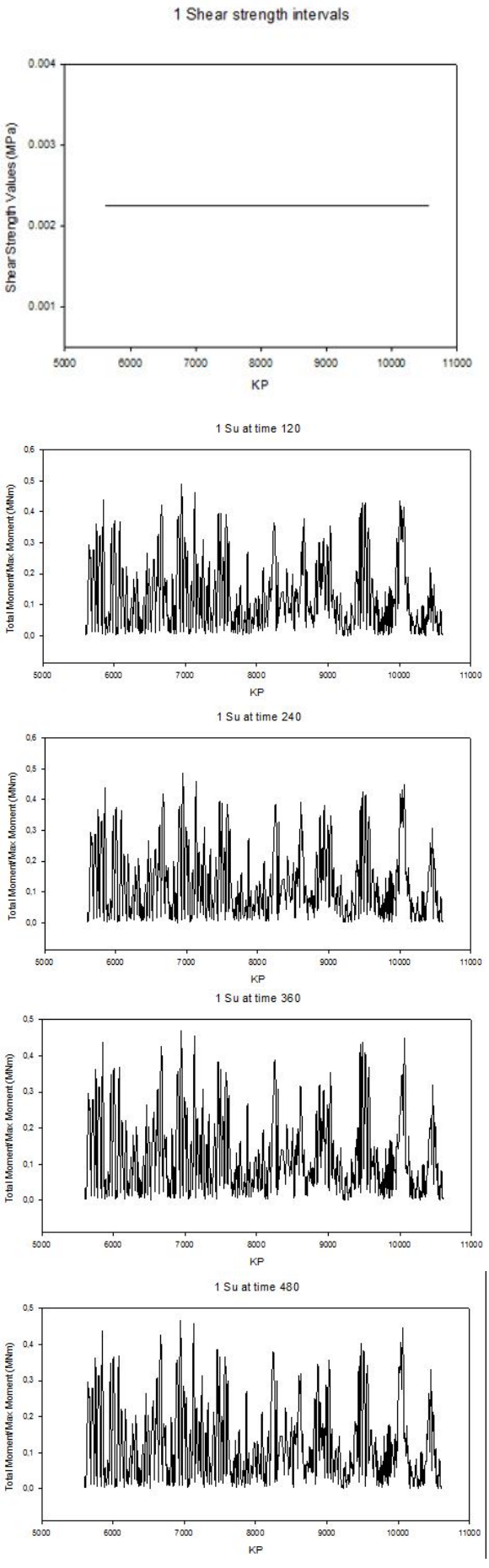


Figure A.1: Moment distributions by cycles with one shear strength over the entire route

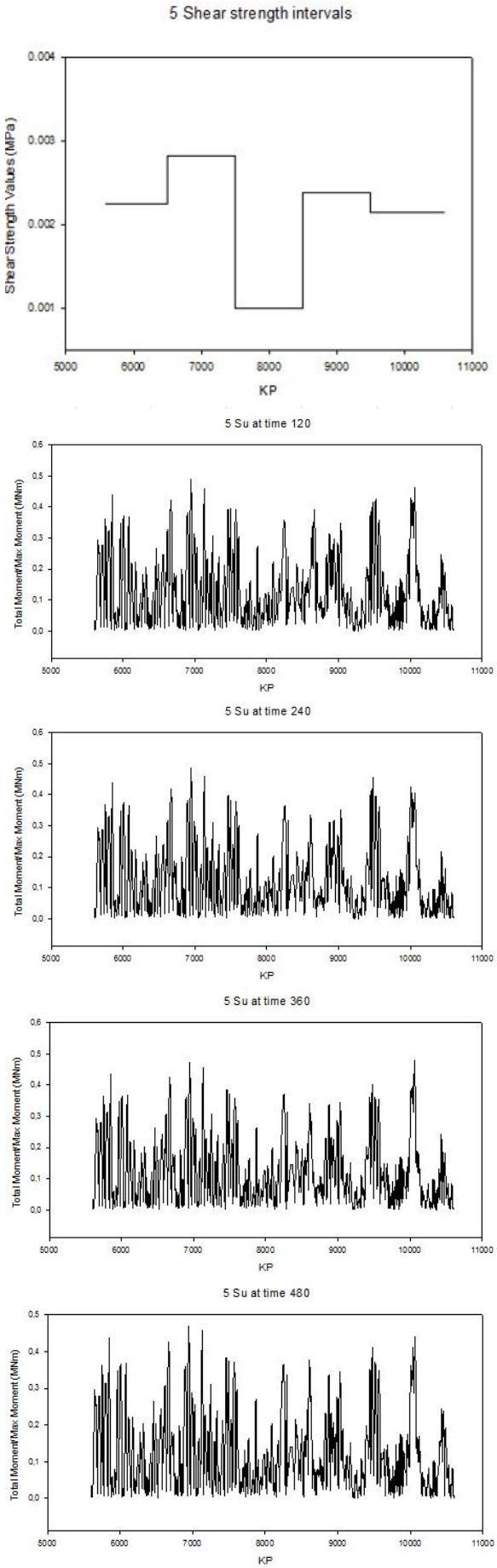


Figure A.2: Moment distributions by cycles with five shear strength intervals

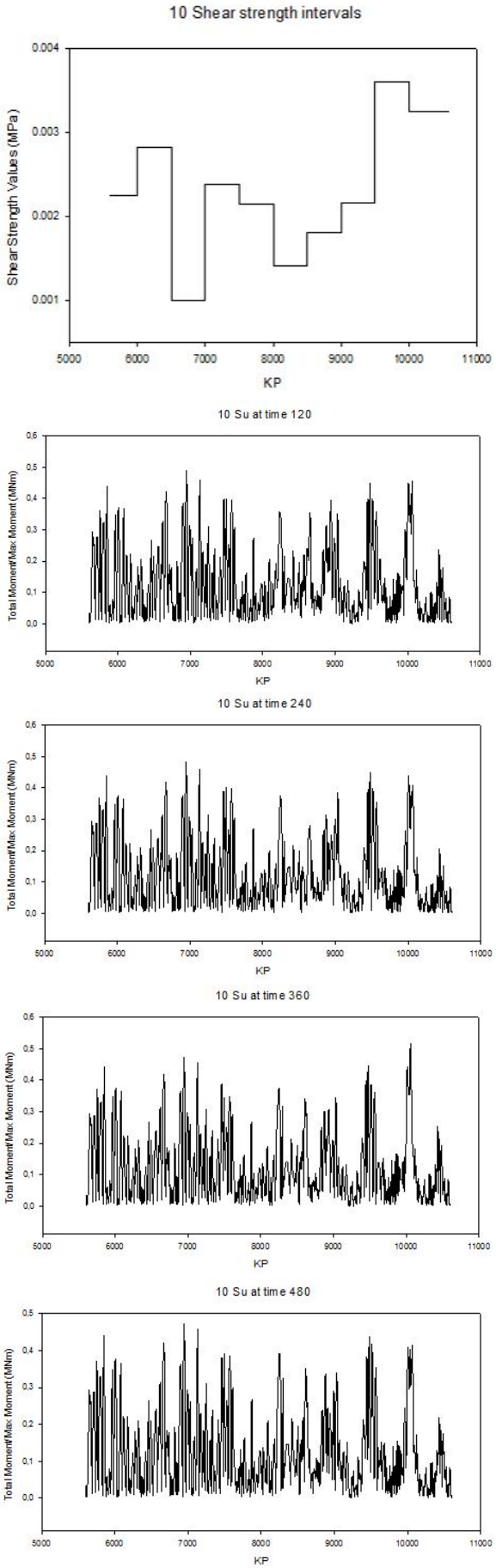


Figure A.3: Moment distributions by cycles with ten shear strength intervals

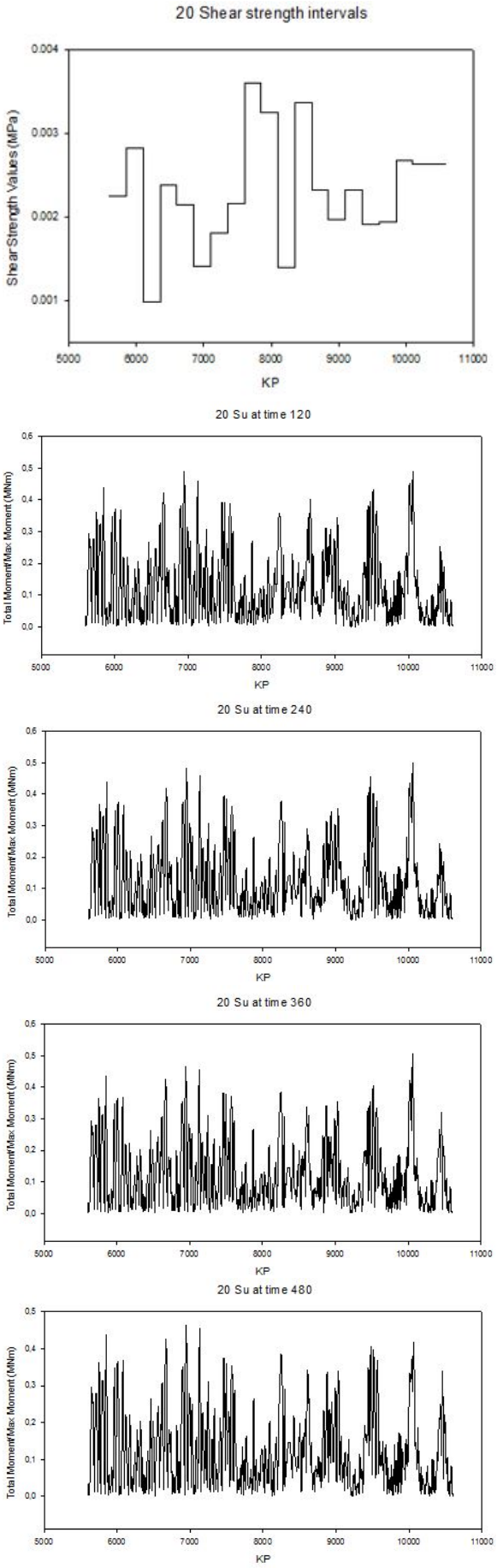


Figure A.4: Moment distributions by cycles with twenty shear strength intervals

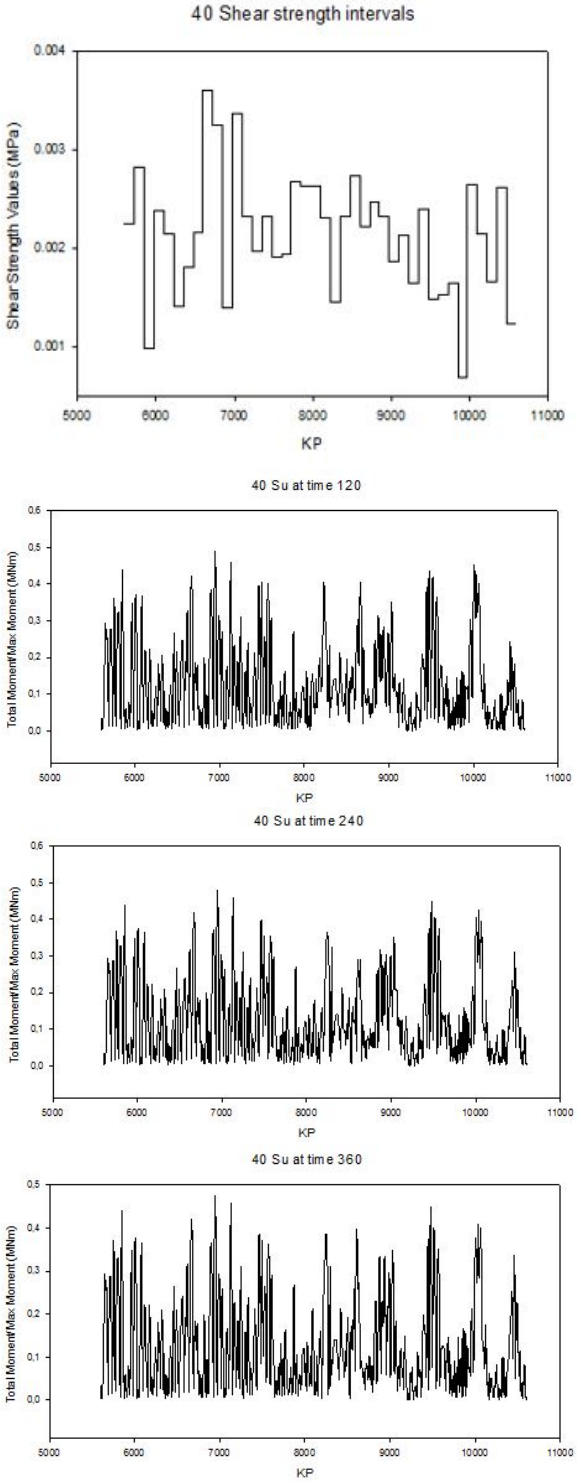


Figure A.5: Moment distributions by cycles with forty shear strength intervals

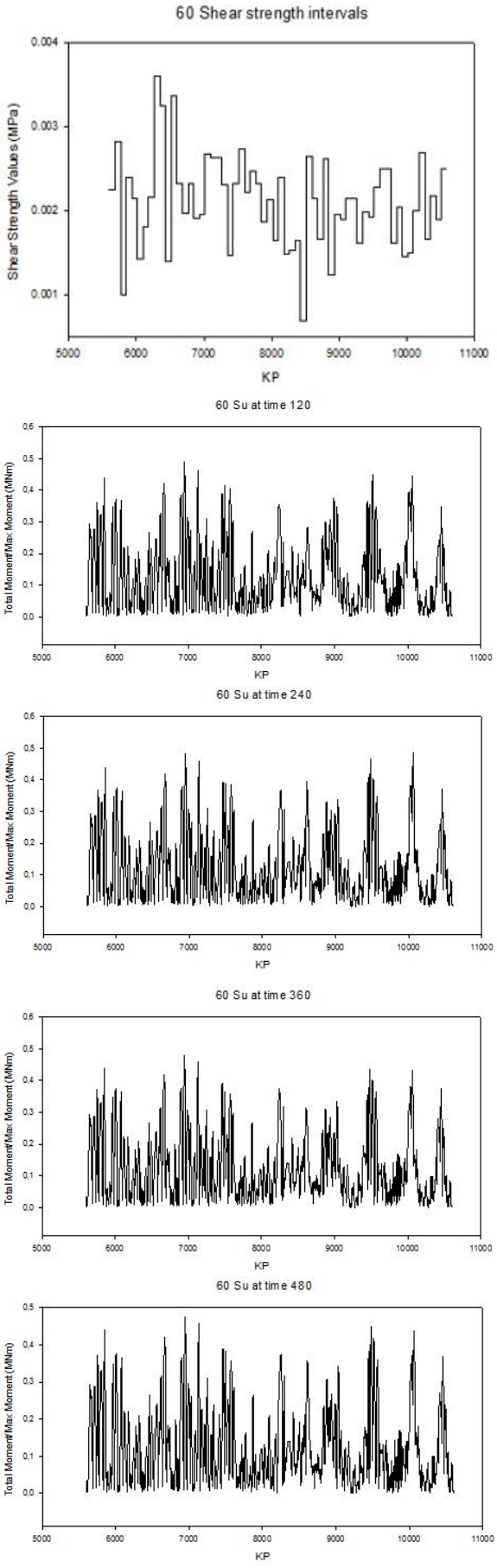


Figure A.6: Moment distributions by cycles with sixty shear strength intervals

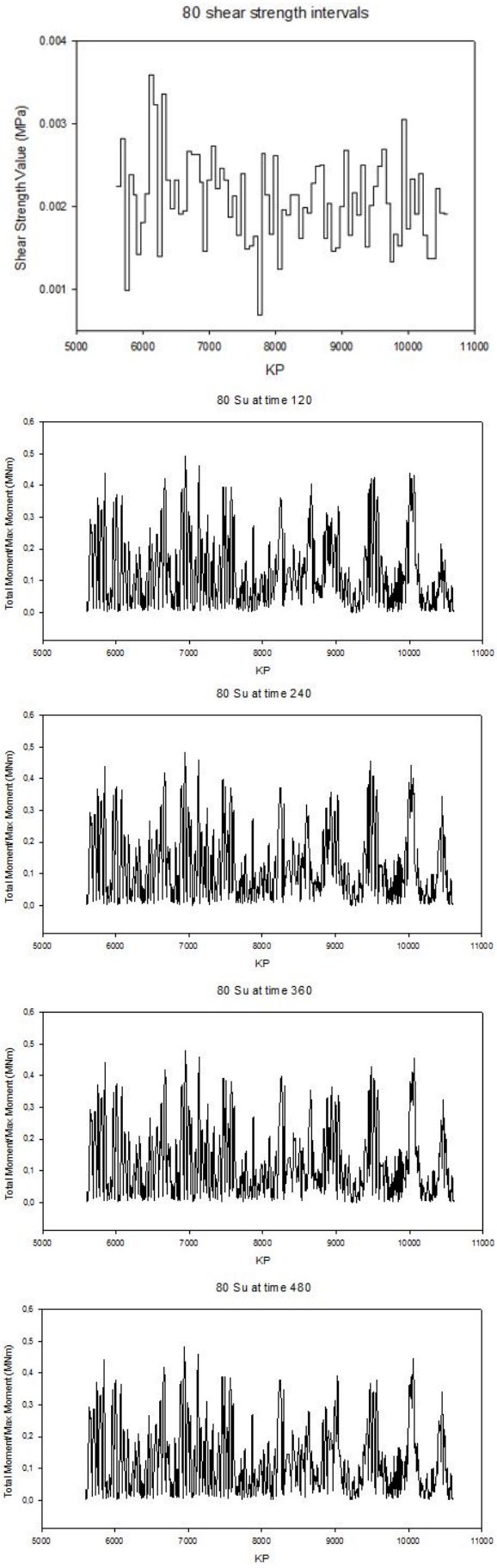


Figure A.7: Moment distributions by cycles with eighty shear strength intervals

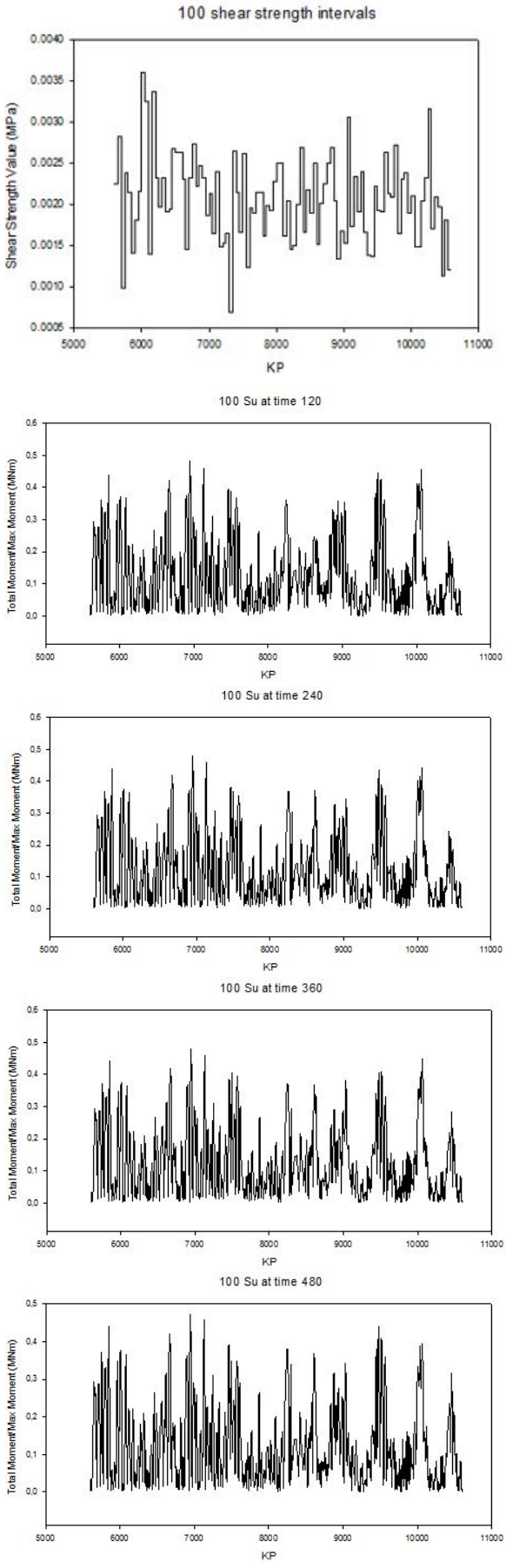


Figure A.8: Moment distributions by cycles with one hundred shear strength intervals

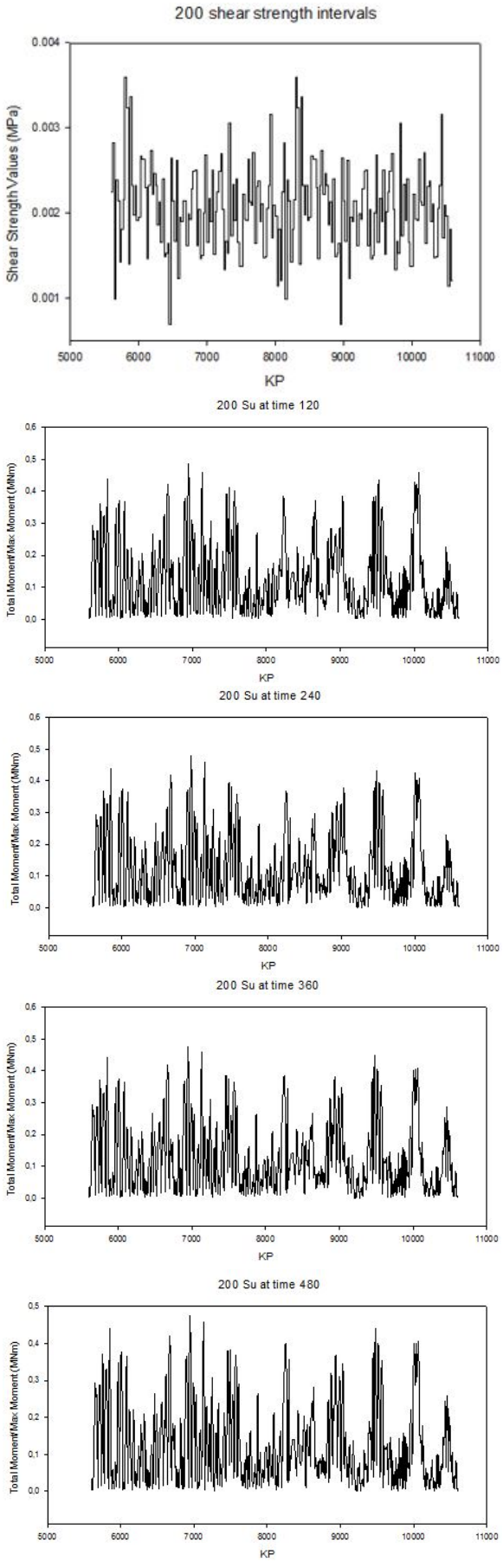


Figure A.9: Moment distributions by cycles with two hundred shear strength intervals

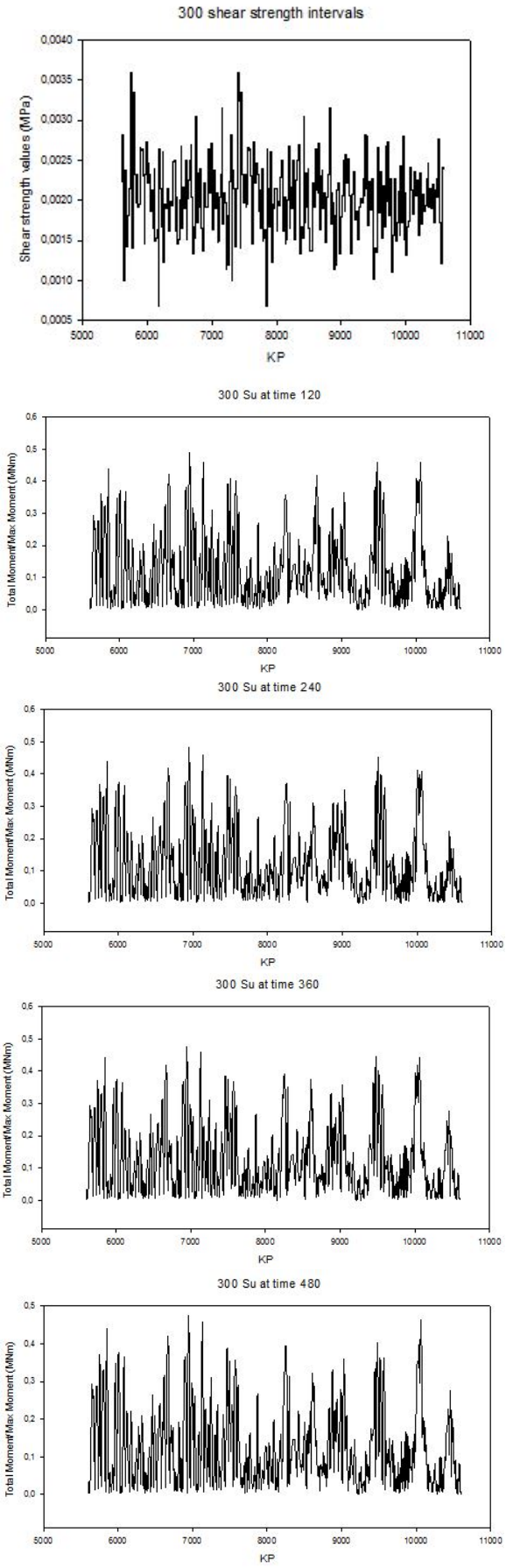


Figure A.10: Moment distributions by cycles with three hundreds shear strength intervals

## A.2 Effects of shear strength intervals in total bending moment

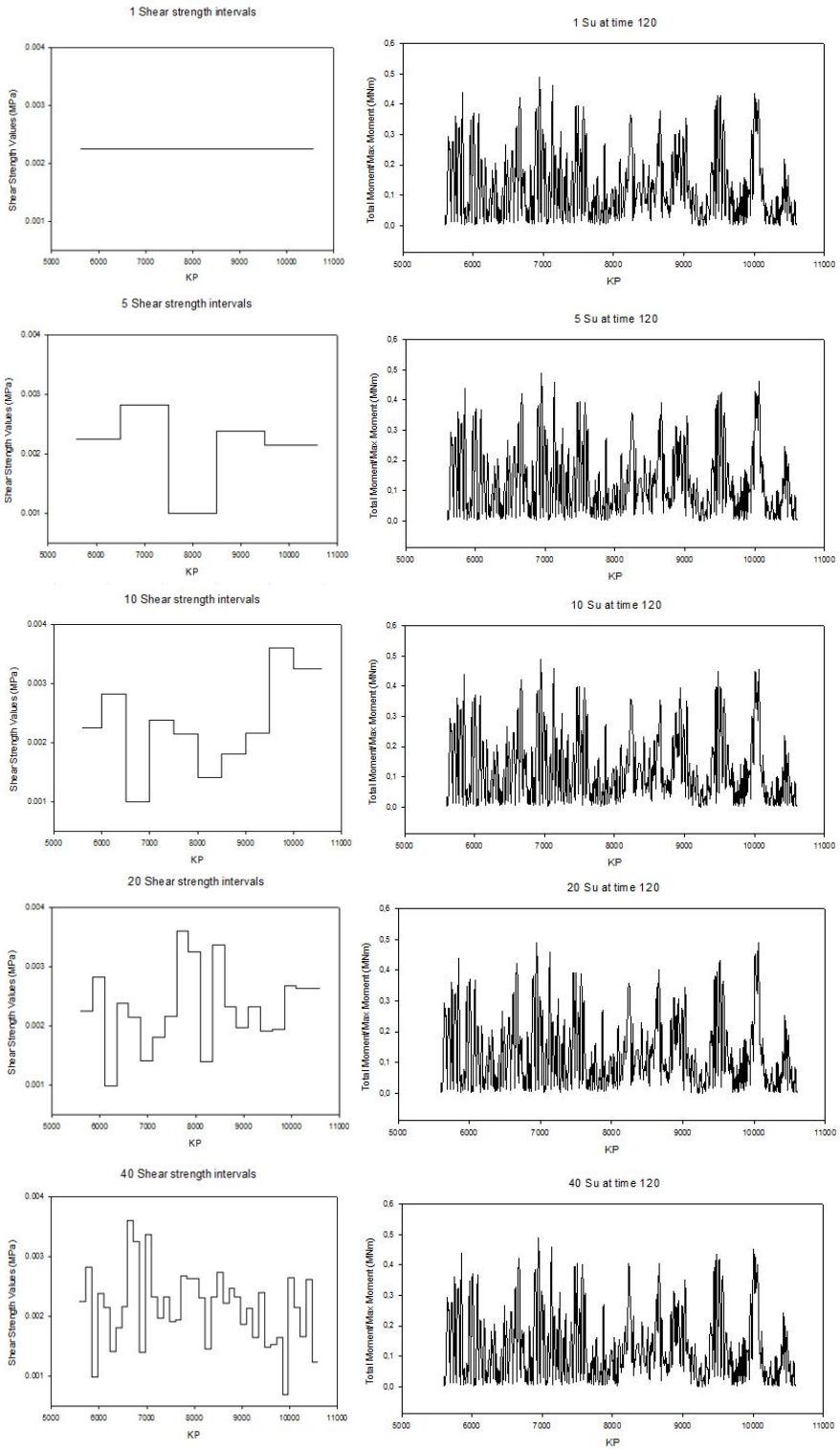

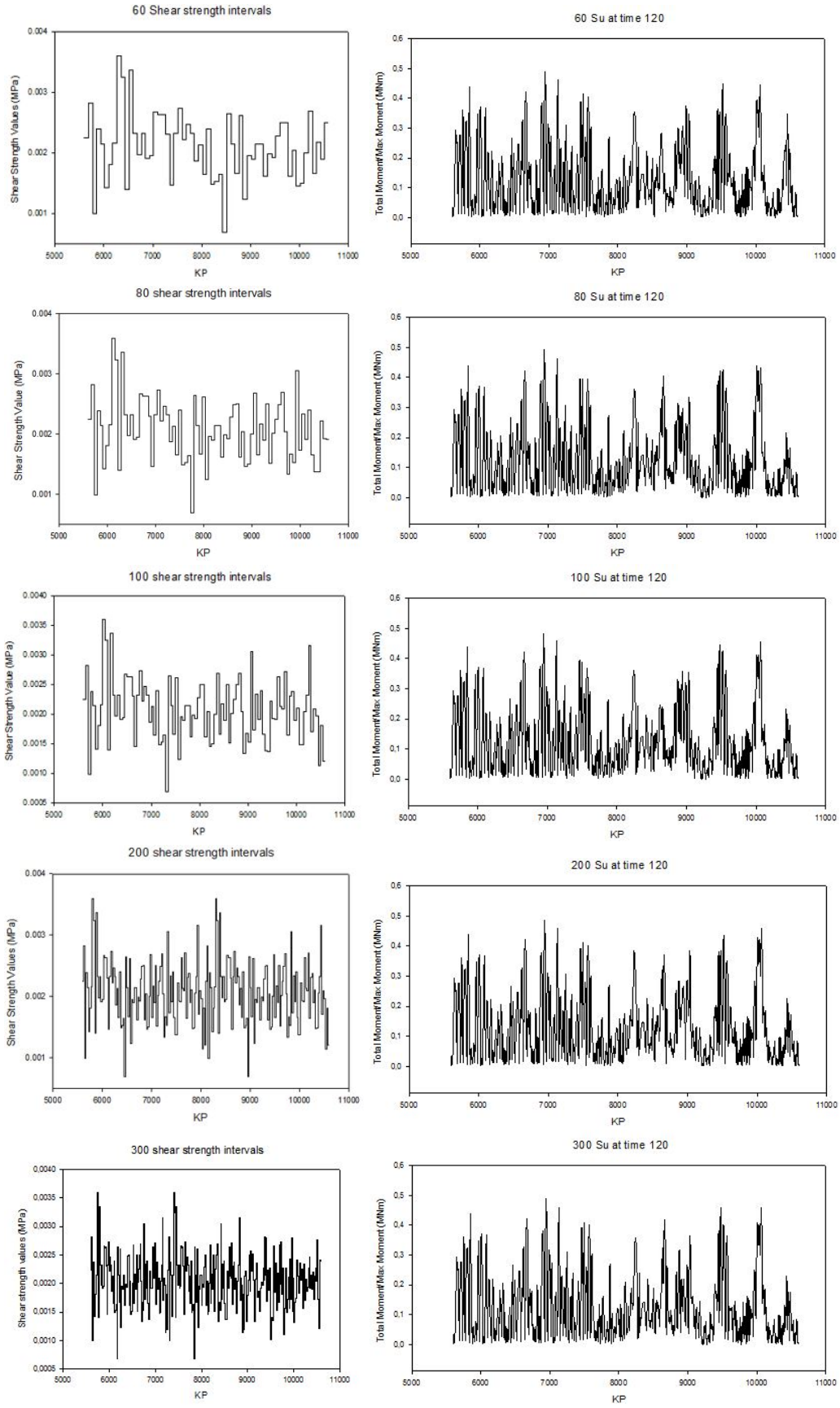


Figure A.11: Moment distributions at time 120s generated by different number of intervals

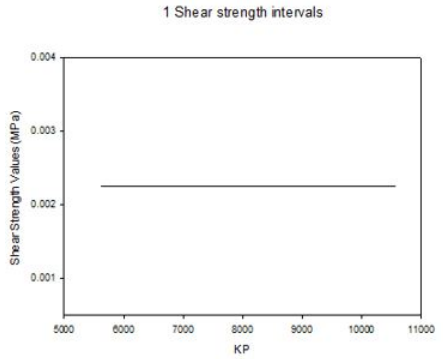
1 Shear strength intervals
Shear Strength Values (MPa)
KP

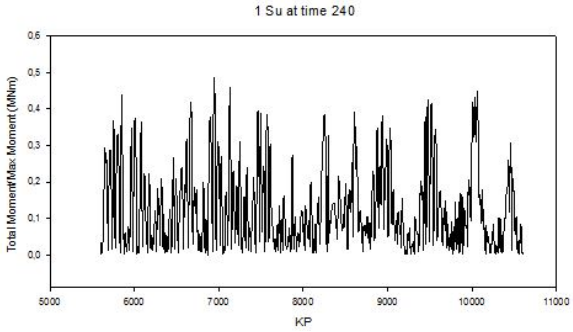
1 Su at time 240
Total Moment/Max Moment (MNm)
KP

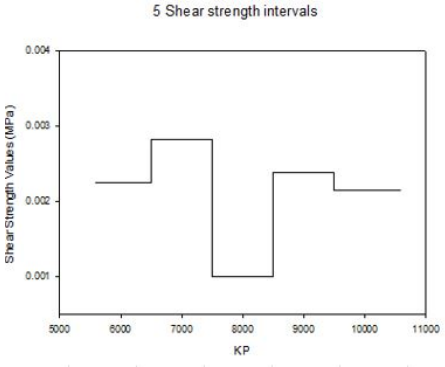
5 Shear strength intervals
Shear Strength Values (MPa)
KP

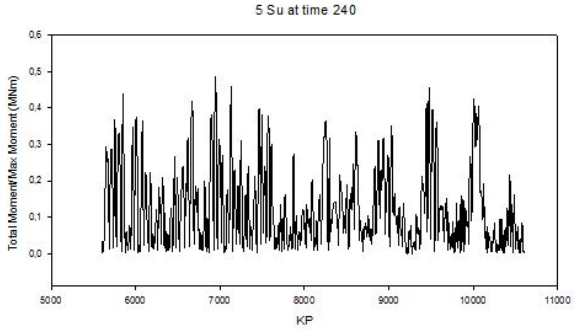
5 Su at time 240
Total Moment/Max Moment (MNm)
KP

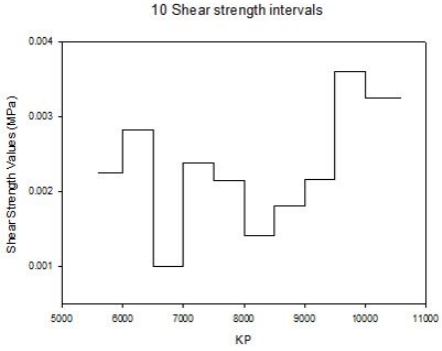
10 Shear strength intervals
Shear Strength Values (MPa)
KP

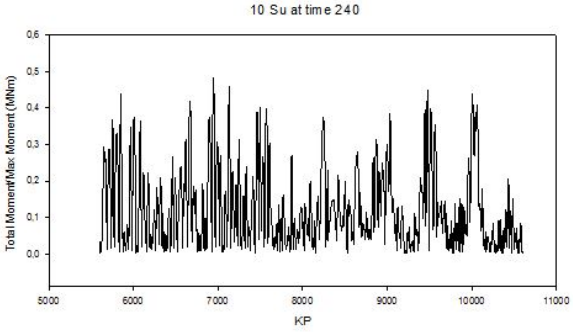
10 Su at time 240
Total Moment/Max Moment (MNm)
KP

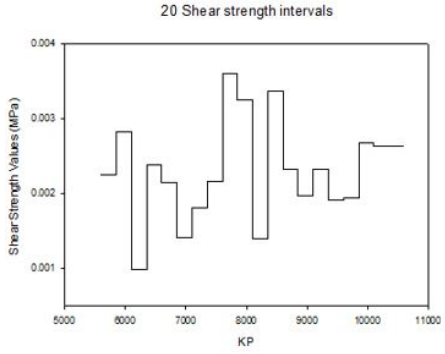
20 Shear strength intervals
Shear Strength Values (MPa)
KP

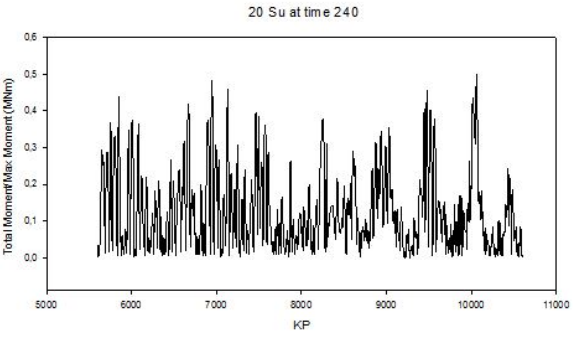
20 Su at time 240
Total Moment/Max Moment (MNm)
KP

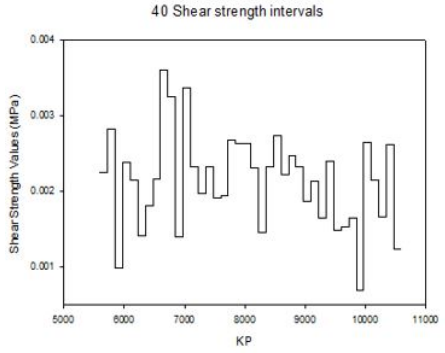
40 Shear strength intervals
Shear Strength Values (MPa)
KP

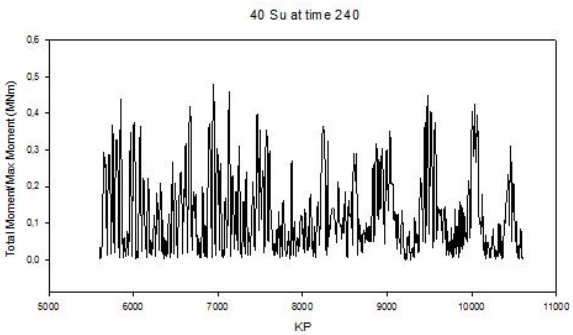
40 Su at time 240
Total Moment/Max Moment (MNm)
KP

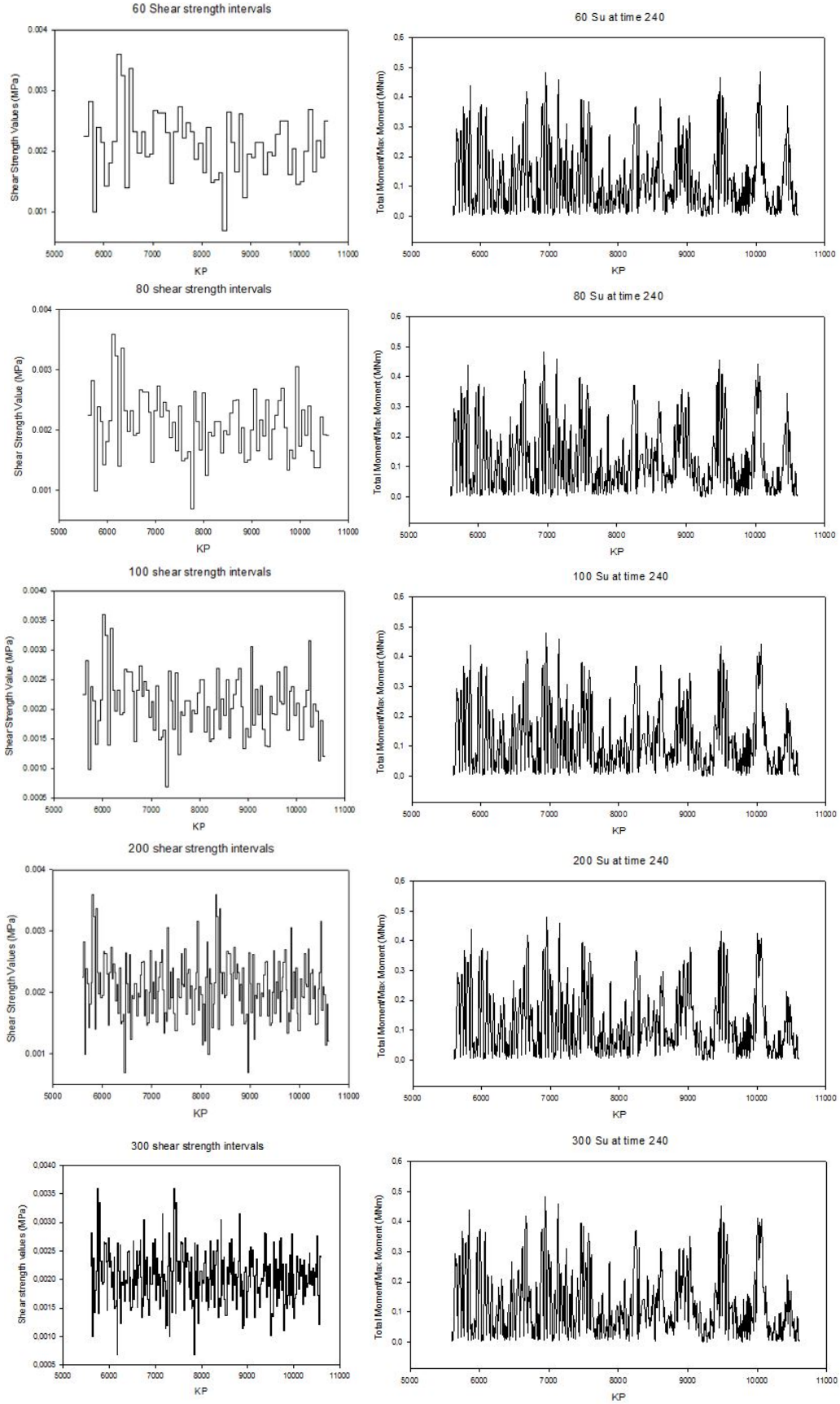


Figure A.12: Moment distributions at time 240s generated by different number of intervals

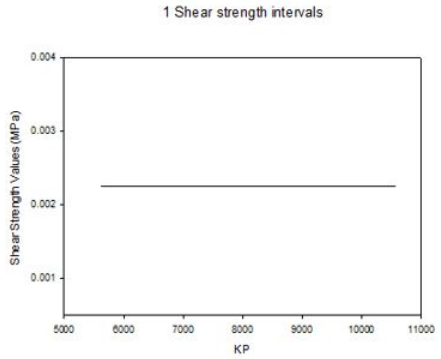
1 Shear strength intervals
Shear Strength Values (MPa)
KP

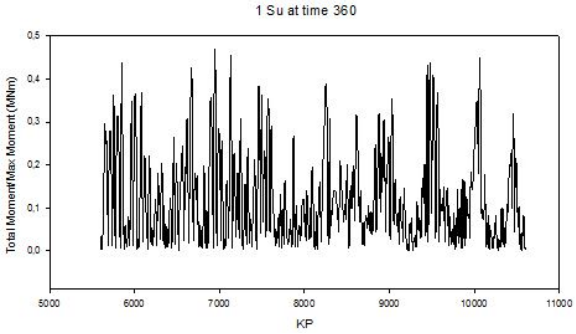
1 Su at time 360
Total Moment/Max Moment (MNm)
KP

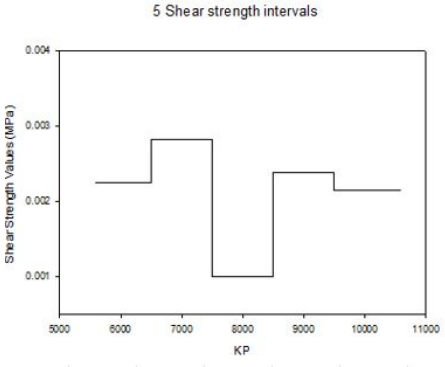
5 Shear strength intervals
Shear Strength Values (MPa)
KP

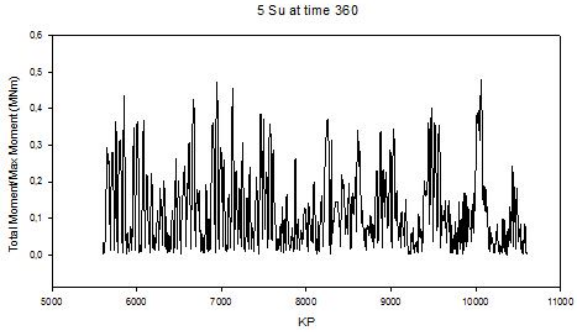
5 Su at time 360
Total Moment/Max Moment (MNm)
KP

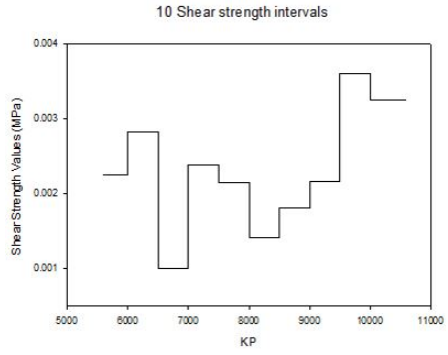
10 Shear strength intervals
Shear Strength Values (MPa)
KP

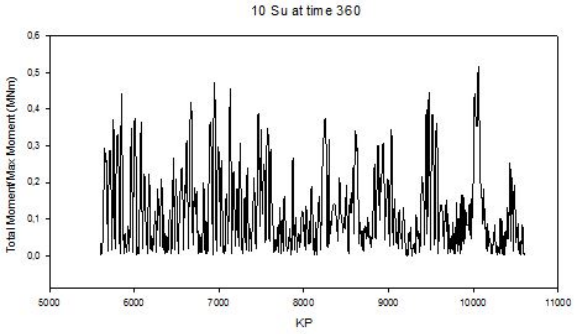
10 Su at time 360
Total Moment/Max Moment (MNm)
KP

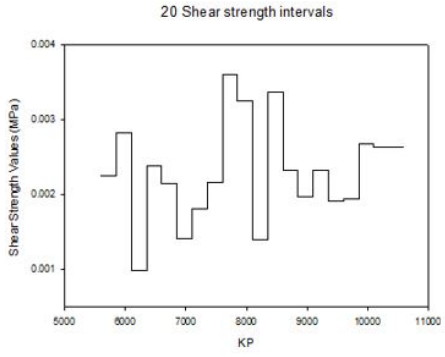
20 Shear strength intervals
Shear Strength Values (MPa)
KP

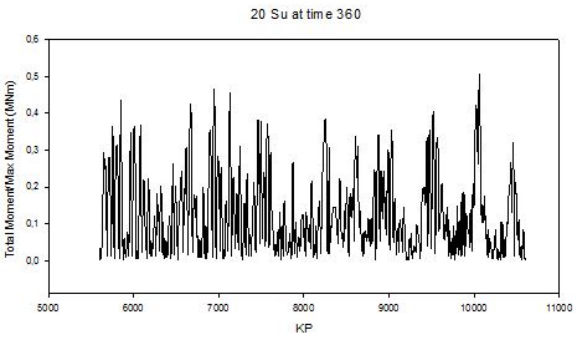
20 Su at time 360
Total Moment/Max Moment (MNm)
KP

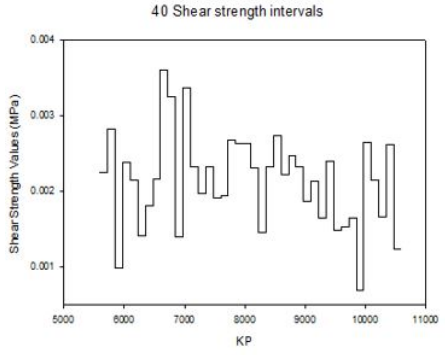
40 Shear strength intervals
Shear Strength Values (MPa)
KP

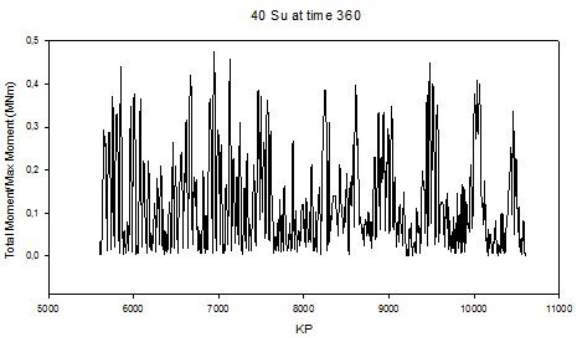
40 Su at time 360
Total Moment/Max Moment (MNm)
KP

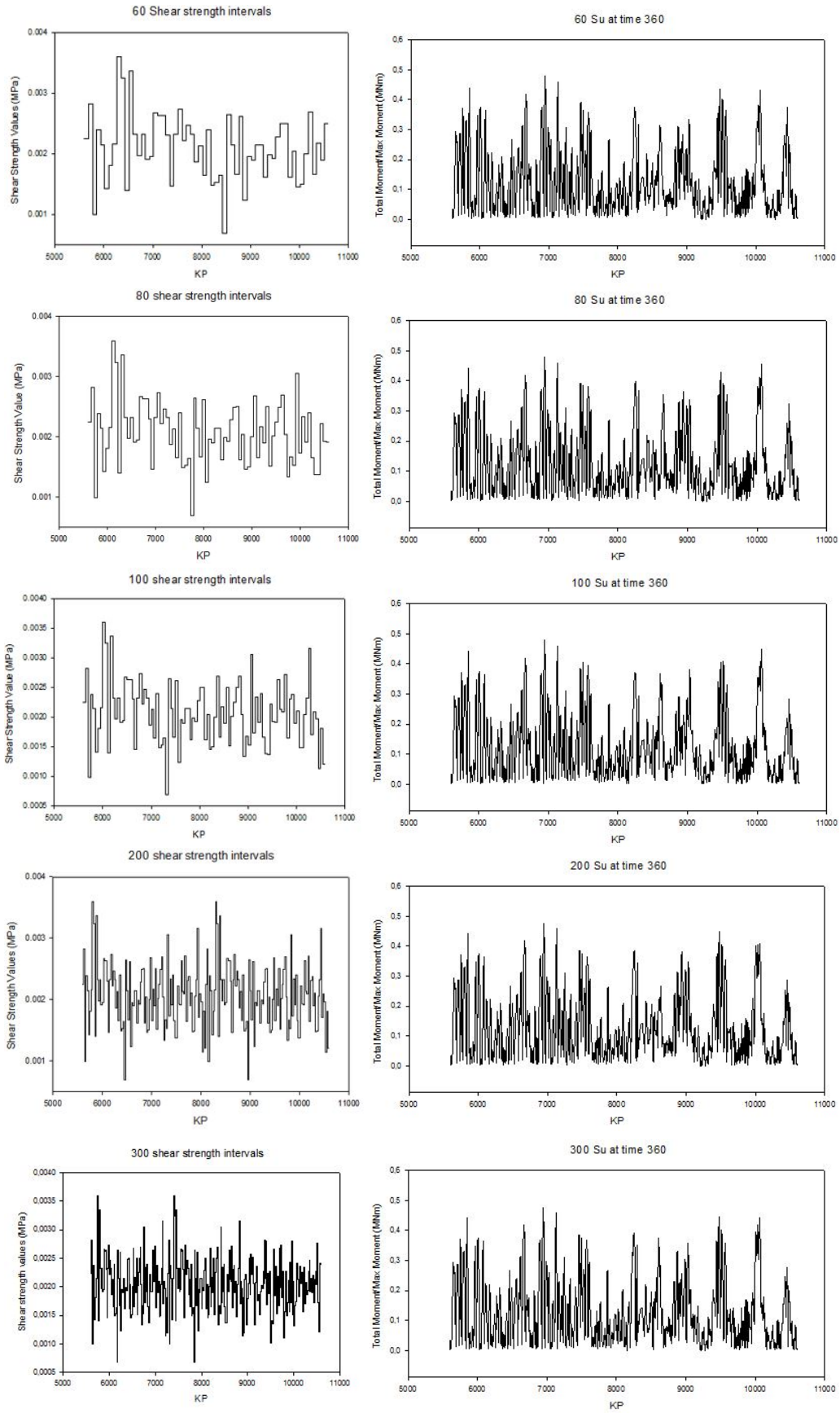


Figure A.13: Moment distributions at time 360s generated by different number of intervals

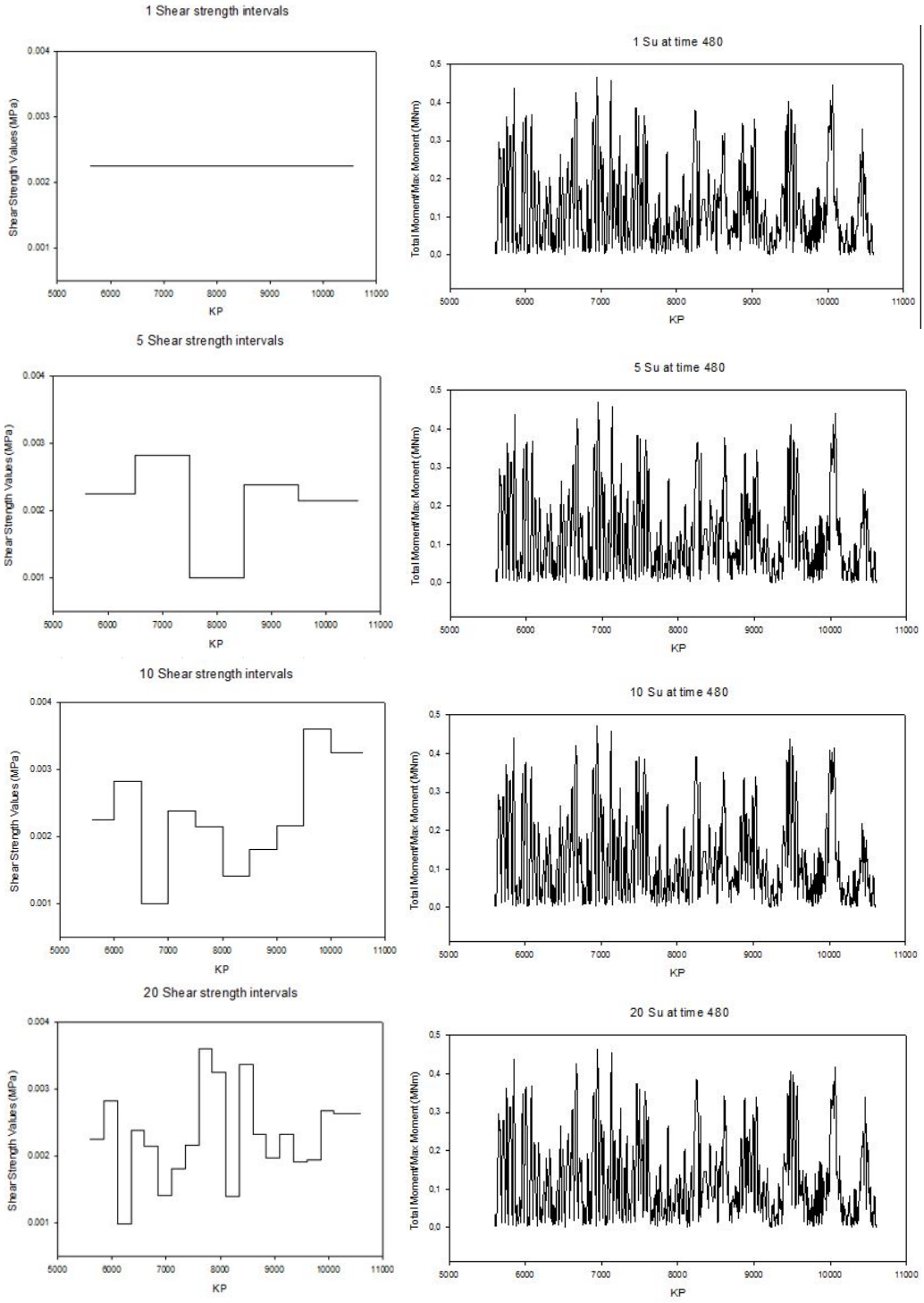
1 Shear strength intervals
Shear Strength Values (MPa)
KP
1 Su at time 480
Total Moment/Max Moment (MNm)
KP
5 Shear strength intervals
Shear Strength Values (MPa)
KP
5 Su at time 480
Total Moment/Max Moment (MNm)
KP
10 Shear strength intervals
Shear Strength Values (MPa)
KP
10 Su at time 480
Total Moment/Max Moment (MNm)
KP
20 Shear strength intervals
Shear Strength Values (MPa)
KP
20 Su at time 480
Total Moment/Max Moment (MNm)
KP

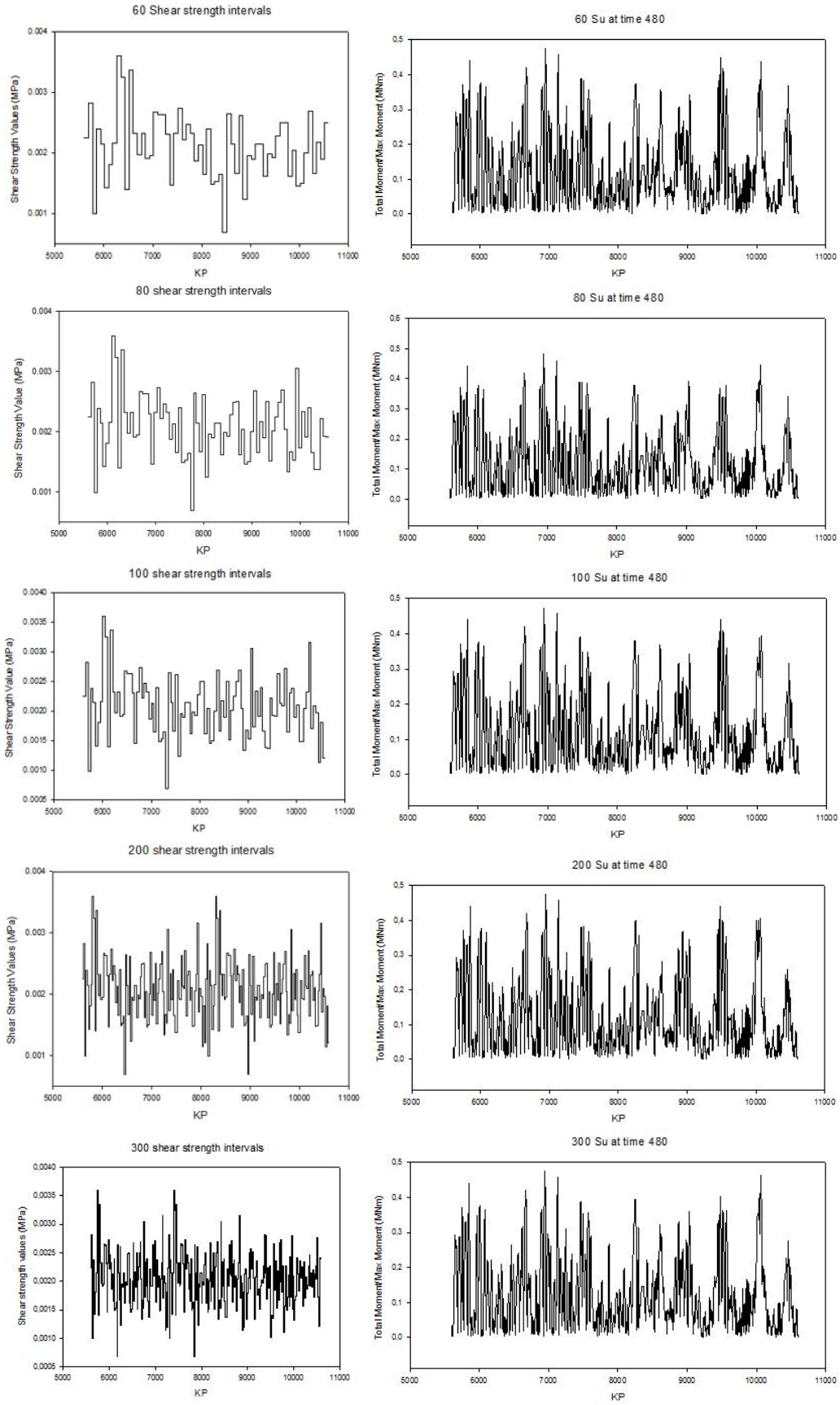


Figure A.14: Moment distributions at time 480s generated by different number of intervals

## A.3 Effects of cyclic loads in Z-moment

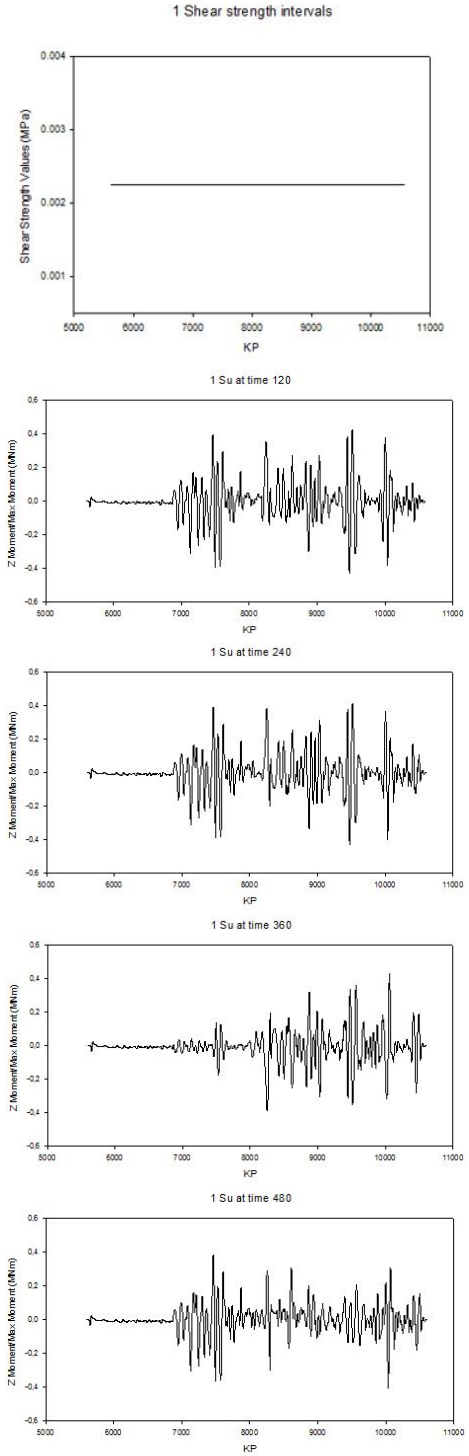


Figure A.15: Moment distributions by cycles with one shear strength over the entire route

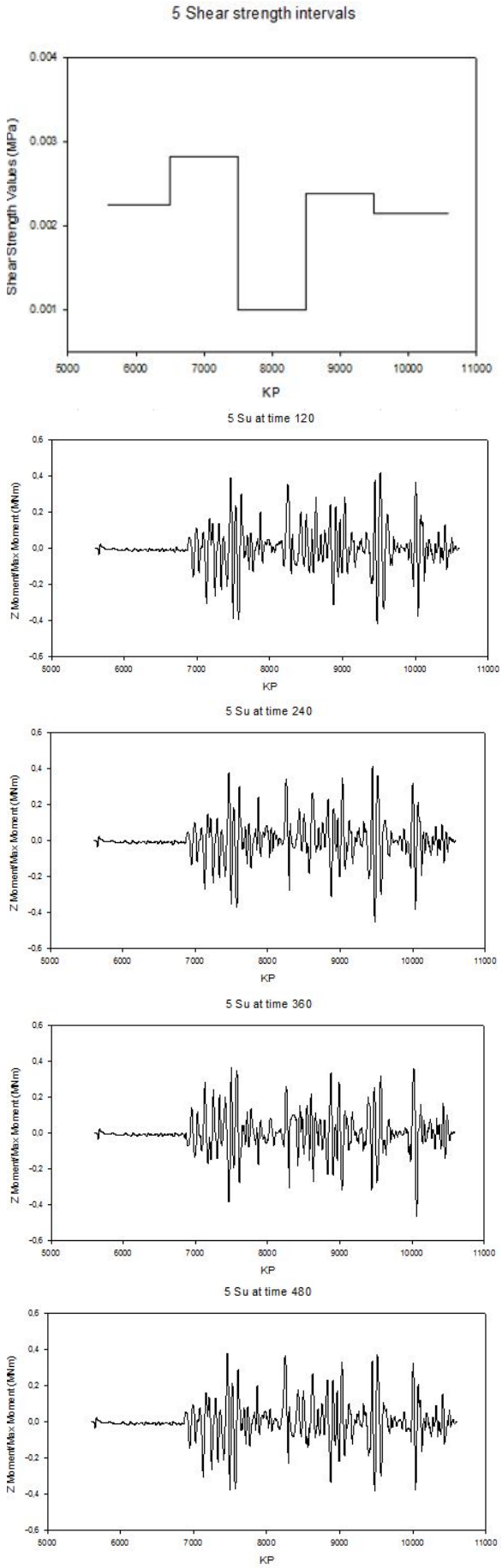


Figure A.16: Moment distributions by cycles with five shear strength intervals

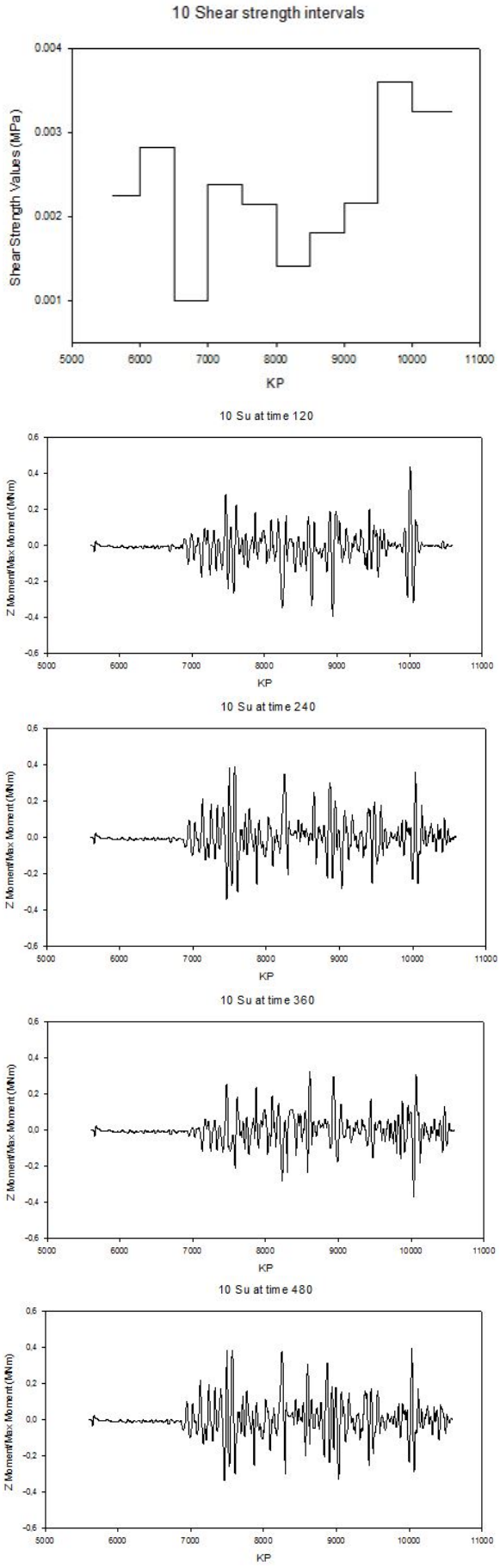


Figure A.17: Moment distributions by cycles with ten shear strength intervals

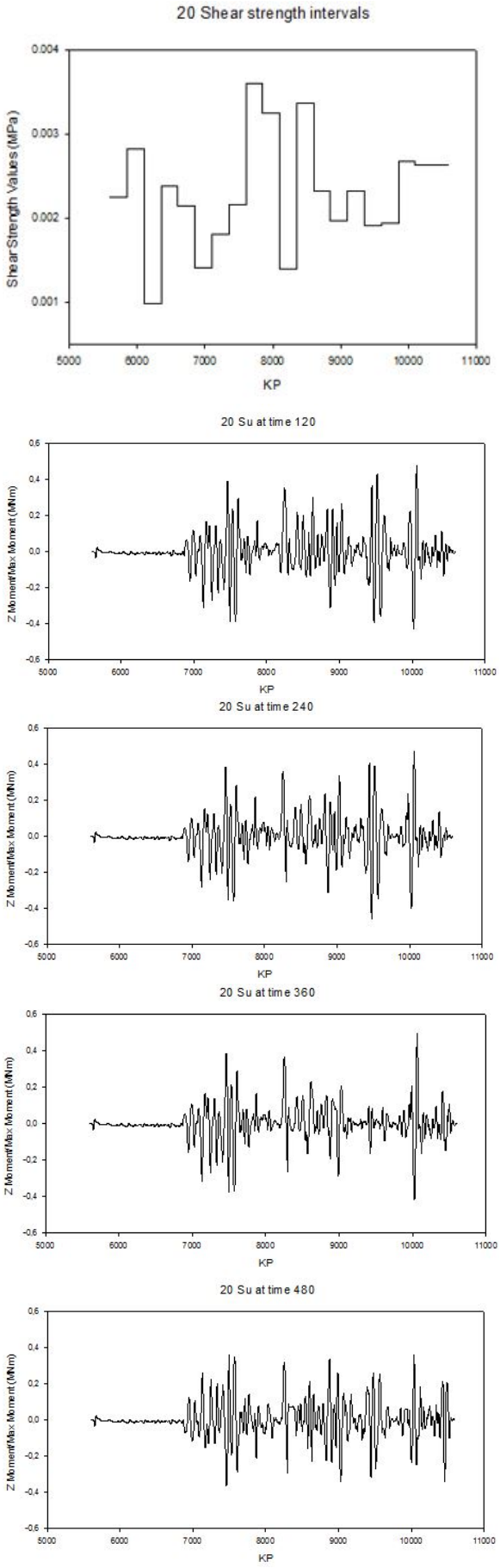


Figure A.18: Moment distributions by cycles with twenty shear strength intervals

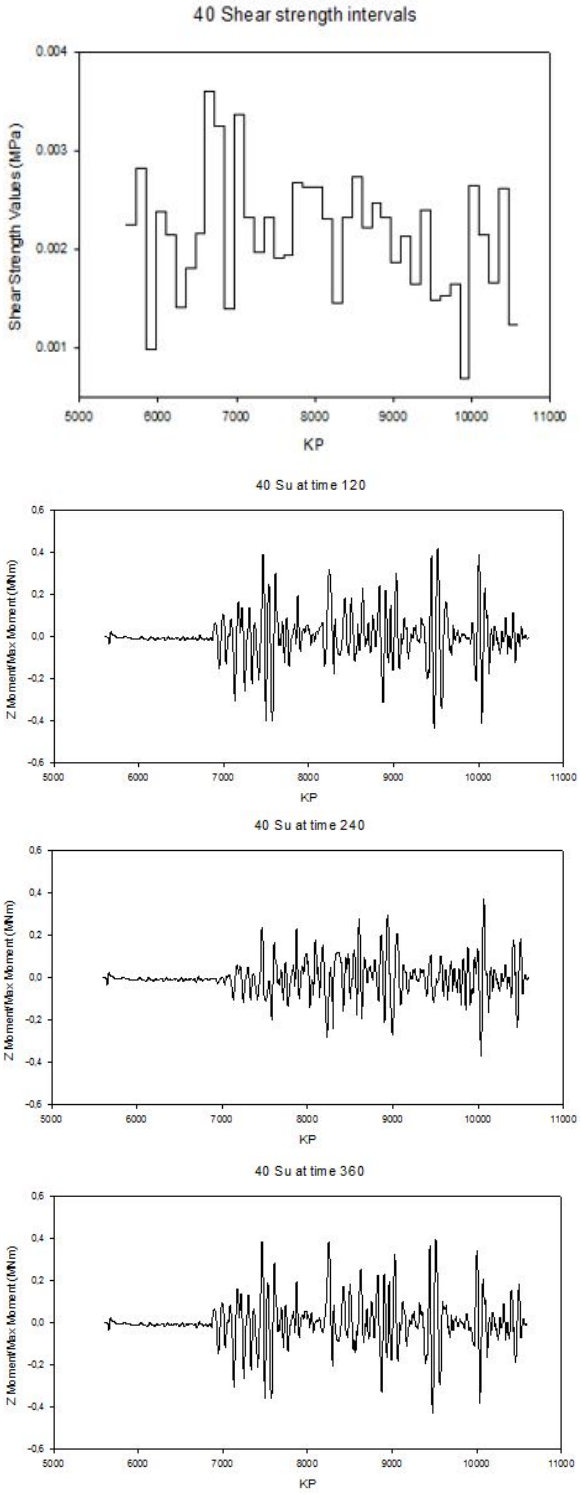


Figure A.19: Moment distributions by cycles with forty shear strength intervals

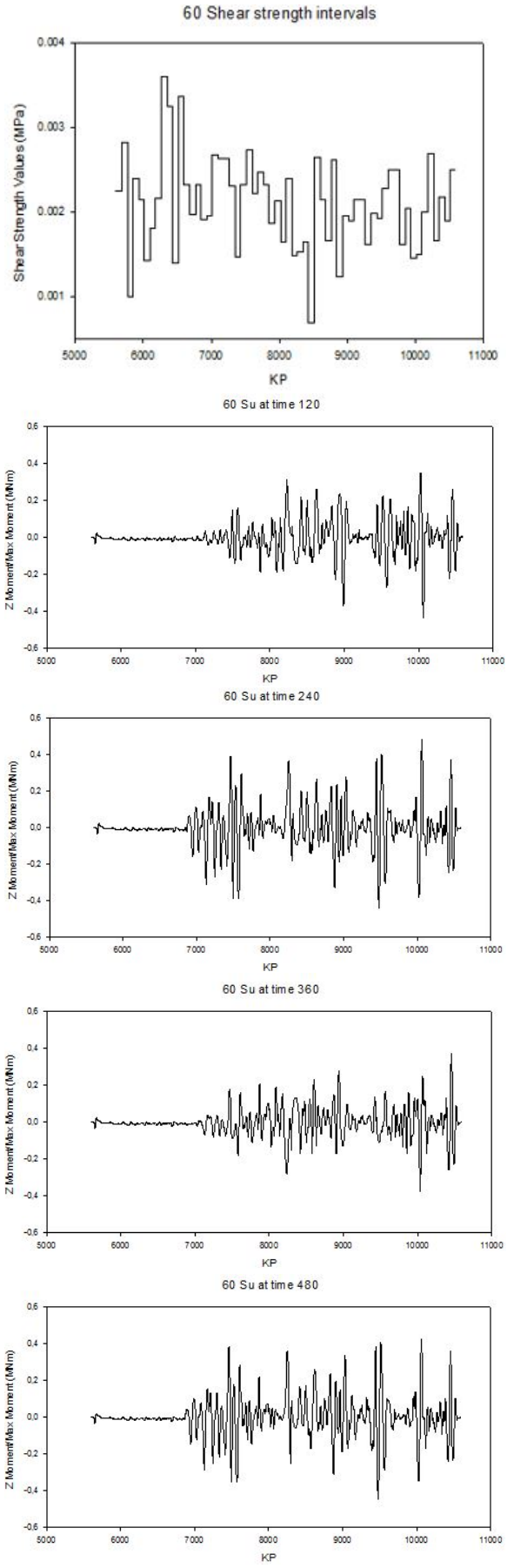


Figure A.20: Moment distributions by cycles with sixty shear strength intervals

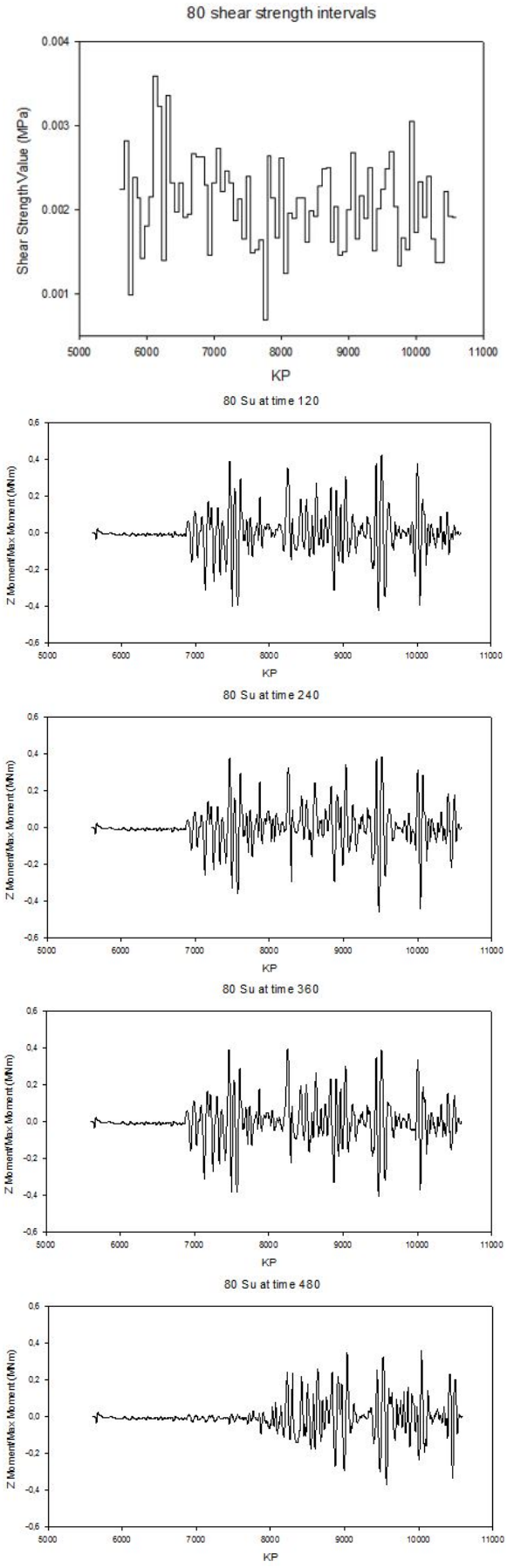


Figure A.21: Moment distributions by cycles with eighty shear strength intervals

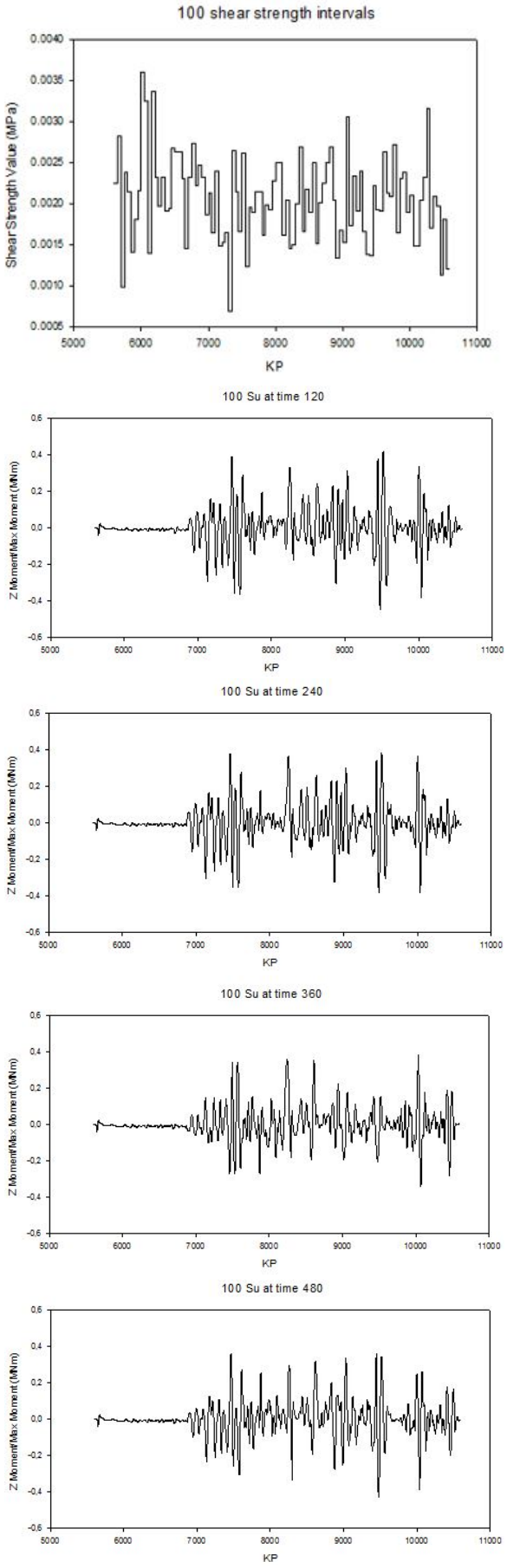


Figure A.22: Moment distributions by cycles with one hundred shear strength intervals

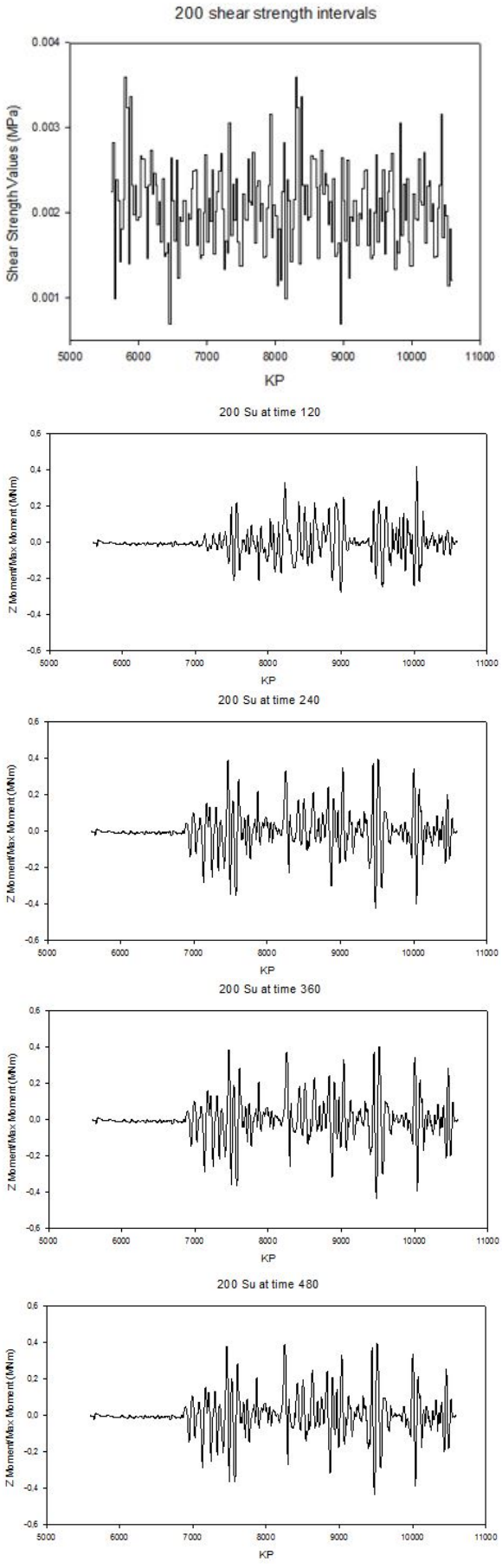


Figure A.23: Moment distributions by cycles with two hundred shear strength intervals

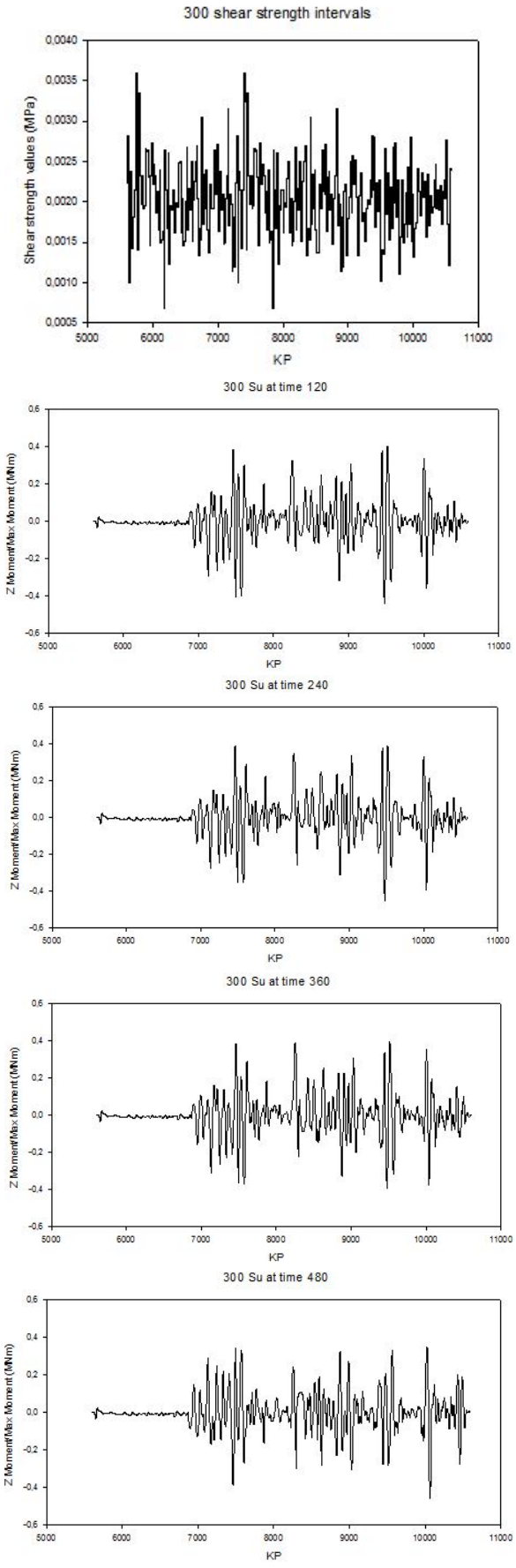


Figure A.24: Moment distributions by cycles with three hundreds shear strength intervals

## A.4 Effects of shear strength intervals in Z-moment

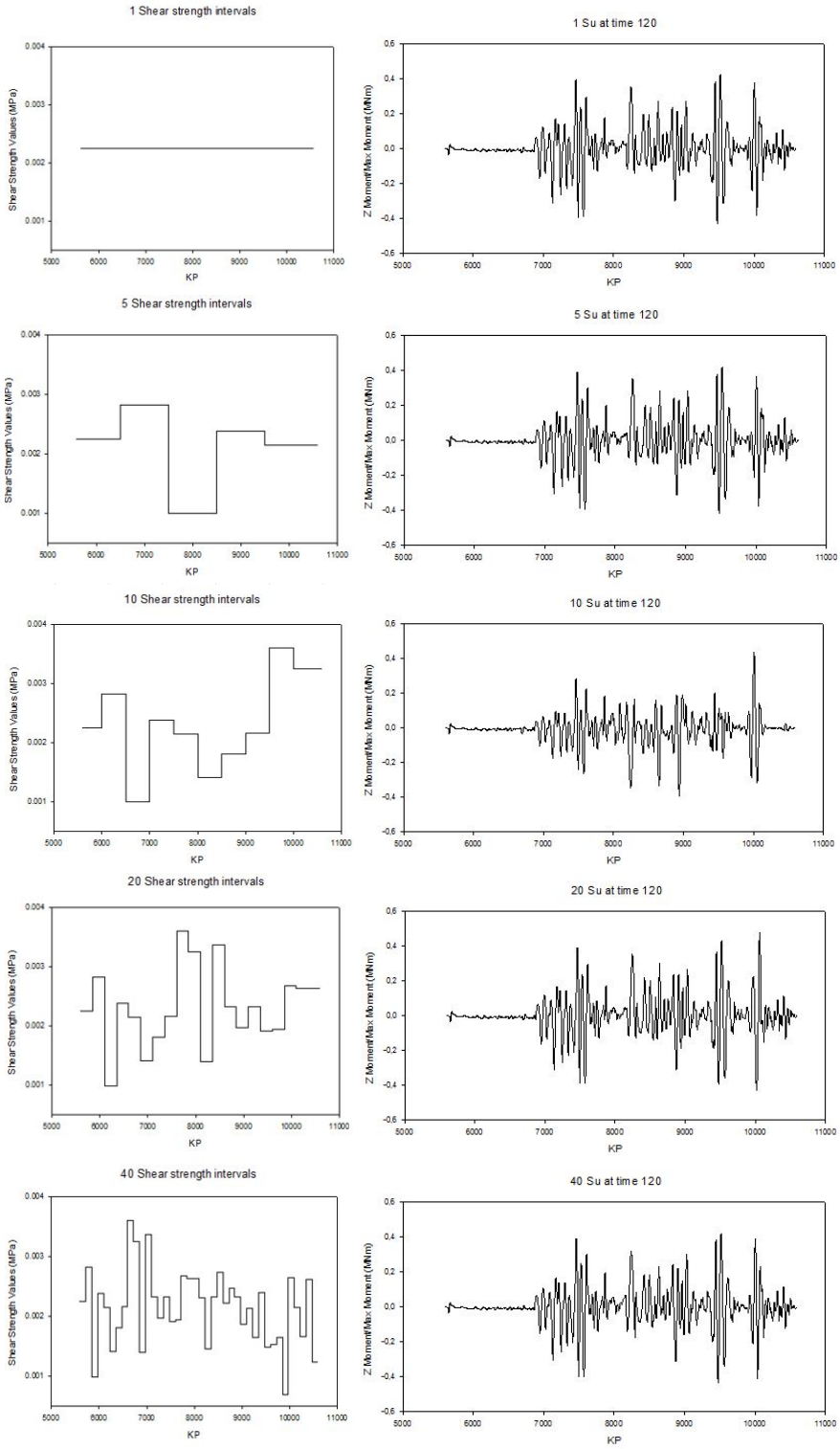

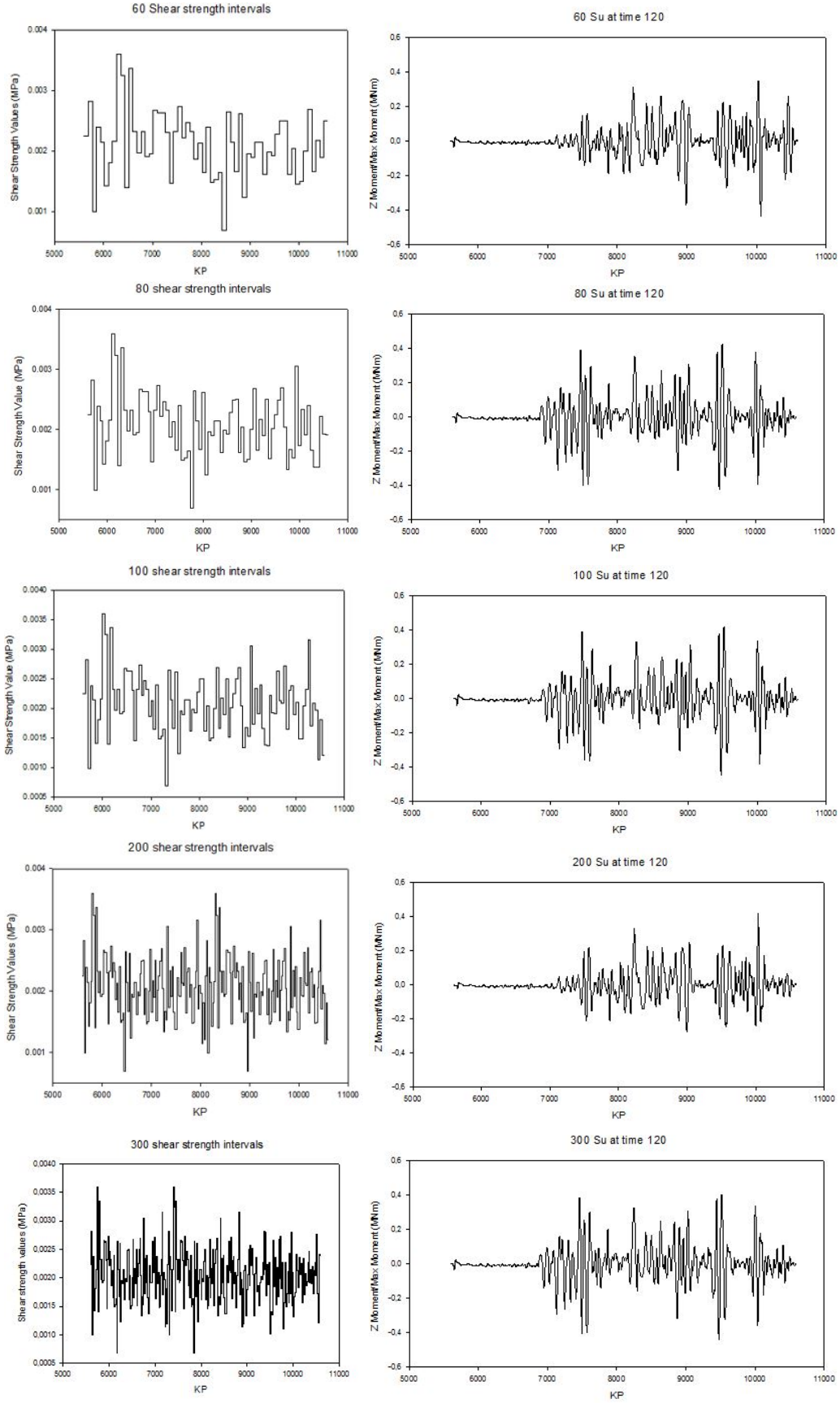


Figure A.25: Z-moment distributions at time 120s by different number of intervals

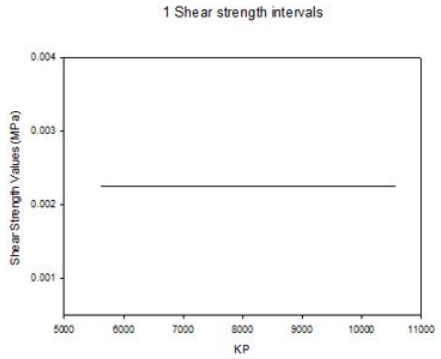
1 Shear strength intervals
Shear Strength Values (MPa)
KP

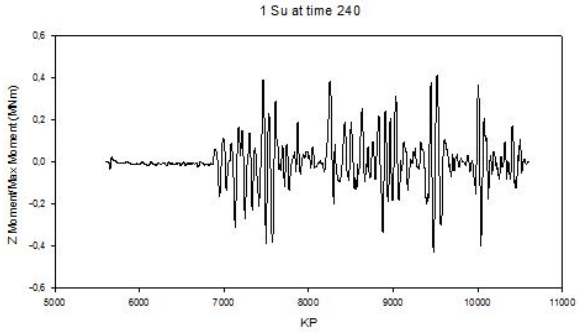
1 Su at time 240
Z Moment/Max Moment (MNm)
KP

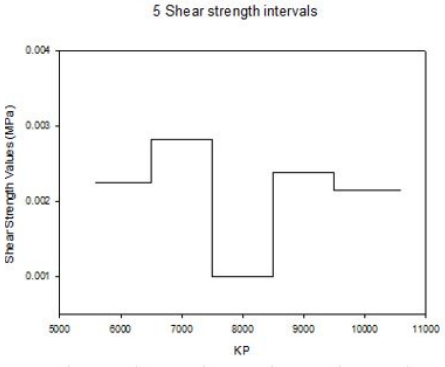
5 Shear strength intervals
Shear Strength Values (MPa)
KP

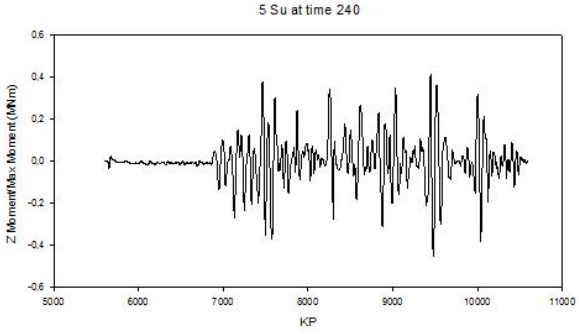
5 Su at time 240
Z Moment/Max Moment (MNm)
KP

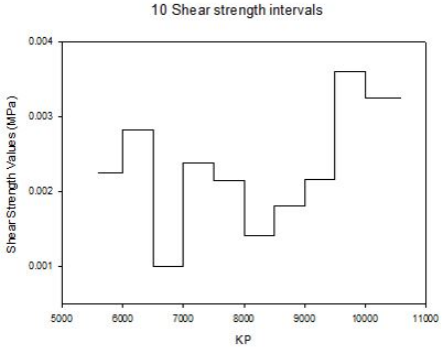
10 Shear strength intervals
Shear Strength Values (MPa)
KP

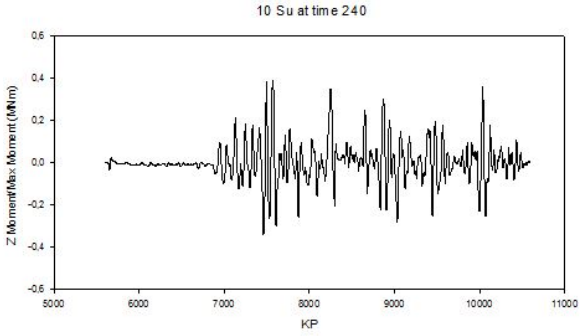
10 Su at time 240
Z Moment/Max Moment (MNm)
KP

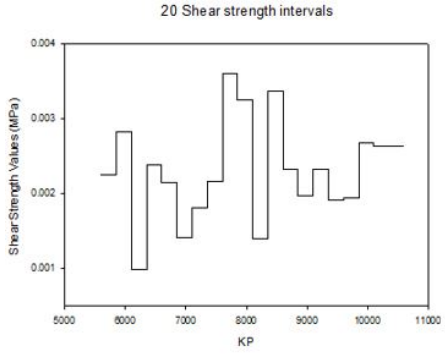
20 Shear strength intervals
Shear Strength Values (MPa)
KP

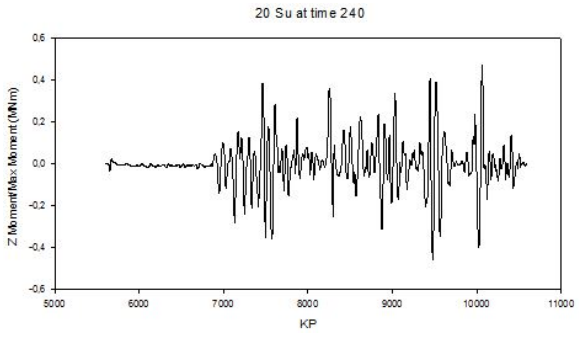
20 Su at time 240
Z Moment/Max Moment (MNm)
KP

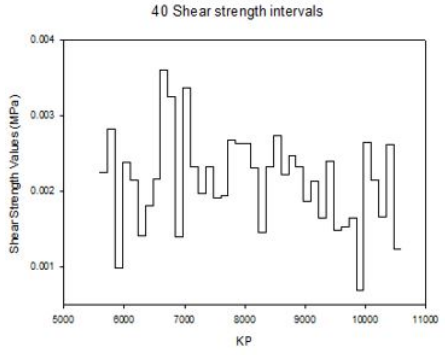
40 Shear strength intervals
Shear Strength Values (MPa)
KP

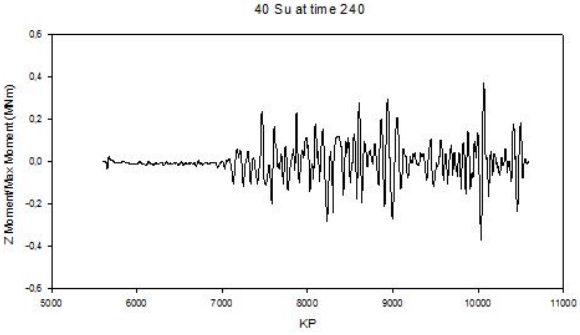
40 Su at time 240
Z Moment/Max Moment (MNm)
KP

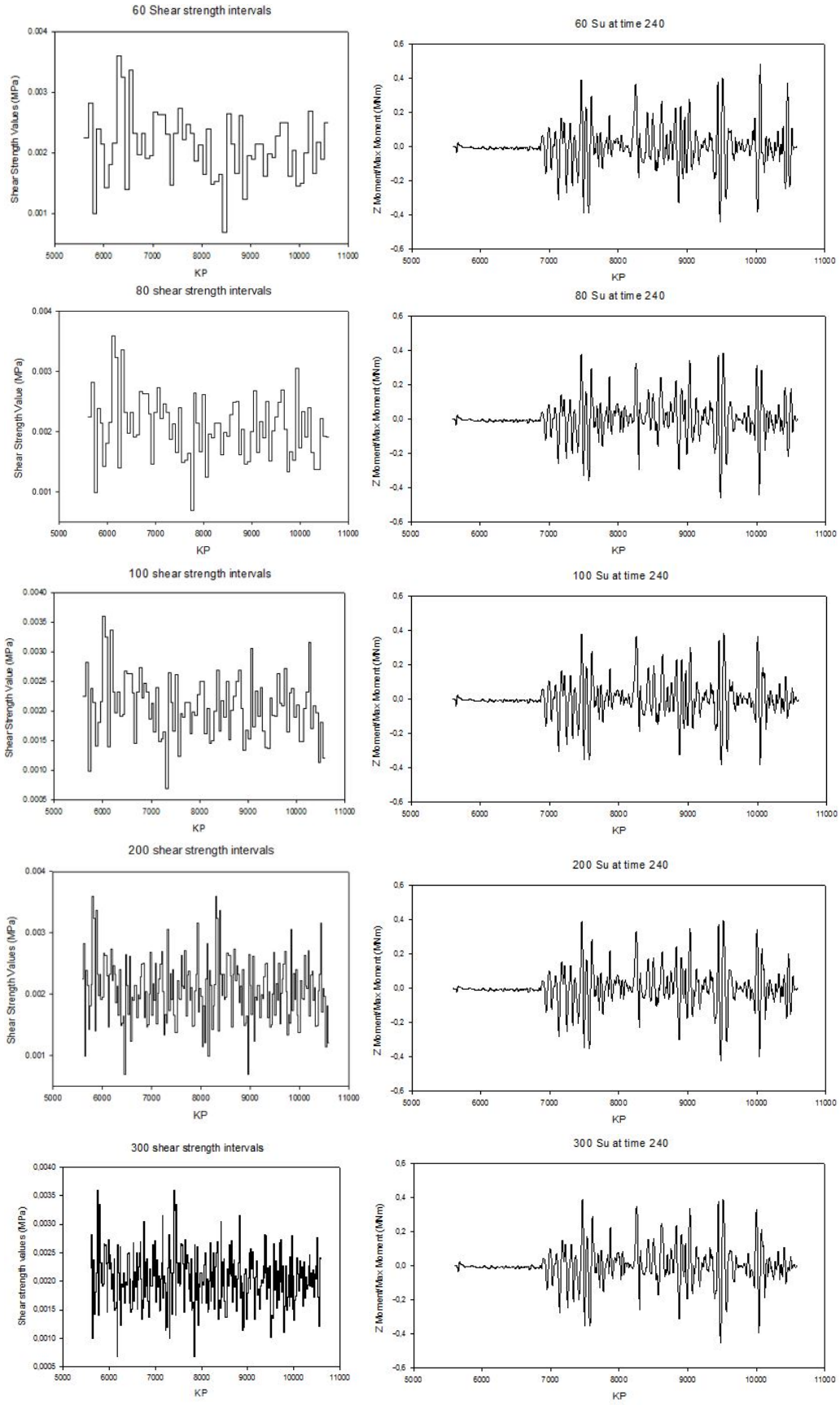


Figure A.26: Z-moment distributions at time 240s by different number of intervals

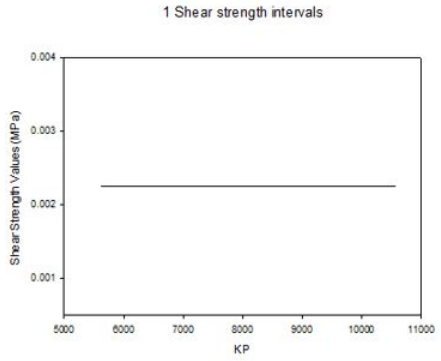
1 Shear strength intervals
Shear Strength Values (MPa)
KP

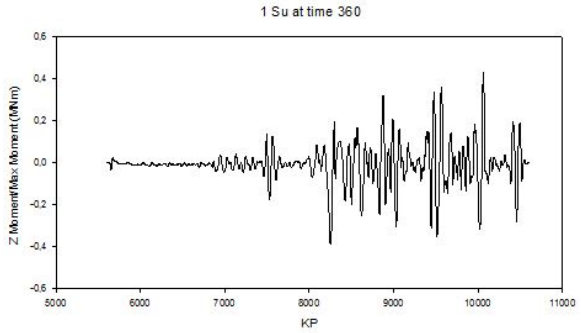
1 Su at time 360
Z Moment/Max Moment (MNm)
KP

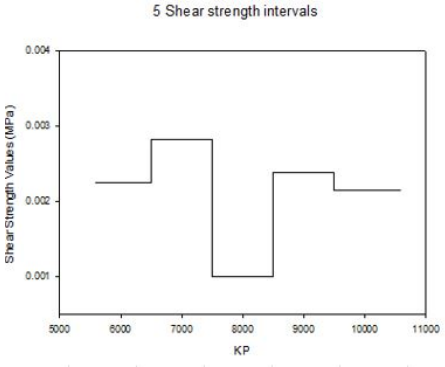
5 Shear strength intervals
Shear Strength Values (MPa)
KP

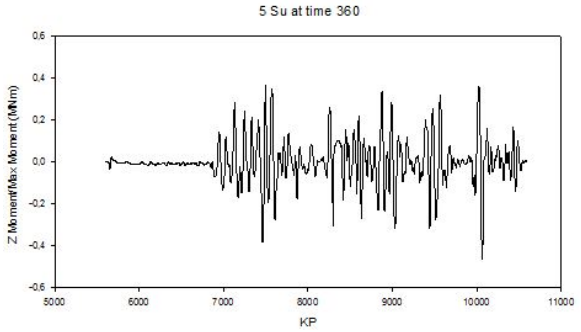
5 Su at time 360
Z Moment/Max Moment (MNm)
KP

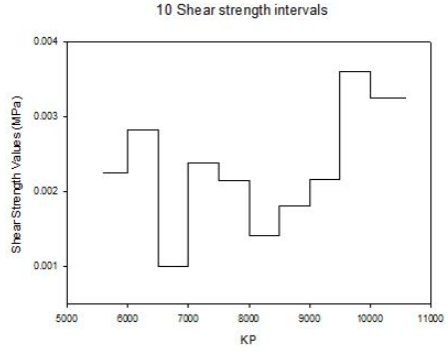
10 Shear strength intervals
Shear Strength Values (MPa)
KP

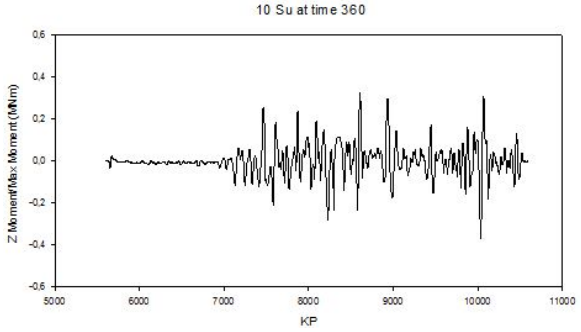
10 Su at time 360
Z Moment/Max Moment (MNm)
KP

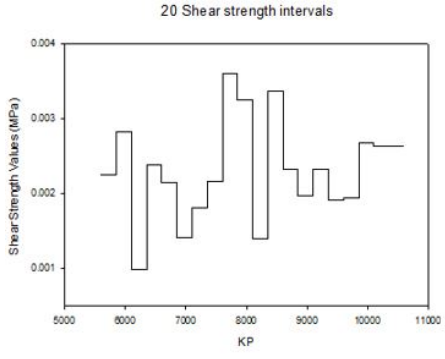
20 Shear strength intervals
Shear Strength Values (MPa)
KP

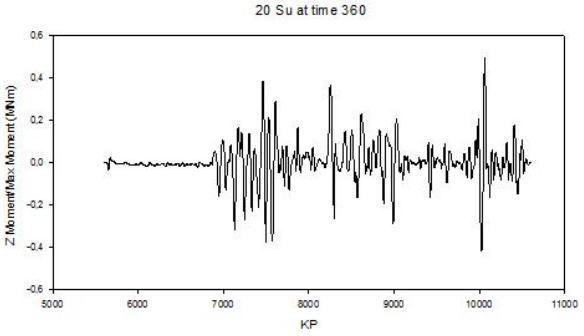
20 Su at time 360
Z Moment/Max Moment (MNm)
KP

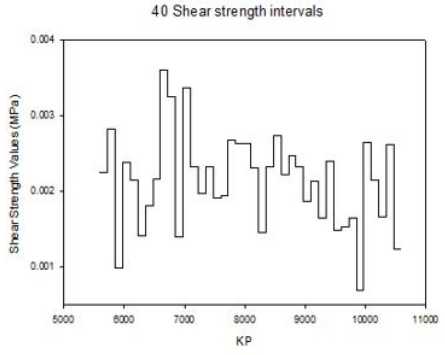
40 Shear strength intervals
Shear Strength Values (MPa)
KP

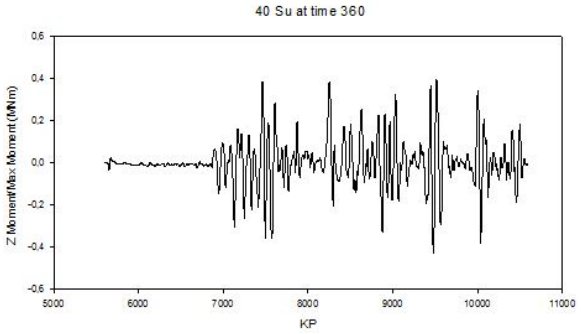
40 Su at time 360
Z Moment/Max Moment (MNm)
KP

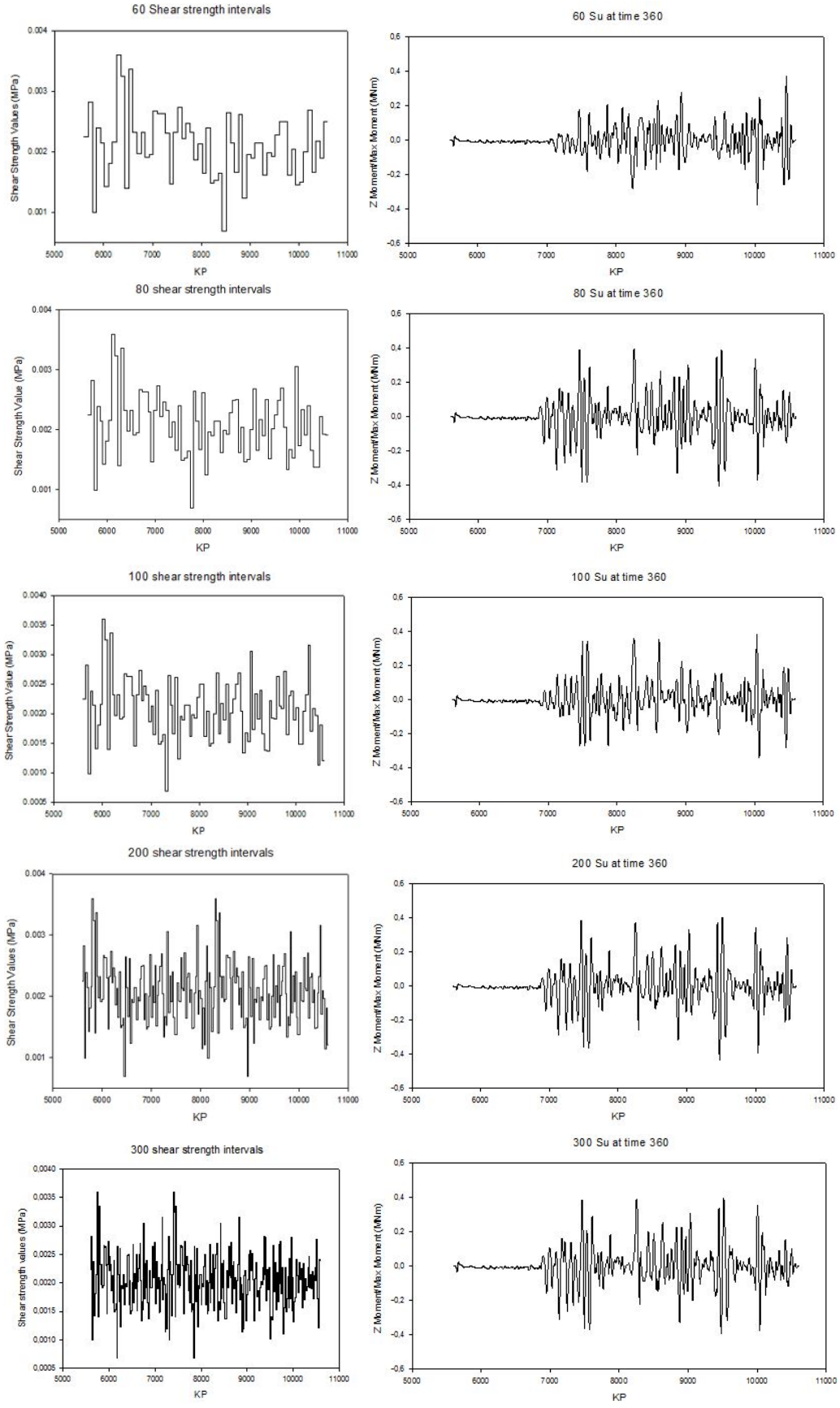


Figure A.27: Z-moment distributions at time 360s by different number of intervals

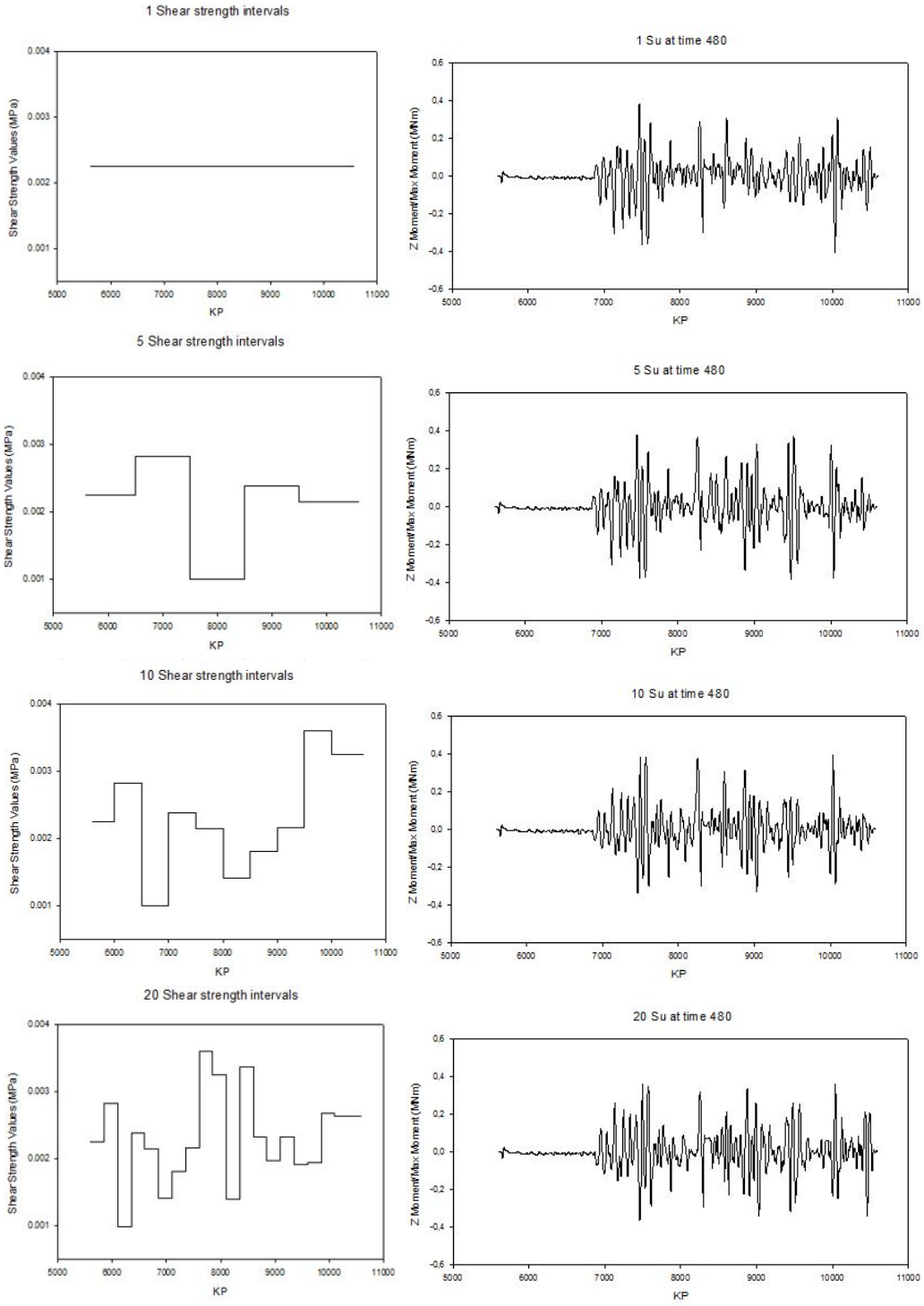
1 Shear strength intervals
Shear Strength Values (MPa)
KP
1 Su at time 480
Z Moment/Max Moment (MNm)
KP
5 Shear strength intervals
Shear Strength Values (MPa)
KP
5 Su at time 480
Z Moment/Max Moment (MNm)
KP
10 Shear strength intervals
Shear Strength Values (MPa)
KP
10 Su at time 480
Z Moment/Max Moment (MNm)
KP
20 Shear strength intervals
Shear Strength Values (MPa)
KP
20 Su at time 480
Z Moment/Max Moment (MNm)
KP

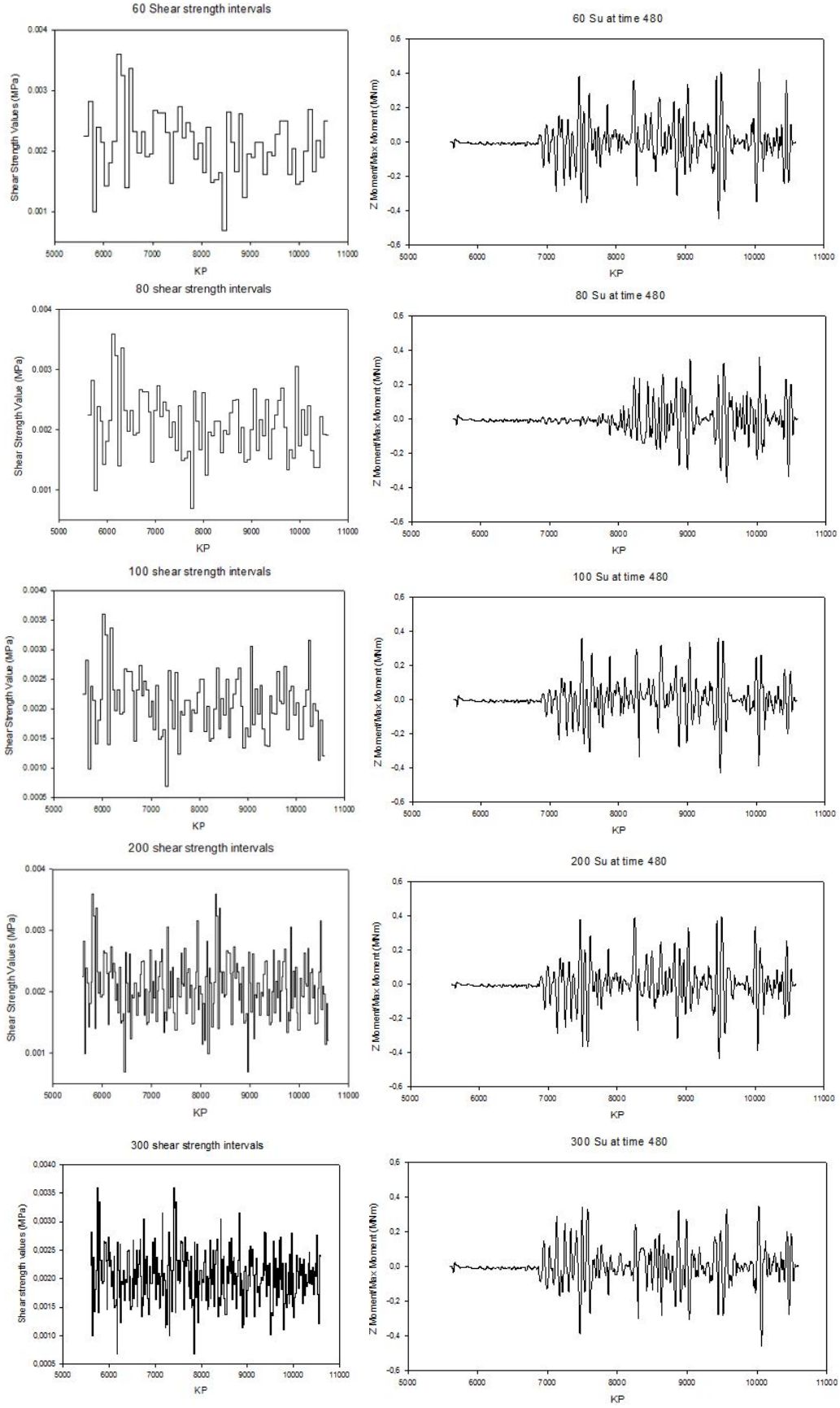


Figure A.28: Z-moment distributions at time 480s by different number of intervals

# Appendix B

# Case study 2

## B.1 Total moment by different shear strength distributions

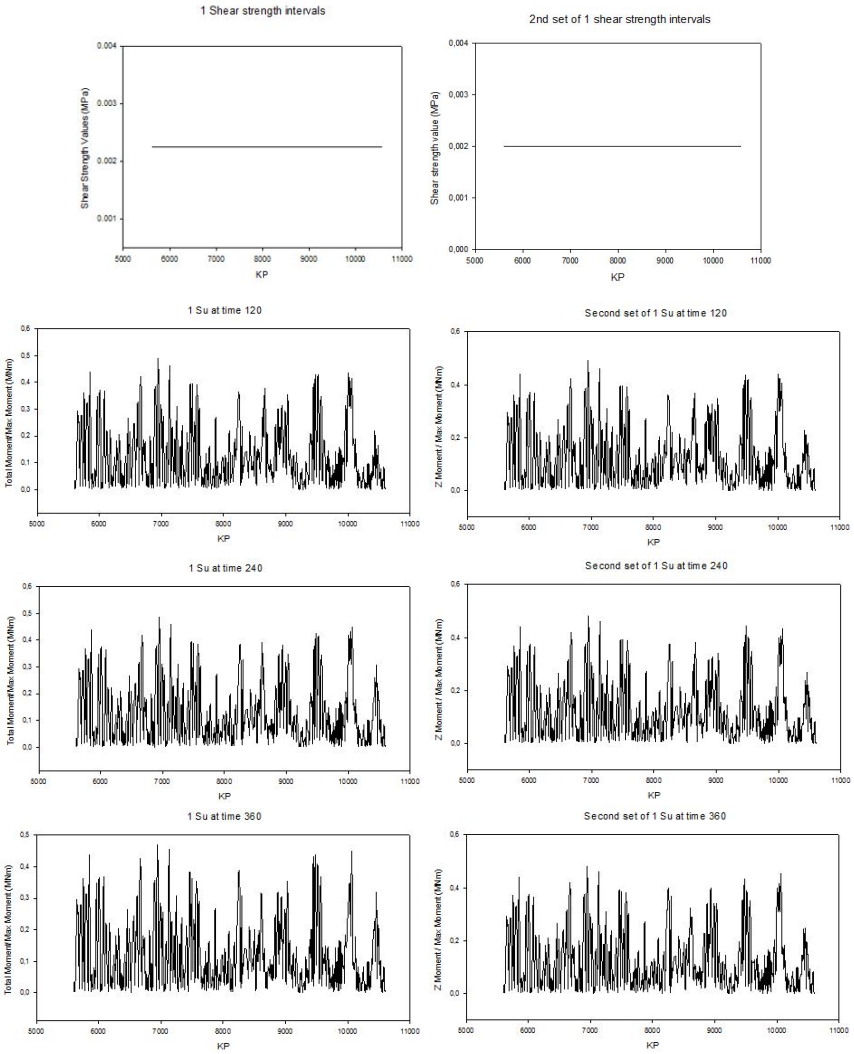


Figure B.1: Moment distributions by 1 interval generated by different set of $S_u$

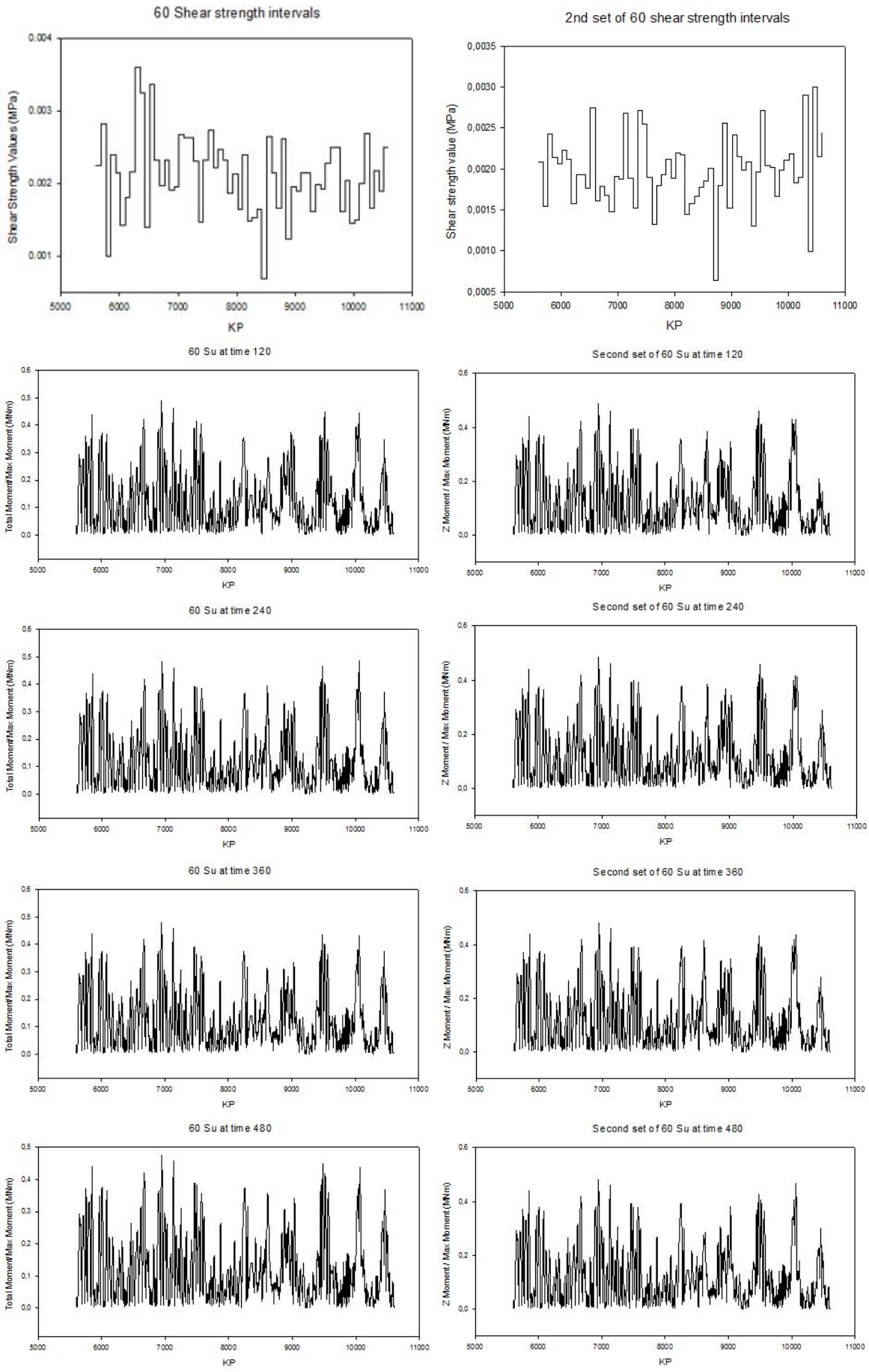


Figure B.2: Moment distributions by 60 intervals generated by different set of $S_u$

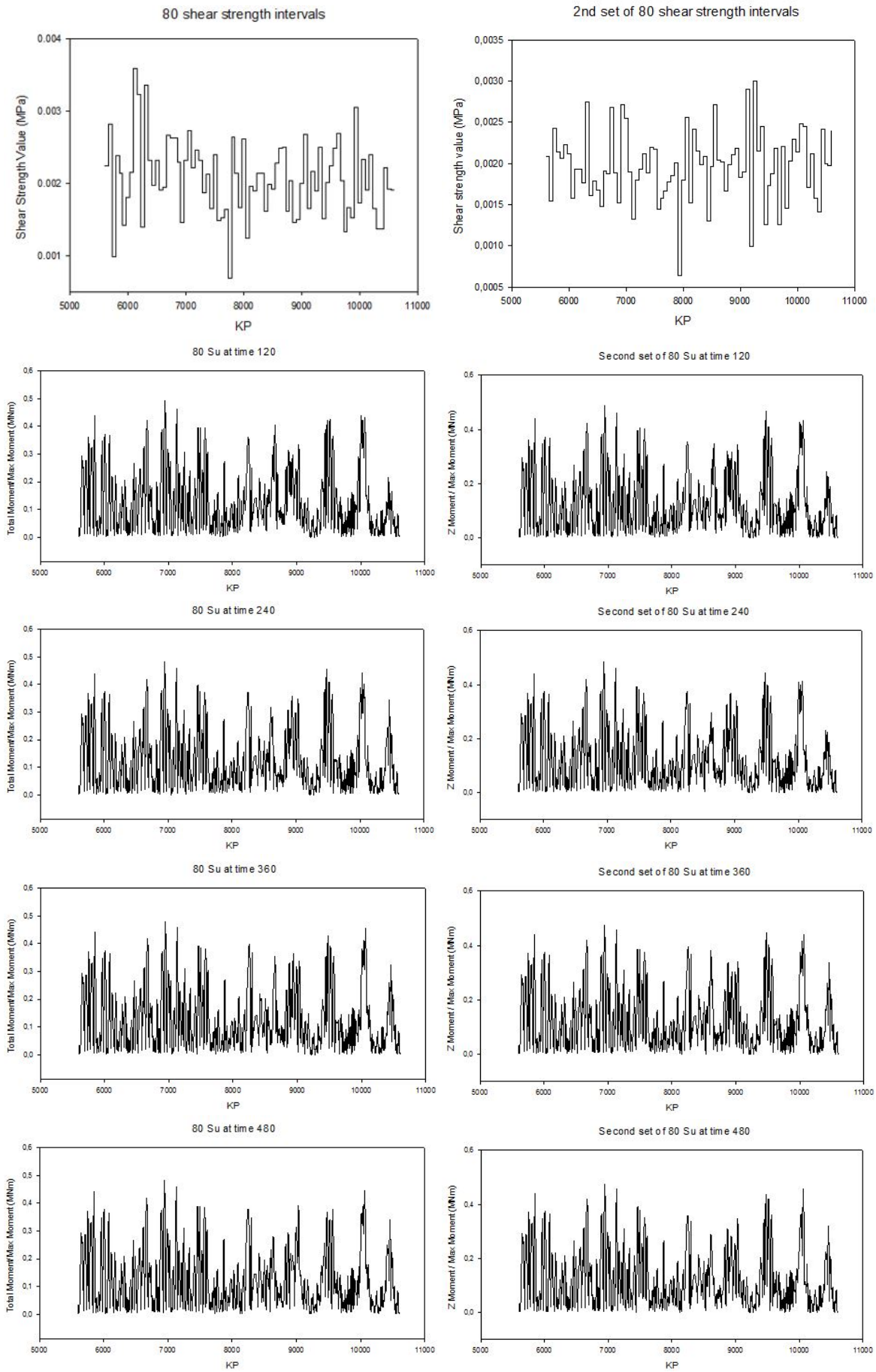


Figure B.3: Moment distributions by 80 intervals generated by different set of $S_u$

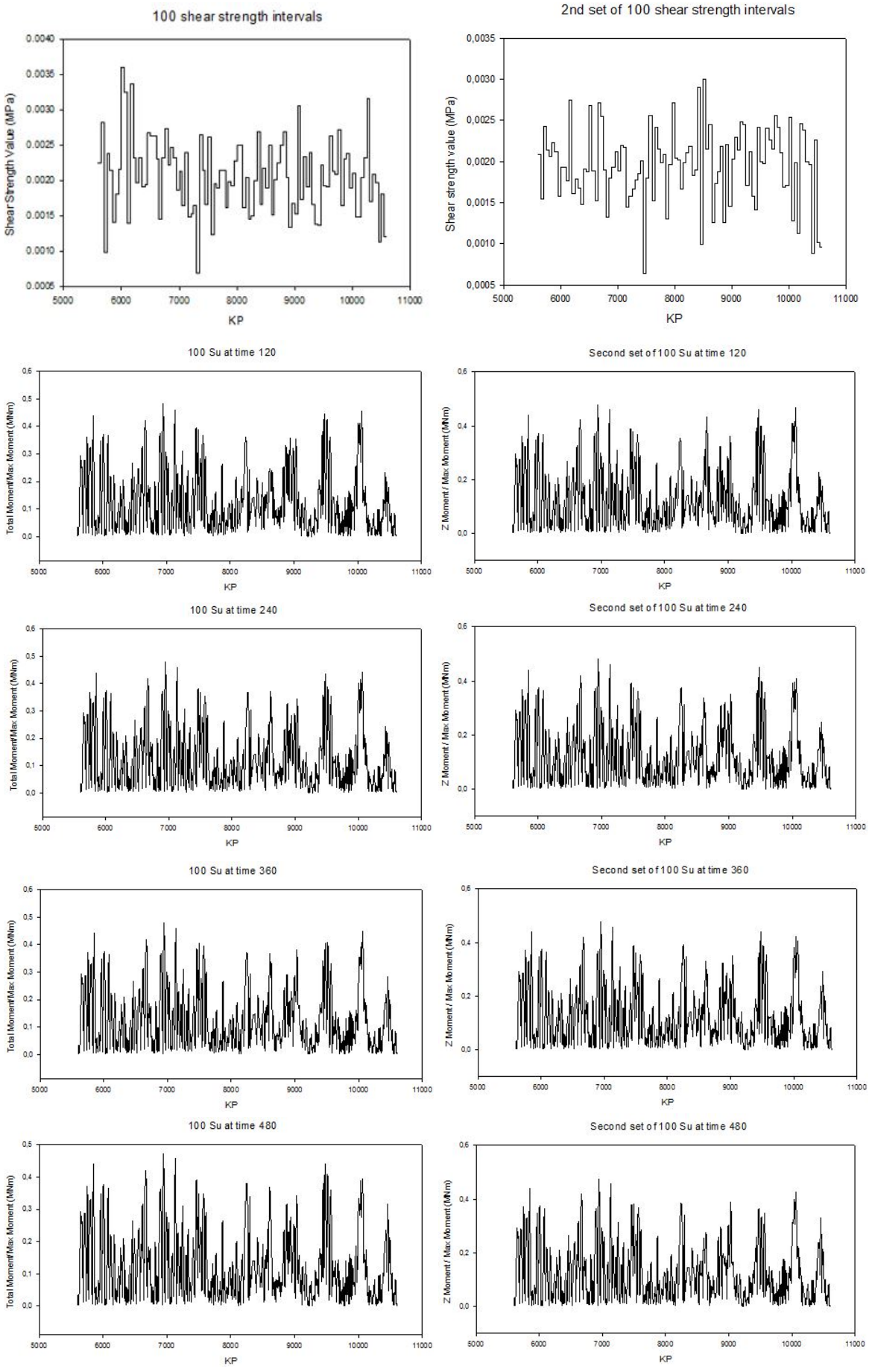


Figure B.4: Moment distributions by 100 intervals generated by different set of $S_u$

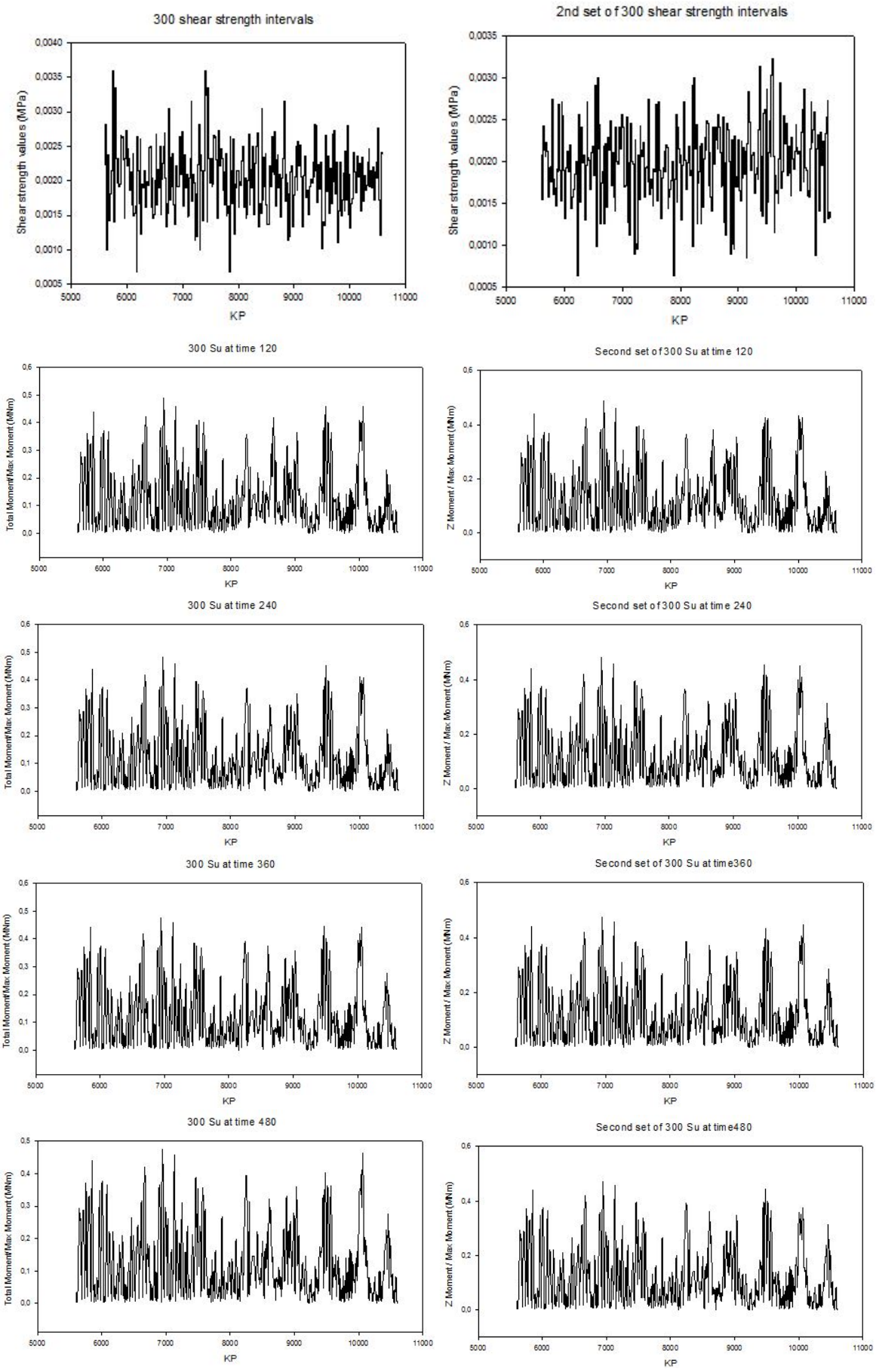


Figure B.5: Moment distributions by 300 intervals generated by different set of $S_u$

## B.2 Comparison of different shear strength distributions

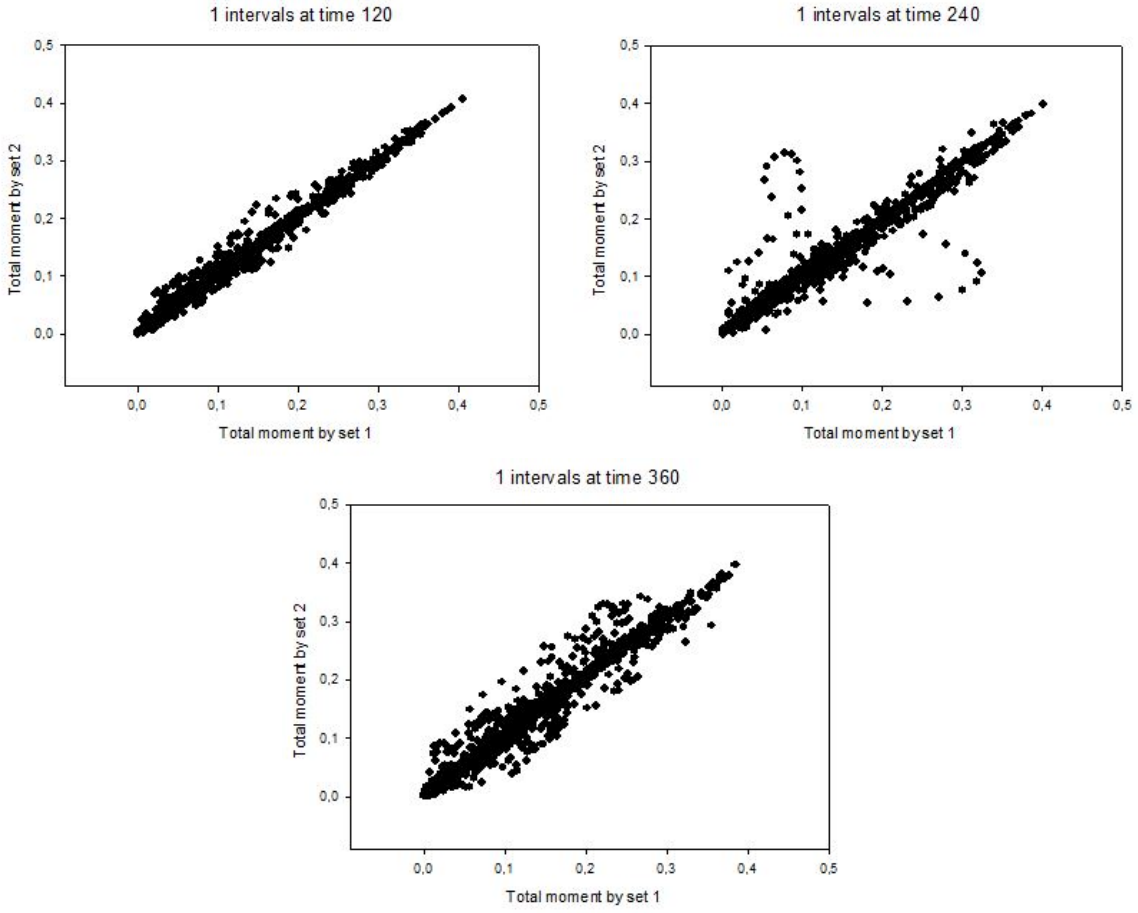


Figure B.6: Comparisons of moment distributions generated by different $S_u$ sets with 1 interval

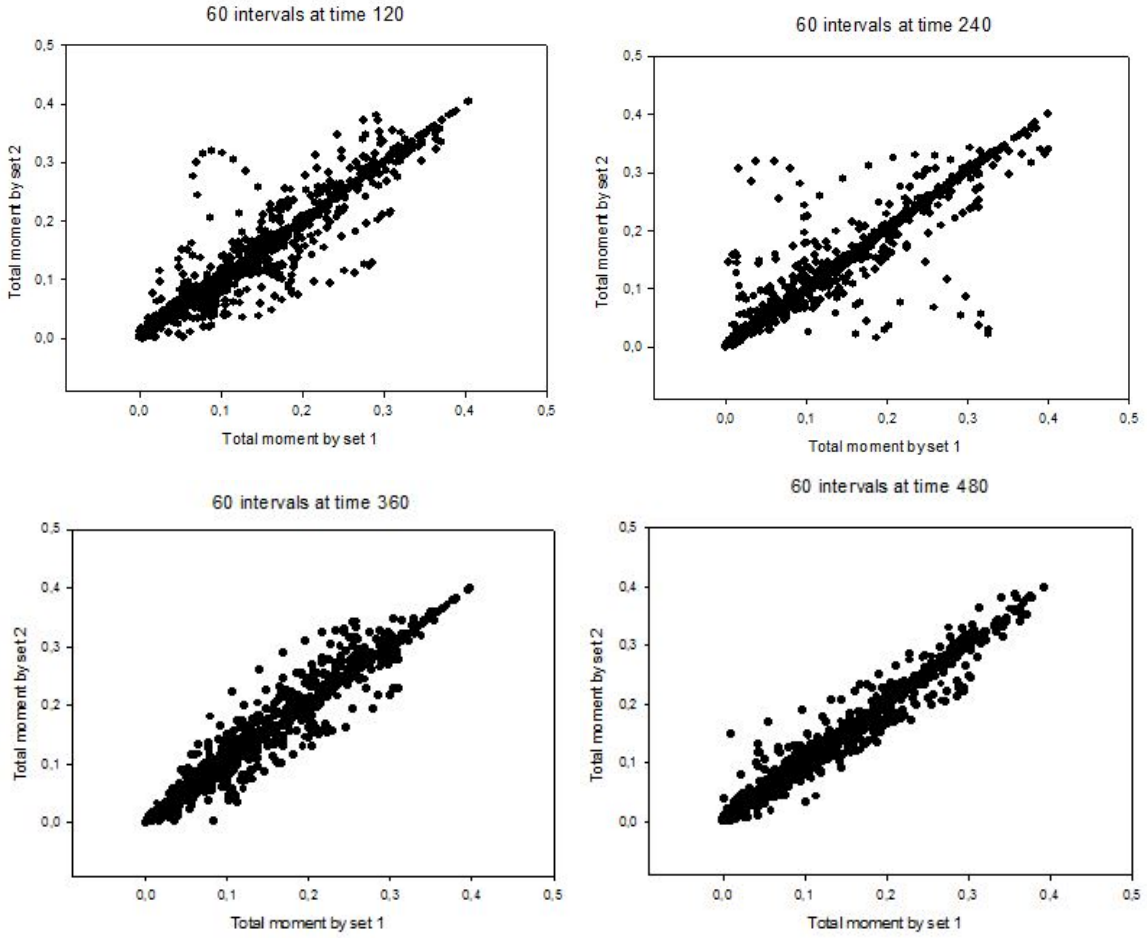


Figure B.7: Comparisons of moment distributions generated by different $S_u$ sets with 60 interval

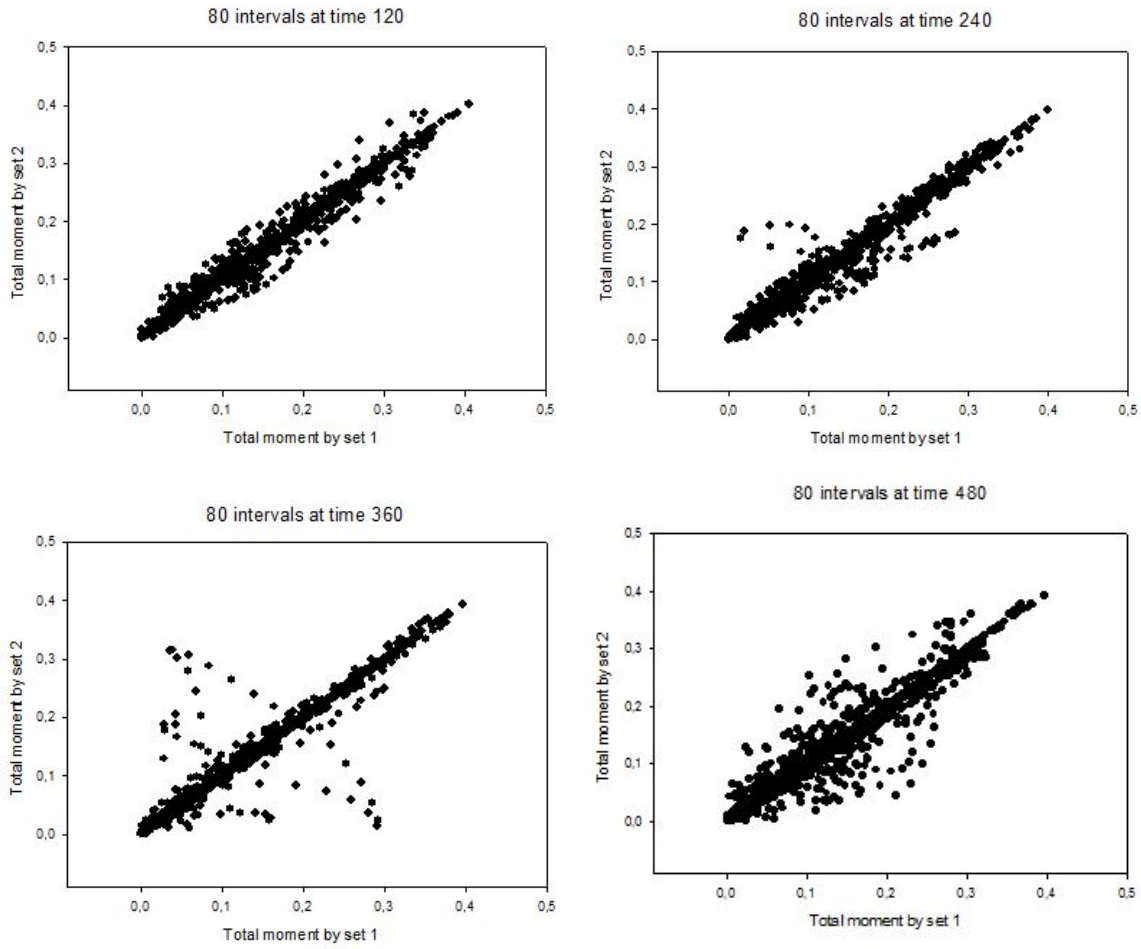


Figure B.8: Comparisons of moment distributions generated by different $S_u$ sets with 80 interval

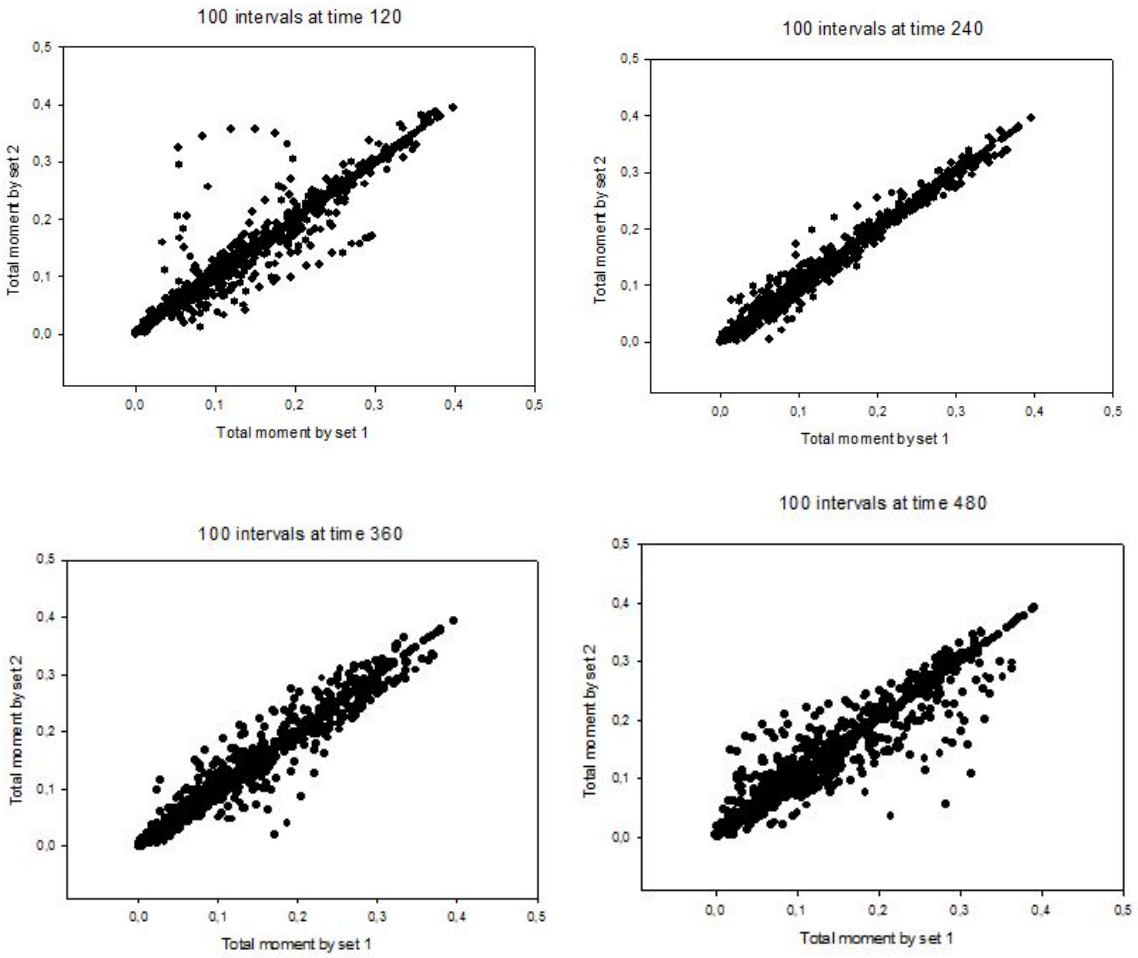


Figure B.9: Comparisons of moment distributions generated by different $S_u$ sets with 100 interval

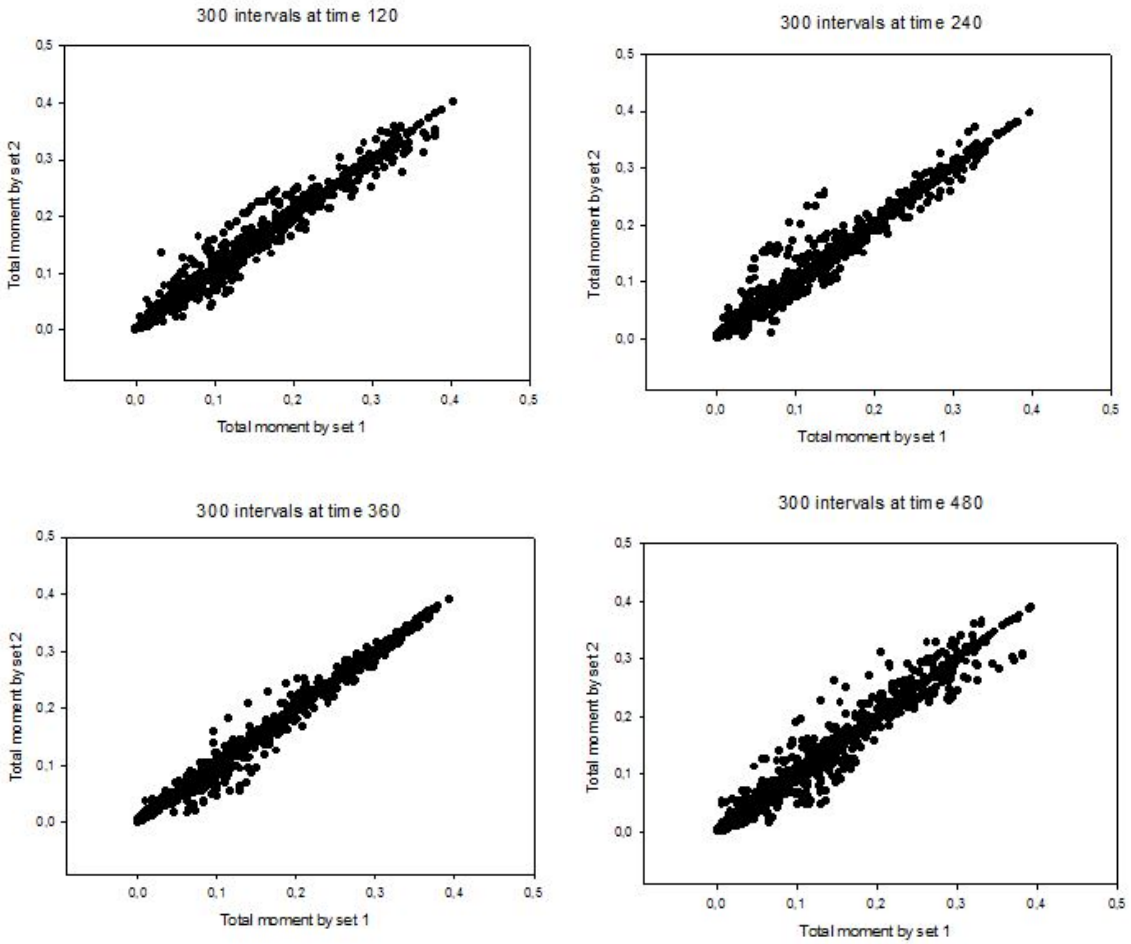


Figure B.10: Comparisons of moment distributions generated by different $S_u$ sets with 300 interval